

Collective Dynamics in Networks of Pulse-Coupled Oscillators

Dissertation

zur Erlangung des Doktorgrades
der Mathematisch-Naturwissenschaftlichen Fakultäten
der Georg-August-Universität zu Göttingen

vorgelegt von

Marc Timme

aus Soltau

Göttingen 2002

D7

| | |
|-------------|-----------------------|
| Referent: | Prof. Dr. Theo Geisel |
| Koreferent: | Prof. Dr. Reiner Kree |

| | |
|-----------------------------|-------------------|
| Tag der mündlichen Prüfung: | 11. Dezember 2002 |
|-----------------------------|-------------------|

Contents

| | | |
|----------|---|-----------|
| 1 | Introduction | 7 |
| 2 | Fundamentals | 13 |
| 2.1 | Basic notions from graph theory | 13 |
| 2.1.1 | Graphs and adjacency | 13 |
| 2.1.2 | Paths, distance, connectivity, and irreducibility | 14 |
| 2.2 | Concepts of stability and attractors | 15 |
| 2.2.1 | Stability of invariant sets | 15 |
| 2.2.2 | Different concepts of an attractor | 17 |
| 3 | The Mirollo-Strogatz model | 21 |
| 3.1 | Mirollo-Strogatz model of pulse-coupled oscillators | 21 |
| 3.1.1 | Pulse-coupled single variable threshold oscillators | 22 |
| 3.1.2 | Nonlinear transformation of variables | 23 |
| 3.1.3 | A brief history of investigations | 24 |
| 3.1.4 | Phase model by Mirollo and Strogatz | 25 |
| 3.2 | Advantages of the Mirollo-Strogatz model | 27 |
| 3.2.1 | Equivalence to other models | 27 |
| 3.2.2 | Numerical advantages | 32 |

| | | |
|----------|---|-----------|
| 4 | Unstable attracting periodic orbits | 35 |
| 4.1 | Unstable attractors? | 36 |
| 4.2 | Perpetual synchronization and desynchronization | 37 |
| 4.3 | Stability analysis | 39 |
| 4.4 | Unstable attractors | 44 |
| 4.5 | Unstable attractors in large networks | 47 |
| 4.6 | Prevalence and persistence | 48 |
| 4.7 | Structural modifications | 51 |
| 4.8 | Summary and outlook | 52 |
| | | |
| 5 | Networks with a complex structure | 55 |
| 5.1 | Structure and dynamics of complex networks | 55 |
| 5.2 | Structured networks of Mirollo-Strogatz oscillators | 57 |
| 5.3 | Construction of stroboscopic maps | 57 |
| 5.4 | First order operators | 60 |
| 5.5 | Bounds on the eigenvalues | 61 |
| 5.5.1 | General properties of matrix elements | 62 |
| 5.5.2 | Eigenvalues for inhibitory coupling | 63 |
| 5.5.3 | Eigenvalues for excitatory coupling | 65 |
| 5.6 | Stability and instability | 65 |
| 5.6.1 | Stability for inhibitory coupling | 66 |
| 5.6.2 | Asymptotic stability for inhibitory coupling | 67 |
| 5.6.3 | Instability for excitatory coupling | 71 |
| 5.7 | Coexistence of regular and irregular dynamics | 72 |
| 5.8 | Summary and discussion | 74 |

| | | |
|----------|--|------------|
| 6 | Robust synchronization | 77 |
| 6.1 | Equivalence of synchronization and diffusion | 78 |
| 6.2 | Location of eigenvalues in large random networks | 81 |
| 6.2.1 | Networks with constant in-degree | 82 |
| 6.2.2 | Networks with constant connection probability | 82 |
| 6.3 | Estimates from random matrix theory | 83 |
| 6.3.1 | Ensembles of symmetric and asymmetric random matrices | 84 |
| 6.3.2 | Stability matrices and the Gaussian asymmetric ensemble | 85 |
| 6.4 | Numerical tests of eigenvalue estimates | 88 |
| 6.4.1 | Networks with constant in-degree | 88 |
| 6.4.2 | Networks with constant connection probability | 91 |
| 6.5 | Summary and outlook | 93 |
| 7 | Conclusions | 95 |
| A | Appendix: Two exact derivations | 99 |
| A.1 | Return map of unstable attracting periodic orbit | 99 |
| A.1.1 | Periodic orbit dynamics | 99 |
| A.1.2 | Dynamics of a general perturbation to the periodic orbit | 103 |
| A.2 | Derivation of the expansion (5.17) | 106 |
| | References | 109 |
| | Acknowledgments | 117 |

Chapter 1

Introduction

Complex systems are one of the central subjects of modern science [1]. Although there is no agreement on the very definition of complexity [2], it is commonly accepted that complex systems are typically comprised of a large number of possibly very different units [3]. Interactions occur between spatially neighboring units or on an underlying network which frequently exhibits a complicated structure. Since these interactions are generally nonlinear, it is often hard to deduce the dynamics of a single entity from the behavior of the entire system. Conversely, collective phenomena arise which may not have been anticipated from the dynamics of the individual units [4]. A textbook example from equilibrium statistical mechanics (see, e.g. [5,6]) is provided by a ferromagnet where a phase transition from a disordered phase to spontaneous magnetization occurs as an external parameter, the temperature, passes a critical value.

Current interdisciplinary research focusses on systems in which the interactions are manifestly nonlinear, ranging from fluid dynamics, biophysics and neural networks via complex technical systems to ecological, economical, and social dynamical systems. To model a complex system, it is often a sensible first step to bridge one and the next higher level of abstraction [3] by idealizing the interacting units in such a way that the single unit is as simple as possible, at the same time trying to keep the characteristic features underlying the collective phenomenon under consideration. This method of reduction is already introduced in first courses on mechanics where the collision of two rigid bodies is described neglecting a wealth of influencing factors, such as the friction with the surrounding air and the less obvious motion of atoms in the bodies. Here, such a reduction might seem justified a priori, but in systems exhibiting more complicated dynamics one has to analyze carefully which aspects can be neglected and which have to be kept.

Many complex systems that are comprised of discrete units are modeled within the important class of complex networks [7]. Here, the lowest level of abstraction is the assumption of elementary individual units which interact on the network. It is bridged to the next higher

level, the collective dynamics of a network, which itself is considered in isolation from the influences of its environment. Nevertheless, the dynamics of such networks is often inherently difficult to understand because a number of complications arise. The structure of the network, determined by the coupling architecture between units, may be complicated and even change with time. The dynamics of single units may already be complicated when considered in isolation and may even differ from unit to unit. Deeper insights into the dynamics of such networks are therefore often only possible if the single units as well as the interactions are idealized.

Pulse-coupled oscillators constitute a paradigmatic class of dynamical systems interacting on networks. These are threshold elements, which are slowly driven by an external force and discharge rapidly whenever a trigger threshold is reached, similar to a capacitor which is charged by a voltage source and shorts whenever its voltage exceeds a threshold. Such a unit is said to fire at the time when the threshold is reached. It results in a reset of that unit to a state far from the threshold, its rest value. At the same time the discharge activity, a pulse of brief duration compared to the typical charging time, induces a state change of other units which interact with the original one. Such interactions are termed pulse-coupling because they depend on singular temporal events, such as the firing of one unit, rather than on the temporally evolving state of that unit. Since the state of an isolated individual unit repeatedly cycles through the same values in an approximately periodic time course, they are considered as oscillators. Pairs of oscillators which interact are considered connected. The set of all connections determines the structure of an underlying network.

Networks of pulse-coupled oscillators are used to model various natural systems including earthquakes and forest fires, flashing fireflies and chirping crickets as well as pacemaker cells of the heart and neural networks (see [8–12] and references therein). Let us briefly discuss two seemingly distinct examples. First, single faults between tectonic plates, responsible for earthquakes, are modeled by two-dimensional lattices of such oscillators [8]. Here, each oscillator represents a local patch near the fault, the state of which reflects the current amount of stress of that patch. The stress is assumed to increase slowly due to the opposed motion of two tectonic plates. When the stress of a single patch is too large, it discharges stress and distributes it among spatially neighboring patches on the lattice. An earthquake occurs if discharges of one or a few patches trigger an avalanche of discharges of very many patches. Since the duration of a single earthquake is typically of the order of one minute whereas times between subsequent earthquakes are of the order of years, these two time scales are well separated such that the coupling may be assumed as an instantaneous pulse. Second, neural networks driven by an external current may be viewed as pulse-coupled oscillators [12]. Here an oscillator represents a single neuron, the state of which reflects the electrical potential across the cell's membrane between the inside and the outside of the cell, which is sustained by ionic channels and pumps [13]. To a reasonable degree of approximation, a neuron sends a signal, termed an action potential or a spike, whenever a threshold potential is reached. After about one millisecond the neuron is reset to a resting potential, and an action potential, a short-lasting, stereotyped pulse, travels

along the axon of that neuron through which it is connected to many other neurons. Via synapses at the terminal end of the axon the pulse arrives at the other neurons and induces a change in their potentials. Although both earthquake and neuronal dynamics may be modelled by networks of pulse-coupled oscillators, they differ in important characteristics: the most obvious difference concerns the time scales. Whereas the two relevant time scales in earthquakes are minutes and years, those in neurons are about one millisecond and tens or hundreds of milliseconds. Since for the assumption of pulse-coupling the separation of time scales is important, but not the absolute durations of events and inter-event times, this difference is only of minor importance. Some less obvious differences are more relevant. Whereas shocks in earthquakes may well be considered as instantaneous events, given that stress is released only to spatially neighboring patches, the traveling action potentials of neurons often need a significant amount of time to arrive at and induce a response in a connected cell. Thus a time delay between the sending and reception of the pulse becomes important. Furthermore, single patches in earthquake models may be assumed to be arranged in a regular, two-dimensional array, e.g. a square lattice. In contrast, the intricate connections between neurons creating complicated networks may often be essential for their dynamics, and should in this case not be modeled by regular lattices. In this thesis we will show how interaction delays as well as irregular network structures can have a pronounced effect on the dynamics of pulse-coupled oscillators.

Recently a wealth of different dynamical features of networks of pulse-coupled units has been revealed. A fundamental question concerns the long-time behavior of such networks at given parameters and fixed connectivity structure, i.e. the dynamics on attractors of the system. The simplest kind of attractor dynamics, besides the complete quiescence of all units, is the fully synchronous state in which all units fire periodically in unison [14–16]. The next simplest class of attractors is given by period-one orbits, in which every oscillator fires exactly once during each period. In such states either one [14] or several groups [17, 18] of oscillators are synchronized resulting in cluster states, or the oscillators just exhibit constant differences between their firing times, called phase-locked states [19]. Periodic orbits of periods larger than one are also possible. Another possibility is the occurrence of partially synchronous and completely asynchronous states [20–22]. A kind of dynamics more complicated than these temporal patterns are spatio-temporal patterns [23] such as waves in the simplest case traveling along a one-dimensional chain of oscillators [24].

Temporal interaction delays and irregular network structures add conceptually new aspects to the dynamics of pulse-coupled oscillators. Since delays induce complicated dynamics even in systems with only one dynamical state variable [25], it is expected that delays present between the sending and reception of a pulse may have a particularly strong effect on the dynamics of a large network of oscillators. For instance, it becomes possible that some oscillators may be quiescent while others fire perpetually. This is known as delay induced oscillator death [26, 27]. Furthermore, the presence of delays can imply that a unique, global attractor towards which all initial states converge [14] is replaced by a multitude of attractors, such that the choice of initial state determines which attractor is

selected [17]. Whereas most previous studies on pulse-coupled oscillators have focussed on simple regular networks, studies on networks with a more complicated structure reveal new kinds of interesting dynamics. For instance, a state of balanced activity constitutes a novel phenomenon discovered recently in sparsely connected networks [28–30]. This balanced state displays apparently chaotic dynamics, in which single units fire irregularly.

From these considerations we may discern the frontier of current research on networks of pulse-coupled oscillators. Even these highly idealized model systems exhibit not only simple but also very complicated dynamics, due to the large number of units which collectively interact in a nonlinear fashion. On the other hand, since detailed insights become possible only through these idealizations, simple models open new perspectives for understanding the mechanisms underlying collective dynamical behavior.

In this thesis, we consider two main complications which arise when considering networks of pulse-coupled oscillators. These complications are motivated by biological networks of neurons: The first complication is the presence of interaction delays, the second the complexity of the network structure. Beyond standard physicists' tools, we adopt methods from nonlinear dynamics and random matrix theory and concepts from graph theory to reveal the fundamental mechanisms of their dynamics. In parts of this thesis we not only use methods adapted from other areas of science, but conversely, also present new mathematical phenomena which arise in the analysis of the particular system studied here and may well be useful elsewhere. The unstable attractors discussed in Chapter 4 and the multi-operator stability problem analyzed in Chapter 5 constitute promising candidates.

The thesis is organized as follows. The introduction is followed by Chapter 2 which provides the fundamentals used throughout. We provide graph theoretical foundations to describe the connectivity structure of a network and give an overview of the different concepts of stability and an attractor. In Chapter 3 we derive a class of models of pulse-coupled oscillators which was originally introduced by Mirollo and Strogatz and is studied throughout this thesis. Subsequently, the advantages of this class of models for analytical as well as numerical studies are discussed. In Chapter 4 we consider networks of oscillators with delayed, global pulse-coupling. We analyze a switching phenomenon which arises in the presence of arbitrary weak noise but not in the absence of noise. We show that the network considered naturally exhibits periodic orbits that are simultaneously attracting and unstable [31]. It constitutes the first example of a dynamical system with this property. We present strong evidence that those unstable attractors become prevalent in large networks for a wide range of parameters [32]. In Chapters 5 and 6 we consider networks exhibiting a complex structure. In Chapter 5 we present an exact stability analysis for synchronous states in networks with an arbitrary connectivity. Our treatment reveals that this is a multi-operator problem. We solve it analytically. Furthermore, we provide the first theoretical demonstration that the synchronous state displaying regular dynamics coexists with a balanced state exhibiting irregular dynamics [33] in random networks with strong interactions. The question arises whether the results obtained in Chapter 5 are

valid for a more general class of models that are obtained from the original by a structural perturbation of the dynamics. In Chapter 6 we analyze this question in detail identifying a subclass of simpler models: Within this subclass, all multiple operators are degenerate and we are thus confronted with a standard, one operator stability problem. For symmetric networks, the convergence towards the stable synchronous state is shown to be equivalent to the convergence towards the equilibrium of a diffusion process on the same network. Furthermore, we present numerical evidence that random matrix theory provides very useful estimates to the stability problem of synchronization. These estimates suggest that the stable synchronous state analyzed in Chapter 5 is robust against structural perturbations of the original model dynamics. Chapter 7 summarizes the results obtained in this thesis and gives a brief outlook to future research. The Appendix contains the details of two exact derivations.

Chapter 2

Fundamentals

This chapter provides the fundamentals that are used in the main part of the thesis. We first introduce some notions from graph theory relevant to the description of network structures. It follows a definition of stability of invariant sets of a dynamical system and an overview about fundamentally different concepts of an attractor.

2.1 Basic notions from graph theory

In this section we introduce basic graph theoretical concepts. We define a graph, its adjacency properties, connectivity and the relation between the connectivity of a graph and the irreducibility of a matrix. A concise introduction to graph theory is provided by the textbooks [34–37].

We focus on directed graphs. Most notions are readily adaptable to undirected graphs, so these are discussed only briefly. Undirected graphs are often simply called graphs in the literature, but we will use undirected graph and directed graph here and refer to a graph, if the respective concept applies to both kinds.

2.1.1 Graphs and adjacency

A directed graph, or digraph, is a pair $G = (V, E)$ where V is a finite set of vertices v and $E \subset V \times V$ is a set of edges (v, w) from v to w . In an undirected graph an edge is an un-ordered pair of vertices such that $E \subset [V]^2$. A graph is thus determined by its vertices $v \in V$, also called nodes or corners, and its edges $(v, w) \in E$, also called links or connections, as well as arcs for directed graphs. The vertices are usually labeled by the

natural numbers such that $V = \{1, \dots, N\}$ if the graph has N vertices, $|V| = N$. We assume that a graph has no loops, also called self-connections, $(v, v) \notin E$. A subgraph $S \subset G$ of a graph G is determined by a subset of vertices $V_S \subset V$ and a subset of edges $E_S \subset V_S \times V_S \cap E$. If for every edge (v, w) the graph also contains the edge (w, v) , it is an undirected graph and associated pairs of edges are identified. Otherwise the graph is directed and the edges (v, w) and (w, v) are considered to be distinct.

From now on we slightly depart from common terminology used in graph theory and also use terminology adopted from neuroscience. For a directed graph, the vertex v is presynaptic to w , denoted $v \in \text{Pre}(w)$ if $(v, w) \in E$. Similarly, the vertex v is postsynaptic to w , denoted $v \in \text{Post}(w)$ if $(w, v) \in E$. It is obvious that if v is presynaptic to w , then w is postsynaptic to v and vice versa. For an undirected graph, two vertices v and w are adjacent if there is an edge between them, $(v, w) \in E$. For directed and undirected graphs we define the adjacency matrix, also called connectivity matrix of a graph by

$$C_{vw} := \begin{cases} 1 & \text{if } (w, v) \in E \\ 0 & \text{otherwise} \end{cases} \quad (2.1)$$

such that it is symmetric, $C = C^T$, for undirected graphs, but in general asymmetric, $C \neq C^T$, for directed graphs.

For directed graphs, the number of outgoing edges of a vertex v , is called its out-degree

$$d_v^{\text{out}} := |\{(v, w) \in E \mid w \in V\}| = \sum_{w=1}^N C_{vw} \quad (2.2)$$

and the number of incoming edges its in-degree

$$k_v := d_v^{\text{in}} := |\{(w, v) \in E \mid w \in V\}| = \sum_{w=1}^N C_{wv}. \quad (2.3)$$

By definition, every vertex v of an undirected graph has the same in- and out-degree, then just called degree d_v of that vertex.

2.1.2 Paths, distance, connectivity, and irreducibility

A path $P = (V, E)$ of length L is a graph of the form

$$V = \{v_1, v_2, \dots, v_L\}, \quad E = \{(v_1, v_2), (v_2, v_3), \dots, (v_{L-1}, v_L)\} \quad (2.4)$$

where all vertices v_i are distinct. If such a path P from $v = v_1$ to $w = v_L$ exists as a subgraph of some graph G , P is said to connect $v \in G$ to $w \in G$. If no such path exists, w is called disconnected from v . The concept of a path as a subgraph is useful for both

directed and undirected graphs with directed edges replaced by undirected edges in the latter case.

The distance $d(v, w)$ from vertex v to w is the length L of the shortest path from $v = v_1$ to $w = v_L$ in (2.4). If v is disconnected from w , we set $d(v, w) := \infty$. For an undirected graph $d(v, w) = d(w, v)$. The greatest distance between any two vertices of a graph G is called the diameter of G . A directed graph is called **strongly connected** if there is a directed path from every vertex v to every other vertex w , i.e. $d(v, w) < \infty$ for all $v, w \in V$. Similarly, it is called weakly connected if $d(v, w) < \infty$ or $d(w, v) < \infty$ for all $v, w \in V$, i.e. there is a directed path or an inverted directed path connecting any v and w . An undirected graph is called connected if $d(v, w) < \infty$ for all $v, w \in V$.

The property of strong connectivity will be of importance to the dynamics considered in Chapter 5. In particular, we will use the fact that strong connectivity of a graph is equivalent to the statement that its adjacency matrix C is irreducible. Here a matrix A is called reducible if there is a permutation matrix P such that

$$B = P^{-1}AP = \begin{pmatrix} X & 0 \\ Y & Z \end{pmatrix} \quad (2.5)$$

has block-tridiagonal form where X and Z are square matrices. A is irreducible if it is not reducible.

2.2 Concepts of stability and attractors

The concepts of stability and attractors are important throughout this thesis. The different notions of attractors are of special interest in Chapter 4.

In this section we give a brief introduction to the concepts of stability and attractivity of invariant sets in dynamical systems described by continuous maps $f : X \rightarrow X$ where (X, d) is a complete metric space, e.g. $X = \mathbb{R}^N$ and $d(\mathbf{x}, \mathbf{y}) = \max_i |x_i - y_i|$ for $\mathbf{x}, \mathbf{y} \in X$.

Time-continuous dynamical systems, described by flows, are easily mapped onto time-discrete maps. For brevity of presentation, we only treat the case of maps here. We follow the presentation of Milnor [38, 39], Buescu [40], Ashwin and Terry [41], as well as standard text books on nonlinear dynamics [42–46].

2.2.1 Stability of invariant sets

Definition 2.2.1 (Forward Invariance). *A subset $A \subset X$ is said to be forward invariant if $f(A) \subset A$.*

If A is forward invariant, then $f^n(A) \subset A$ for all $n \geq 0$, i.e. all trajectories through points in A remain in A for all future times.

Definition 2.2.2 (Invariance). *A subset $A \subset X$ is said to be invariant if $f(A) = A$.*

Invariance is more stringent than forward invariance. If A is invariant, it is forward invariant and every point in A has a pre-image in A , i.e. $f^{-1}(A) \subset A$.

Definition 2.2.3 (Omega limit set). *The ω -limit set of a point $x \in X$ is the set*

$$\omega(x) = \bigcap_{N>0} \overline{\bigcup_{n>N} f^n(x)}$$

of accumulation points of the forward orbit of x .

We now formally define two criteria for local stability of an invariant set.

Definition 2.2.4 ((Lyapunov) stability). *A compact invariant set $A \subset X$ is said to be Lyapunov stable if, for every open neighborhood U of A , there exists an open neighborhood $V \subset U$ such that $f^n(V) \subset U$ for all $n > 0$.*

Intuitively, a compact invariant set A is Lyapunov stable if orbits through a point x sufficiently close to A remain close to A for all future times. A stronger version of the notion of stability is asymptotic stability.

Definition 2.2.5 (Asymptotic stability). *A compact invariant set $A \subset X$ is said to be asymptotically stable if it is Lyapunov stable and there is an open neighborhood W of A such that $\omega(x) \subset A$ for all $x \in W$.*

Asymptotic stability guarantees that all trajectories sufficiently close to A converge towards A in the long time limit.

Both plain (Lyapunov) and asymptotic stability are local properties. Under general conditions (cf. the Hartman-Grobman Theorem, [42]) these local stability properties may be proven by only considering the local, first order approximation of a given map. This guarantees Lyapunov stability or asymptotic stability of a fixed point or a periodic orbit, if they are linearly stable or linearly asymptotically stable, respectively. In the analyses presented in this thesis we use the terms stability and asymptotic stability instead of linear stability and linear asymptotic stability because we do not consider non-linear stability. For linear stability of a fixed point x^* of a map f , no eigenvalue λ of the local Jacobian $Df(x^*)$ may exceed one in absolute value, $|\lambda| \leq 1$. For linear asymptotic stability, all eigenvalues must be smaller than one in absolute value, $|\lambda| < 1$. Periodic orbits of time-continuous systems display the same stability properties as a return map from a section through state space to itself, that is transverse to the orbit. Another possibility to obtain a map from a time-continuous flow is to strobe the system periodically. Periodic orbits are thus conveniently studied by considering one of such maps. We will use this fact in Chapters 4 and 5.

2.2.2 Different concepts of an attractor

The concept of an attractor is important to describe the long-time behavior of trajectories through given initial conditions. Up to date, there is no common agreement about what the best definition of an attractor should be. In fact, it might be sensible to use different definitions depending on the problem at hand.

The set of initial conditions that converge towards an invariant set in the long-time limit is called the basin of attraction of this set.

Definition 2.2.6 (Basin of attraction). *Let A be a compact invariant set. The basin of attraction of A is defined by*

$$\mathcal{B}(A) := \{x \in X \mid \omega(x) \subset A\}.$$

We now first introduce a conventional definition of an attractor.

Definition 2.2.7 ((Conventional) attractor). *An attractor is a compact invariant set $A \subset X$ that has an open neighborhood $U \supset A$ such that $f^n(U) \subset U$ for all $n > 0$ and $\bigcap_{n>0} f^n(U) = A$.*

Thus, a conventional attractor A has an open neighborhood that shrinks towards A under the time evolution. Since the shrinking neighborhood is open, A has a basin of attraction of positive measure, $\mu(\mathcal{B}(A)) > 0$. Here and in the following, we denote the Lebesgue measure of a (Borel-) subset $S \subset X$ by $\mu(S)$. The existence of a shrinking neighborhood also implies that a conventional attractor A is asymptotically stable, because all sufficiently close trajectories ultimately converge towards A .

We now introduce three different definitions of an attractor that do not imply stability.

Definition 2.2.8 (Weak attractor). *A weak attractor is a compact invariant set $A \subset X$ that satisfies*

$$\mu(\mathcal{B}(A)) > 0.$$

The definition of a weak attractor thus only emphasizes its attractivity property, a positive measure (a volume) of state space must be attracted towards A . Following Milnor we define a Milnor attractor and a minimal Milnor attractor.

Definition 2.2.9 (Milnor attractor). *A weak attractor A is said to be a Milnor attractor if any proper compact invariant subset $A' \subsetneq A$ satisfies*

$$\mu(\mathcal{B}(A) \setminus \mathcal{B}(A')) > 0.$$

This condition on the measure guarantees that no proper compact invariant subset $A' \subset A$ demands the full volume of the basin of A . A Milnor attractor A is called minimal if no proper compact invariant subset demands any basin volume of A :

Definition 2.2.10 (Minimal Milnor attractor). *A Milnor attractor A is said to be a minimal Milnor attractor if any proper compact invariant subset $A' \subsetneq A$ satisfies*

$$\mu(\mathcal{B}(A')) = 0.$$

These definitions are successively more restrictive, formally,

$$\text{Weak attractor} \Leftarrow \text{Milnor attractor} \Leftarrow \text{minimal Milnor attractor}.$$

For instance, the collection $A = \{x, y\}$ of two asymptotically stable fixed points, constitutes a weak attractor and a Milnor attractor with basin $\mu(\mathcal{B}(A)) > 0$ but not a minimal Milnor attractor: Since the proper compact invariant subset $A' = \{y\}$ is an asymptotically stable fixed point, it individually has a basin of positive measure, $\mu(\mathcal{B}(A')) > 0$ such that A is not minimal. It is a Milnor attractor because the basin of $A \setminus A' = \{x\}$ also has positive measure, $\mu(\mathcal{B}(\{x\})) > 0$.

It is important to note that, in contrast to the conventional definition of an attractor, the latter three definitions of an attractor do not imply stability of the invariant set but emphasize a basin of attraction of positive state space volume. For example, the map

$$x_{n+1} = f(x_n) = ax_n \sin(\pi x_n) \tag{2.6}$$

on $[0, 1]$ exhibits a minimal Milnor attractor at $a = 1$, see Fig. 2.1. It has two fixed points $\bar{x}_1 = 0$ and $\bar{x}_2 = \frac{1}{2}$. The point \bar{x}_1 is a stable minimal Milnor attractor as well as a conventional attractor. The point \bar{x}_2 attracts all points from the right such that its basin is $\mathcal{B}(\bar{x}_2) = [\frac{1}{2}, x^*]$, where $x^* \approx 0.778$ is the non-trivial solution of $x^* \sin(\pi x^*) = \frac{1}{2}$. At the same time \bar{x}_2 repels trajectories starting arbitrarily close to the left of it. These, in turn, converge to \bar{x}_1 which has the basin $\mathcal{B}(\bar{x}_1) = [0, \frac{1}{2}) \cup (x^*, 1]$. Thus \bar{x}_2 is a minimal Milnor attractor, but not asymptotically stable. In particular, \bar{x}_2 is not a conventional attractor.

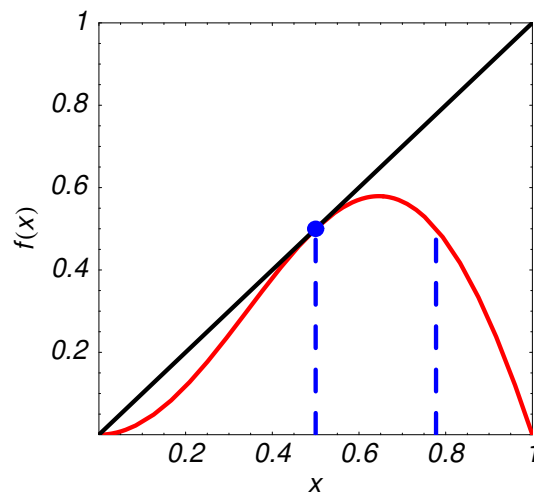


Figure 2.1: The map $f(x) = ax \sin(\pi x)$ (2.6) exhibits a minimal Milnor attractor at $a = 1$. There is one trivial stable attractive fixed point $\bar{x}_1 = 0$ for all parameters $a > 0$. At $a = 1$ (red function) an unstable attracting fixed point \bar{x}_2 exists that is a minimal Milnor attractor: Points in the interval $[0, \frac{1}{2})$ are repelled whereas points in some interval $[\frac{1}{2}, x^*]$ (between the dashed lines) are attracted.

Chapter 3

The Mirollo-Strogatz model

In this thesis, we consider a class of models of pulse-coupled oscillators that was introduced by Mirollo and Strogatz [14] and modified later to include interaction delays by Ernst, Pawelzik, and Geisel [17]. In these models, an individual oscillator is described by a phase variable, that encodes the time until its next firing event in the absence of interactions. A nonlinear function mediates the interactions such that a specific model is not explicitly defined by differential equations but by certain interaction rules that are specified by an interaction function. Due to this approach certain complications that arise from nonlinear differential equations are circumvented.

The first section of this chapter introduces the Mirollo-Strogatz model, starting from differential equation models of pulse-coupled oscillators. A number of related earlier results, are briefly reviewed. In the second section we elaborate and analyze several advantages of the model class considered. We show that a large class of well-known models, defined originally by differential equations, are captured by an associated Mirollo-Strogatz model. This is illustrated by a selection of important examples of differential equation models, for which we explicitly derive conditions for equivalence to the Mirollo-Strogatz model. Finally, we discuss the numerical advantages of the Mirollo-Strogatz formulation compared to differential equation models of pulse-coupled oscillators.

3.1 Mirollo-Strogatz model of pulse-coupled oscillators

In this section we introduce a class of pulse-coupled oscillators captured by the model by Mirollo and Strogatz. We start from systems of differential equations in which individual oscillators are modelled by one dynamical state variable. By a nonlinear transformation of variables, the explicit dependence of the pulse-coupling term on the state of the receiving oscillator can be removed. After a brief summary of investigations related to this model

class, we define the model introduced originally by Mirollo and Strogatz.

3.1.1 Pulse-coupled single variable threshold oscillators

In studies of synchronization phenomena in networks of pulse-coupled oscillators, single elements are often modelled as phase oscillators, assuming that the dynamics of the amplitude of the oscillation is less important because amplitude perturbations decay rapidly. In these models there is thus only one relevant dynamical variable, W_i , that describes the dynamics of an individual oscillator i . In models of many natural systems, the oscillator variable W_i represents an analog of a potential, like the membrane potential in the case of a externally driven nerve cells.

The dynamics of a network of pulse-coupled oscillators can be described by a system of coupled ordinary differential equations

$$\frac{dW_i}{dt} = A(W_i) + B(W_i)S_i(t) \quad (3.1)$$

for $i \in \{1, \dots, N\}$ where A and B are continuous functions and S_i represents the interactions within the network. The free dynamics is thus given by $dW_i/dt = A(W_i)$, taking $S_i(t) \equiv 0$ in Eq. (3.1). The pulse-like interactions between the oscillators are given by

$$S_i(t) = \sum_{j=1}^N \sum_{m=-\infty}^{\infty} \varepsilon_{ij} K_{ij}(t - t_{j,m}) \quad (3.2)$$

where ε_{ij} is the strength of the coupling from oscillator j to oscillator i and the response kernels $K_{ij}(t)$ have the property that $K_{ij}(t) \geq 0$, $K_{ij}(t) = 0$ for $t < 0$, and $\int_{-\infty}^{\infty} K_{ij}(t) dt = 1$. The sum includes all times $t_{j,m}$ at which oscillator j reaches a threshold $W_\theta := 1$ (from below) for the m^{th} time,

$$W_j(t_{j,m}) \geq W_\theta = 1, \quad \left. \frac{dW_j(t)}{dt} \right|_{t=t_{j,m}} > 0 \quad (3.3)$$

where dW_j/dt denotes the left derivative. If this threshold is reached, W_j is reset to a potential

$$W_j(t_{j,m}^+) := W_{\text{reset}} = 0 \quad (3.4)$$

and a signal is generated that is sent to oscillators i . Commonly, a unit that is reset and sends out a pulse when it reaches a threshold is said to “fire” at that instant of time. This form of pulse-coupling idealizes the fact that in diverse natural systems such as populations of flashing fireflies or networks of spiking neurons in the brain, units interact by stereotyped short-lasting signals that are generated as the state of a unit reaches a threshold. Note that the normalizations $W_\theta = 1$ and $W_{\text{reset}} = 0$ are made without loss

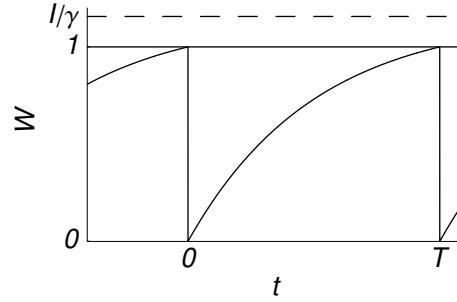


Figure 3.1: Dynamics of a non-interacting integrate-and-fire oscillator. Without threshold, the potential W would converge to its long-time limit I/γ (dashed line). Every time the threshold $W_\theta = 1$ is reached, the potential W is reset to $W_{\text{reset}} = 0$ and a pulse is sent.

of generality. Whereas Eqs. (3.1)–(3.4) describe the interaction dynamics without explicit delays between sending and reception of a pulse, a delay $\tau > 0$ can easily be included by a transformation $K_{ij}(t) \rightarrow K_{ij}(t - \tau)$ of the response kernels. If the duration of the response of a unit i to an incoming pulse is sufficiently brief, the kernels K_{ij} in (3.2) may be idealized by the Dirac distribution

$$K_{ij}(t) = \delta(t) \quad (3.5)$$

such that the coupling becomes discontinuous, i.e. the state variable of the receiving unit jumps.

For the commonly used leaky integrate-and-fire models [12] of oscillators the dynamics is given by the linear inhomogeneous differential equation

$$\frac{dW}{dt} = -\gamma W + I + S(t) \quad (3.6)$$

where $A(W) = -\gamma W + I$, I is an external current, $\gamma > 0$ measures the dissipation in the system, and $B(W) = 1$ is independent of the dynamical variable W . This linear differential equation has the advantages that the solution is known explicitly and the response to an additional current can be found by superposition arguments. For sufficiently large external current, $I > \gamma$, the free ($S(t) \equiv 0$) dynamics

$$W(t) = I/\gamma (1 - e^{-\gamma t}) \quad \text{for } 0 < t \leq T \quad \text{and} \quad W(t+T) = W(t) \quad (3.7)$$

is periodic (Fig. 3.1) with period $T = \frac{1}{\gamma} \ln \left(1 - \frac{\gamma}{I}\right)^{-1}$.

3.1.2 Nonlinear transformation of variables

In the analysis of a pulse-coupled systems given by Eq. (3.1), two principal complications may arise. First, the differential equation may not be linear such that superposition arguments fail. Second, the pre-factor $B(W)$ of the coupling term may not be constant as

it is for the integrate-and-fire model (3.6). The first point may be circumvented by using the limit of infinitely fast responses (3.5). For the treatment of the second complication, it is often convenient and under weak conditions possible [20] to transform the variables W_i according to

$$V_i(t) := \frac{1}{C} \int_0^{W_i(t)} B(w)^{-1} dw \quad (3.8)$$

where

$$C = \int_0^1 B(w)^{-1} dw \quad (3.9)$$

such that (3.1) becomes

$$\frac{dV_i}{dt} = \hat{A}(V_i) + \frac{1}{C} S_i(t) \quad (3.10)$$

for $i \in \{1, \dots, N\}$ where

$$\hat{A}(V) = C^{-1} A(W(V)) / B(W(V)) \quad (3.11)$$

and $W(V)$ is determined by solving Eq. (3.8) for W . Specific examples for transformations of variables will be given in Subsection 3.2.1.

3.1.3 A brief history of investigations

To study the synchronization of pacemaker cells in the heart, Peskin considered a simple, globally coupled network of such leaky integrate-and-fire oscillators [11] where the coupling is not delayed, $\tau = 0$, and the responses are infinitely fast, $K_{ij}(t) = \delta(t)$, excitatory, and homogeneous, $\varepsilon_{ij} = \varepsilon > 0$. In his 1975 book he conjectured that arbitrary initial conditions converge towards the fully synchronous state in which all oscillators fire simultaneously. He gave a proof for $N = 2$ oscillators assuming that both coupling strength and dissipation are small, $\varepsilon \ll 1$, $\gamma \ll 1$.

In a seminal work of 1990, Mirollo and Strogatz generalized the approach of Peskin [11]. Contrary to Peskin, whose analysis was based on the linearity of the differential equations, Mirollo and Strogatz's only assumptions were that the free ($S_i(t) \equiv 0$) dynamics can be described by a phase-like variable and that the interactions are mediated by some potential function U that is a monotonically increasing and concave down function of this phase [14] (for model details see below). This framework includes many cases for which the associated differential equation is nonlinear such that its solution may not be known explicitly and superposition arguments fail. Within this general framework, they proved that, for all N , almost all initial conditions will ultimately end up in the fully synchronous state. For systems without dissipation ($\gamma = 0$ in Eq. (3.6)), equivalent to linear functions U , Senn and Urbanczik [16] proved that the dynamics becomes fully synchronous even if the intrinsic

frequencies and the thresholds of the oscillators are not quite identical. Like the previous investigators, they treated the case without delay, $\tau = 0$, for which the fully synchronous state is the only attractor. This periodic orbit is an example of period-one dynamics, for which every oscillator fires exactly once during one period.

Within the framework introduced by Mirollo and Strogatz, it was, moreover, shown that the introduction of a delay time $\tau > 0$, that occurs ubiquitously in natural systems, changes this situation drastically [17, 18]: With increasing network size, an exponentially increasing number of attractors coexist. In a large region of parameter space, these are typically periodic orbits with period-one dynamics, that exhibit several groups of synchronized oscillators (clusters), which reach threshold and send pulses alternately. It was also shown [17, 18] that these kinds of attractors arise not only in excitatorily coupled networks ($\varepsilon > 0$) but also if the oscillators are coupled inhibitorily ($\varepsilon < 0$).

3.1.4 Phase model by Mirollo and Strogatz

To define the Mirollo-Strogatz model, we consider networks of N pulse-coupled oscillators with delayed interactions. A phase-like variable $\phi_j(t) \in (-\infty, 1]$ specifies the state of each oscillator j at time t such that the difference between the phases of two oscillators quantifies their degree of synchrony, with identical phases for completely synchronous oscillators. The free dynamics of oscillator j is given by

$$\frac{d\phi_j}{dt} = 1. \quad (3.12)$$

Whenever oscillator j reaches a threshold

$$\phi_j(t) = 1 \quad (3.13)$$

the phase is reset to zero

$$\phi_j(t^+) = 0 \quad (3.14)$$

and a pulse is sent to all other postsynaptic oscillators $i \in \text{Post}(j)$. These oscillators i receive this signal after a delay time τ . The interactions are mediated by a function $U(\phi)$ specifying a 'potential' of an oscillator at phase ϕ . The function U is twice continuously differentiable, monotonically increasing,

$$U' > 0, \quad (3.15)$$

concave (down),

$$U'' < 0, \quad (3.16)$$

and normalized such that

$$U(0) = 0 \quad \text{and} \quad U(1) = 1. \quad (3.17)$$

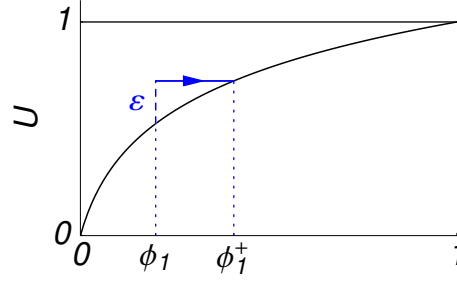


Figure 3.2: An incoming pulse of strength ε induces a phase jump $\phi_1^+ := \phi_1(t^+) = U^{-1}(U(\phi_1(t)) + \varepsilon) = H_\varepsilon(\phi_1)$ that depends on the state $\phi_1 := \phi_1(t)$ of the oscillator at time t of pulse reception. Due to the curvature of U , an excitatory pulse ($\varepsilon > 0$) induces an advancing phase jump. If the incoming pulse puts the potential above threshold ($U(\phi_1) + \varepsilon > 1$), the phase is reset to zero ($\phi_1^+ = 0$). An inhibitory pulse ($\varepsilon < 0$) would induce a regressing phase jump such that the phase may assume negative values (not shown).

For a general $U(\phi)$ we define the transfer function

$$H_\varepsilon(\phi) = U^{-1}(U(\phi) + \varepsilon) \quad (3.18)$$

that represents the response of an oscillator at phase ϕ to an incoming subthreshold pulse of strength ε . Depending on whether the input ε_{ij} received by oscillator i from j is subthreshold,

$$U(\phi) + \varepsilon_{ij} < 1, \quad (3.19)$$

or suprathreshold,

$$U(\phi) + \varepsilon_{ij} \geq 1, \quad (3.20)$$

the pulse sent at time t (Eq. (3.13)) induces a phase jump after a delay time τ at time $t + \tau$ according to

$$\phi_i((t + \tau)^+) = \begin{cases} H_{\varepsilon_{ij}}(\phi_i(t + \tau)) & \text{if } U(\phi_i(t + \tau)) + \varepsilon_{ij} < 1 \\ 0 & \text{if } U(\phi_i(t + \tau)) + \varepsilon_{ij} \geq 1 \end{cases}. \quad (3.21)$$

This phase jump (Fig. 3.2) depends on the phase $\phi_i(t + \tau)$ of the receiving oscillator i at time $t + \tau$ after the signal by oscillator j has been sent at time t , the effective coupling strength ε_{ij} , and the nonlinear potential U . The interaction from unit j to unit i is either excitatory ($\varepsilon_{ij} > 0$) inducing advancing phase jumps (cf. Fig. 3.2) or inhibitory ($\varepsilon_{ij} < 0$) inducing retarding phase jumps. If there is no interaction from j to i , we have $\varepsilon_{ij} = 0$ and . There are two immediate differences between inhibitory and excitatory inputs. First, while inhibitory input $\varepsilon_{ij} < 0$ is always subthreshold, excitatory input $\varepsilon_{ij} > 0$ may also be suprathreshold and thus induce an instantaneous reset to zero according to Eq. (3.21). Second, in response to the reception of an inhibitory pulse, the phases of the oscillators may assume negative values whereas for excitatory coupling they are confined to the interval $[0, 1]$.

The general class of functions U captures the dynamics of a variety of systems. In particular, given any differential equation of the form (3.10) the free ($S_i(t) \equiv 0$) dynamics of which has a monotonic periodic solution $V(t)$ with period T and negative curvature, the function U can be taken as the scaled solution,

$$U(\phi) := V(\phi T). \quad (3.22)$$

By the transformations (3.8) and (3.22), the general class of pulse-coupled oscillators (Eqs. (3.1)–(3.4)) with infinitely brief response (3.5) is mapped onto a normalized phase description (Eqs. (3.12)–(3.21)).

3.2 Advantages of the Mirollo-Strogatz model

The class of models introduced in the previous section has a number of advantages. It captures a large class of models which in their original form appear as nonlinear differential equations that lack a simple solution and cannot be treated using linear superposition arguments. Within the framework of the Mirollo-Strogatz model, in which responses are considered infinitely fast (cf. Eqs. (3.5) and (3.2)) and the state of each oscillator is represented by a phase variable, it becomes possible to treat problems analytically that could not be solved before. This constitutes the basis for nearly all analytical calculations performed in this thesis. Furthermore, the model formulation provides advantages for numerical simulations. We discuss both aspects in the following.

3.2.1 Equivalence to other models

The nonlinear transformation of variables (Subsection 3.1.2), and the rescaling of the time axis (Eq. (3.22)) leads to the question whether the original models are equivalent to the Mirollo-Strogatz model in the sense that resulting dynamical equations lead to monotonic and concave down interaction functions. Here we derive conditions under which several specific single-variable models from the general class described above (Eqs. (3.1)–(3.4)) is equivalent to the Mirollo-Strogatz model. In particular, we consider cases where single units represent neurons or similar threshold units. Reasonable assumptions about $A(W)$ and $B(W)$ below threshold, $W < 1$, are

1. $A(W) \geq 0$. Here we assume a sufficiently large, namely suprathreshold external input that drives the state of the oscillator towards threshold. The assumption leads to a monotonically increasing potential $W(t)$ in the absence of interactions within the network ($S_i(t) \equiv 0$).
2. $A'(W) \leq 0$. Here we assume that the increase is slower for larger potentials.

3. $B(W) = g(W_s - W)$. This is motivated by the fact that a cell's potential typically changes by ion flux through trans-membrane channels of given conductance $g \in \mathbb{R}^+$. Here W_s is the synaptic reversal potential and the conductance g is assumed to be voltage independent.

The third assumption implies

$$B'(W) = -g < 0. \quad (3.23)$$

For inhibitory coupling the synaptic reversal potential W_s is negative, $W_s < 0$, such that

$$B(W) < 0 \quad (3.24)$$

for all $W > W_s$. For excitatory coupling, it is positive, typically $W_s > 1$, such that

$$B(W) > 0 \quad (3.25)$$

for all $W \in [0, 1]$.

Some results, e.g. the proof of stability of the synchronous state in Chapter 5, require only that the potential function U is monotonic and concave down on a certain interval. Under such circumstances, the equivalence discussed here, might not be necessary to produce results valid for a certain kind of dynamics, e.g. synchronous, of the original model.

We now derive general conditions under which the potential rise function $U(\phi)$ in the Mirollo-Strogatz model is monotonically increasing and has negative curvature in the phase interval of interest.

From (3.10) with zero synaptic current $S(t) \equiv 0$ we obtain that

$$\dot{V} = \frac{1}{C} \frac{A(W(V))}{B(W(V))}. \quad (3.26)$$

The condition for monotonicity of $V(t)$ and hence the rescaled function $U(\phi) = V(\phi T)$,

$$\dot{V} > 0, \quad (3.27)$$

thus holds if B does not change sign, $B(W) \neq 0$, in the relevant interval because $A > 0$ and C has the same sign as $B(W)$, i.e. $CB(W) > 0$, cf. Eq. (3.9). For both the inhibitory and excitatory case considered above, V and U are thus monotonically increasing.

Furthermore we have

$$\ddot{V} = \frac{A'B - B'A}{CB^2} \dot{W} = \frac{A'B - B'A}{CB^2} A(W(V)) \quad (3.28)$$

if $S(t) \equiv 0$. The condition for concavity,

$$\ddot{V} < 0, \quad (3.29)$$

is satisfied in particular if $A'B > 0$, $B'A < 0$, and $C < 0$. In the following, we will consider several examples of differential equations of the form (3.1) or (3.10) and check whether the condition (3.29) is met.

As a standard model consider the **leaky integrate-and-fire oscillator** [12] defined by the linear differential equation (3.6)

$$\frac{dW_i}{dt} = I - \gamma W_i + S_i(t) \quad (3.30)$$

together with a threshold at $W_i = 1$ and reset to $W_i = 0$, where $I > 1$ is a suprathreshold external current and

$$S_i(t) = \sum_{j=1}^N \sum_{m=-\infty}^{\infty} \varepsilon_{ij} \delta(t - \tau - t_{j,m}) \quad (3.31)$$

is the pulse-coupling between the oscillators (cf. (3.1)). Because the pre-factor of the pulse-coupling term is constant, $B(W) = 1$, the transformation of variables (3.8) is the identity such that $V_i(t) = W_i(t)$. The interaction-free ($S_i(t) \equiv 0$) solution (3.7) through the initial condition $V_i(0) = 0$ leads to the rescaled version

$$U_{\text{IF}}(\phi) = V_i(\phi T_{\text{IF}}) = \frac{I}{\gamma} (1 - e^{-T_{\text{IF}} \phi}) \quad (3.32)$$

where $T_{\text{IF}} = \frac{1}{\gamma} \ln(1 - \frac{\gamma}{I})^{-1} > 0$ is the period of a non-interacting oscillator.

This leads to derivatives of alternating sign,

$$U'_{\text{IF}}(\phi) = \frac{I}{\gamma} T_{\text{IF}} e^{-\phi T_{\text{IF}}} > 0, \quad U''_{\text{IF}}(\phi) = -\frac{I}{\gamma} T_{\text{IF}}^2 e^{-\phi T_{\text{IF}}} < 0, \dots \quad (3.33)$$

such that the resulting potential function is monotonically increasing and concave down for all I , and all $\gamma > 0$ and for all $\phi \in \mathbb{R}$.

Oscillators described by nonlinear differential equations are also captured by the Mirollo-Strogatz approach. For instance, the standard **conductance based threshold model** of a neuron [12] is defined by

$$\dot{W}_i = \gamma(W_{\text{eq}} - W_i) + g(W_s - W_i)S_i(t) \quad (3.34)$$

where $W_{\text{eq}} > 1$ is the equilibrium potential in the absence of an external current, W_s is the synaptic reversal potential of the neuron, $\gamma > 0$ is the synaptic time constant and $g > 0$ the synaptic conductivity. According to Eq. (3.1), we identify

$$A(W) = \gamma(W_{\text{eq}} - W), \quad B(W) = g(W_s - W). \quad (3.35)$$

First we transform the state variable following subsection 3.1.2. Via this transformation (see Eq. (3.8))

$$V_i(t) := \frac{\ln(1 - W_i(t)/W_s)^{-1}}{gC} \quad (3.36)$$

where

$$C = \frac{\ln(1 - W_s^{-1})^{-1}}{g} \quad (3.37)$$

we obtain the inverse

$$W(V) = W_s (1 - e^{-gCV}). \quad (3.38)$$

Equation (3.10) in the absence of internal interactions ($S_i(t) \equiv 0$) may be solved explicitly via separation of variables

$$t = \int_0^V \frac{CB(W(v))}{A(W(v))} dv \quad (3.39)$$

$$= \int_0^V \frac{Cg}{\gamma \left[1 + \left(\frac{W_{\text{eq}}}{W_s} - 1 \right) e^{Cgv} \right]} dv \quad (3.40)$$

$$= \frac{1}{\gamma} \left[CgV - \ln \left(\frac{W_s}{W_{\text{eq}}} + \left(1 - \frac{W_s}{W_{\text{eq}}} \right) e^{CgV} \right) \right] \quad (3.41)$$

such that inversion leads to

$$V(t) = \frac{1}{Cg} \ln \left(1 + \frac{W_{\text{eq}}}{W_s} (e^{-\gamma t} - 1) \right). \quad (3.42)$$

After determining the time to firing, i.e. the period T_{CB} , from the threshold condition $V(T_{\text{CB}}) = 1$, we obtain a potential function

$$U_{\text{CB}}(\phi) = V_i(\phi T_{\text{CB}}) = \frac{\ln \left(1 + \frac{W_{\text{eq}}}{W_s} \left[(1 - W_{\text{eq}}^{-1})^\phi - 1 \right] \right)}{\ln(1 - W_s^{-1})} \quad (3.43)$$

after substituting the constant C (3.37). Monotonicity and curvature of this function may be determined from the conditions (3.26)–(3.29). For inhibitory coupling, where $W_s < 0$, we have $B(W) = g(W_s - W) < 0$ for all $W > W_s$ such that $C < 0$. (For $W < W_s$ the transformation of variables is undefined such the Mirollo-Strogatz approach is not applicable in this case.) For excitatory coupling, where $W_s > 1$, we have $B(W) > 0$ for all W such that $C > 0$. Since $A(W) = \gamma(W_{\text{eq}} - W) > 0$ the resulting potential function U is always monotonically increasing for both kinds of coupling. For inhibitory coupling, the concavity condition (3.28) together with (3.29) is satisfied for all $W > W_s$. For excitatory coupling, since $B(W) > 0$ and hence $C > 0$, the condition for concavity is equivalent to

$$A'B > B'A \Leftrightarrow \quad (3.44)$$

$$-\gamma g(W_s - W) > -g\gamma(W_{\text{eq}} - W) \Leftrightarrow \quad (3.45)$$

$$W_s < W_{\text{eq}} \quad (3.46)$$

which is satisfied for all $W \in [0, 1]$ if the equilibrium potential W_{eq} is sufficiently large.

Another example given by a nonlinear differential equation is the θ -**neuron** that represents a generic model of an excitable unit [47]. In the potential representation it is described by

$$\dot{W}_i = a(W_i - W_0)^2 + I + g(W_s - W_i)S_i(t) \quad (3.47)$$

where $W_0 < 1$ is the potential above which $W_i(t)$ accelerates towards firing, $I \geq 0$ is an external current, $a > 0$ determines the time scale, and g and W_s are conductivity and synaptic reversal potential as for the standard conductance based threshold model described above.

Following the derivation exemplified for the conductance based threshold model, we obtain

$$U_\theta(\phi) = \frac{\ln(\alpha + \beta f(\phi))}{\ln(1 - W_s^{-1})^{-1}} \quad (3.48)$$

where

$$f(\phi) = \tan(\gamma(1 - \phi) + \delta\phi) \quad (3.49)$$

and

$$\alpha = \frac{aW_s(W_s - W_0)}{J + a(W_0 - W_s)^2} \quad (3.50)$$

$$\beta = \frac{(aJ)^{\frac{1}{2}}W_s}{J + a(W_0 - W_s)^2} \quad (3.51)$$

$$\gamma = \arctan \left[\frac{J + aW_0(W_0 - W_s)}{(aJ)^{\frac{1}{2}}W_s} \right] \quad (3.52)$$

$$\delta = \arctan \left[\frac{J - a(1 - W_0)(W_0 - W_s)}{(aJ)^{\frac{1}{2}}(W_s - 1)} \right]. \quad (3.53)$$

From Eq. (3.47) we see that $A(W) = a(W - W_0)^2 + I > 0$ and $A'(W) = -2a(W_0 - W) < 0$ if $W < W_0$. The latter inequality is satisfied for almost all relevant W if W_0 is sufficiently large, $W_0 \approx 1$. In addition $B(W) = g(W_s - W)$ such that $B'(W) = -g < 0$. Thus the conditions sufficient for monotonicity (3.27) of U is satisfied for inhibitory and excitatory coupling. The conditions sufficient for concavity (3.29) are satisfied for inhibitory coupling for sufficiently large W_0 . Viewed as a condition on ϕ , this means that the potential function U will be concave down if $U(\phi) = V(W(\phi T)) < V(W_0)$, i.e. for those phases that are not too large, $\phi < U^{-1}(V(W_0))$. Here $V(W(t))$ is determined by applying the transformation (3.8). For excitatory coupling, U is also concave (down) if the condition

$$A'(W)B(W) < B'(W)A(W) \Leftrightarrow \quad (3.54)$$

$$-2a(W_0 - W)(W_s - W) < -(a(W - W_0)^2 + I) \Leftrightarrow \quad (3.55)$$

$$(W_s - W)^2 - (W_s - W_0)^2 > I/a \quad (3.56)$$

is satisfied. Since $I/a > 0$, it is thus necessary for concavity of U that $|W_s - W| > |W_s - W_0|$. As for inhibitory coupling, if we assume a large $W_0 \approx 1$, this inequality holds for sufficiently small values of W , i.e. for sufficiently small phases ϕ . Under this assumption, a sufficient condition for concavity of U is that the scaled current I/a is small enough.

The fourth example,

$$U_b(\phi) = \frac{1}{b} \ln(1 + (e^b - 1)\phi), \quad (3.57)$$

was introduced by **Mirollo and Strogatz** [14]. This function is monotonically increasing and, for $b > 0$, also concave (down). Independent of b , it has several advantages when performing numerical simulations as well as analytical calculations because the transfer function

$$H_\varepsilon(\phi) = \alpha\phi + \beta \quad (3.58)$$

is affine with ϕ -independent constants $\alpha = e^{b\varepsilon}$ and $\beta = \frac{e^{b\varepsilon} - 1}{e^b - 1}$.

The above collection of models exemplifies, that the Mirollo-Strogatz model captures a very general class of systems of pulse-coupled oscillators, including the cases of the standard conductance based threshold model and the θ -neuron that do not neglect conductance effects present in biological threshold units such as neurons [13].

Important advantages of the formulation of the Mirollo-Strogatz model are now visible: Given its equivalence to several important models and the idealizations of jump-like interactions, it allows analytical calculations for a variety of problems. Moreover, additional advantages for analytical calculations are present that may be inferred from the following discussion of numerical properties of the model.

3.2.2 Numerical advantages

Compared to systems of nonlinear differential equations, the Mirollo-Strogatz approach has the additional advantage, that numerical calculations can be performed exactly on an event-by-event basis. Given the state of the system at time t , defined by a phase vector $\phi(t)$ and a list of signals sent together with their sending times, the dynamics can be computed numerically by iterating between two kinds of events (in an appropriate order):

1. If the next event is the reception of a signal after a time Δt_1 , shift all phases $\phi_i(t)$ by this amount and apply the maps $H_{\varepsilon_{ij}}$ if oscillator j has sent this signal, according to Eq. (3.21). If the received signal is subthreshold for oscillator $i \in \text{Post}(j)$, its resulting phase is given by

$$\phi_i(t + \Delta t_1) = H_{\varepsilon_{ij}}(\phi_i(t) + \Delta t_1), \quad (3.59)$$

if the signal is suprathreshold for oscillator $i' \in \text{Post}(j)$, $U(\phi_{i'}(t) + \Delta t_1) + \varepsilon_{i'j} \geq 1$, its phase is reset to zero,

$$\phi_{i'}(t + \Delta t_1) = 0.0, \quad (3.60)$$

and a signal is generated, i.e. its sending time $t + \Delta t_1$ and the set of sending oscillators j' is stored. If several signals have been simultaneously sent by synchronized oscillators their simultaneous arrival can simply be numerically realized by enlarging the coupling strength to $\sum_{j \in \text{Pre}'(i)} \varepsilon_{ij}$, where $\text{Pre}'(i)$ is the subset of presynaptic oscillators to i which have fired simultaneously at time t .

2. If the next event is that one or more oscillators reach threshold after the time $\Delta t_2 = 1 - \max_i \phi_i(t)$ (without receiving an additional input signal after a time $\Delta t_1 < \Delta t_2$), those oscillators j are reset to zero,

$$\phi_j(t + \Delta t_2) = 0.0, \quad (3.61)$$

and a signal is generated (see event 1.). The phases of all other oscillators j' are just translated in time according to

$$\phi_{j'}(t + \Delta t_2) = \phi_{j'}(t) + \Delta t_2. \quad (3.62)$$

Besides the uniform increase of all phases, these are the only two possible events that change the state of the system, such that the simulation time is increased by Δt_1 or Δt_2 , depending on the kind of event: To determine the state at the next time step Δt_{MS} after time t numerically, one first finds the minimum of the time Δt_1 after which the next signal would arrive and the time Δt_2 after which the next phase would cross threshold without an additional incoming signal (cf. Eq. (3.21)). Thus, time steps smaller than $\Delta t_{\text{MS}} = \min\{\Delta t_1, \Delta t_2\}$ do not need to be considered. Note that Δt_{MS} depends on the state of the system such that it changes with time t .

This event-based numerics can be exploited for every choice of $U(\phi)$, and is not restricted to $U_{\text{IF}}(\phi)$ derived from the linear differential equation (3.6), for which one may as well exactly numerically integrate the original differential equation due to linear superposition (cf. [48, 49]).

Hence, in contrast to standard numerical integration of nonlinear differential equations, for which the time steps Δt_{DE} have to be taken sufficiently small and the numerics is only approximate, the above numerical algorithm for the Mirollo-Strogatz model is exact. In addition, it is fast, if oscillators constitute synchronized groups, that create a grouping of events such as the simultaneous firing of several oscillators. Under these circumstance, typical time steps are long, $\Delta t_{\text{MS}} \gg \Delta t_{\text{DE}}$.

Chapter 4

Unstable attracting periodic orbits

In this chapter we present and analyze the first example of a dynamical system that naturally exhibits periodic orbits that are simultaneously *attracting* and *unstable*. These unstable attractors occur in networks of globally, homogeneously pulse-coupled oscillators with delayed interactions.

After a brief introduction to the subject, our investigations start from a numerical observation of a collective switching phenomenon: from random initial conditions, groups of synchronized oscillators (clusters) are formed which fire alternately, resulting in a periodic network dynamics. Under the influence of arbitrarily weak noise, this synchronization is followed by a desynchronization of clusters. Perpetual synchronization and desynchronization lead to a switching among attractors. Thus trajectories successively approach and retreat from periodic orbits in the presence of noise. Supported by further systematic numerical investigations, this leads to the hypothesis that the observed dynamics is induced by unstable attracting periodic orbits. To investigate this collective phenomenon, we identify an analytically tractable network exhibiting unstable attractors and perpetual switching in the presence of noise. For this network we perform an exact stability analysis of a specially selected set of periodic orbits. It is followed by an analysis of the dynamics during a switching transition between two states and a numerical investigation of the structure of the basins of attractions in state space. This demonstrates the existence of unstable attractors. They are enclosed by basins of attraction of other attractors and are thus separated from the volume of their own basins. This geometrical fact explains why arbitrarily small noise leads to a switching among attractors. We show strong indications that such unstable attractors prevail in large networks for a wide range of parameters. We discuss which structural modifications of the dynamics of the system conserve the phenomenon of unstable attractors and which are likely to conserve their dynamical consequences, in particular switching in the presence of noise. The chapter closes with a brief summary and outlook.

4.1 Unstable attractors?

Attractors determine the long-term behavior of dissipative dynamical systems. Thus, the concept of attractors is central to the analysis of many natural systems as well as to the design of artificial systems. For instance, the computational capabilities of various neural networks are controlled by their collective dynamics. In models of associative memory function, such as the Hopfield model [50–52], memory patterns are stored and retrieved as the attractors of the collective dynamics of a neural network. Here, starting from a given stimulus pattern – a specific initial condition in the basin of attraction of some attractor – the system converges towards this attractor that represents the stored pattern. Networks of spiking neurons [12] constitute an important example of pulse-coupled systems, in which attractors may be computationally useful. Consequently, the nature and design of attractors in such systems constitute a focus of current research interest [12, 14–24, 28–30, 47, 53–66].

In general, the state space of a nonlinear dynamical system is partitioned into various basins of attraction from which states evolve towards the respective attractors. Since states slightly perturbed from an attractor often stay confined to its vicinity and eventually return to the attractor, attractors are commonly considered to be *stable* [42–45, 67]. In fact, in the conventional definition an attractor is necessarily stable (see also Chapter 2, Def. 2.2.7).

In this chapter, we refer to an attractor as a minimal Milnor attractor (see Chapter 2, Def. 2.2.10), because it will turn out that periodic orbits exist that have a positive basin volume but are simultaneously unstable. Since this definition of an attractor does not presume nor imply stability, these periodic orbits are appropriately described as (minimal) Milnor attractors. In some other systems such Milnor attractors might not be uncommon if these systems exhibit *strange* invariant sets with a fractal geometry such as chaotic attractors [68–70], or strange, non-chaotic attractors [71].

More generally, however, attractors that are not stable seem to be special cases which have to be constructed artificially by precisely tuning parameters. In fact, they may be easily constructed even in one-dimensional maps by appropriately tuning parameters to a point of a tangent bifurcation. Consider, for example, the map

$$x_{n+1} = f(x_n) = ax_n \sin(\pi x_n) \quad (4.1)$$

that was introduced in Chapter 2, Eq. (2.6). For $a = a_c := 1$ this map exhibits a minimal Milnor attractor $A = \{\bar{x}_2\}$ where $\bar{x}_2 = \frac{1}{2}$ (cf. Fig. 4.1). This attractor is unstable. It attracts points from the right, i.e. from its basin of attraction $\mathcal{B}(A) = [\bar{x}_2, x^*]$ where $x^* \approx 0.778$ (see Chapter 2) but is not stable since points to the left, $x < \bar{x}_2$, diverge from it. Precisely at the parameter $a = a_c$ the map undergoes a tangent bifurcation: If a is increased to $a > a_c$ (lower gray curve) instead of an unstable minimal Milnor attractor, it exhibits one asymptotically stable (and hence attractive) fixed point and one unstable, non-attractive fixed point. For $a < a_c$ (lower gray curve) the fixed point \bar{x}_2 disappears,

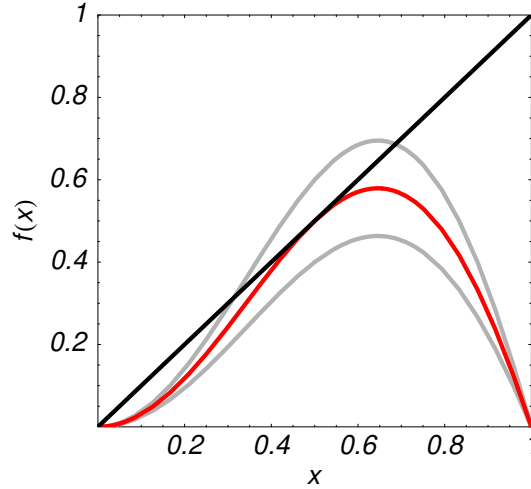


Figure 4.1: The map $f(x) = ax \sin(\pi x)$ (Eq. 4.1) at different values of the parameter a . For $a = a_c = 1$ (red curve) it exhibits a minimal Milnor attractor $A = \{\bar{x}_2\}$, $\bar{x}_2 = \frac{1}{2}$, which is attractive but unstable. It attracts point from the right from its basin of attraction $\mathcal{B}(A) = [\bar{x}_2, x^*]$ where $x^* \approx 0.778$ (see Chapter 2) but is not stable since points to the left, $x < \bar{x}_2$, diverge from it. At the parameter $a = a_c$ the map undergoes a tangent bifurcation: For $a > a_c$ (lower gray curve) instead of an unstable minimal Milnor attractor, it exhibits one asymptotically stable (and hence attractive) fixed point and one unstable, non-attractive fixed point. These two points have annihilated for $a < a_c$ (lower gray curve), such that there is no fixed point at all near $x = \frac{1}{2}$.

such that there is no fixed point near $x = \frac{1}{2}$. In summary, we obtained a minimal Milnor attractor which is unstable only at $a = a_c$. In general, such attracting and unstable fixed points may be obtained by tuning a parameter precisely to its bifurcation value. This is why attractors are commonly considered to be stable, except for very special cases.

Contrary to this intuition, we report here that unstable attractors are typical in large networks of pulse-coupled oscillators. They arise as a collective phenomenon, which is absent if the network is too small, but persist in large networks even if the physical parameters of the model, the coupling strength between oscillators and the time delay of the pulsed interactions, are varied substantially.

4.2 Perpetual synchronization and desynchronization

To specify the model, we specialize from the general presentation of Chapter 3. We consider a network of N globally and homogeneously coupled Mirolo-Strogatz oscillators (Sec. 3.1.4) with interactions that are delayed by a time $\tau > 0$. The coupling strengths obey

$$\varepsilon_{ij} = \begin{cases} \frac{\varepsilon}{N-1} =: \hat{\varepsilon} & \text{for } i \neq j \\ 0 & \text{for } i = j \end{cases} \quad (4.2)$$

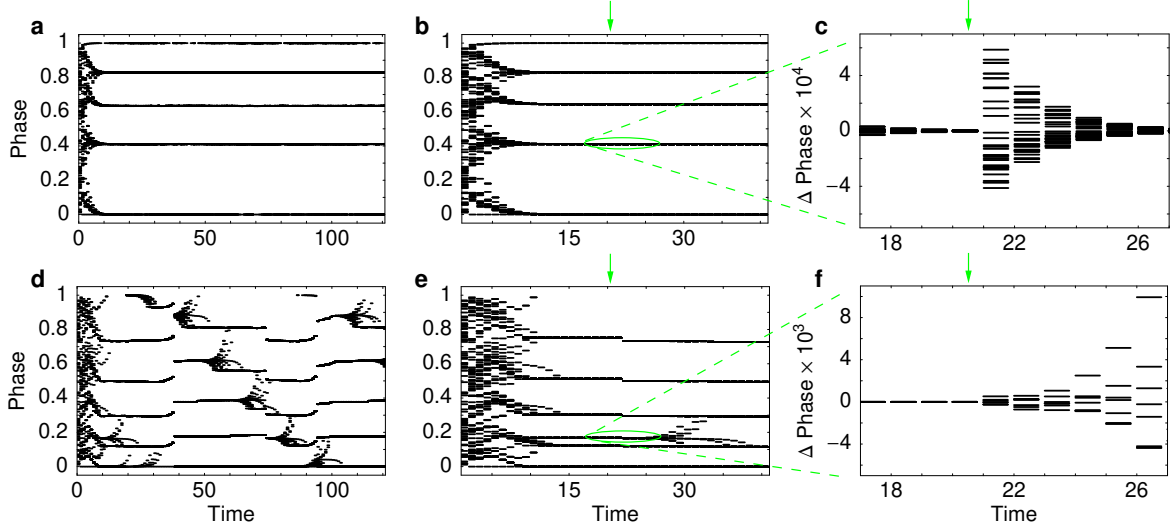


Figure 4.2: Phase dynamics of a large network ($N = 100$, $\tau = 0.15$). Phases of all oscillators are plotted whenever a reference oscillator has been reset such that the axis labeled 'Time' is discrete and nonlinear. (a,b,c) Inhibitory coupling ($\varepsilon = -0.2$). (d,e,f) Excitatory coupling ($\varepsilon = 0.2$). (a,d) Dynamics with noise (noise level $\eta = 10^{-3}$). (b,e) Noiseless dynamics in response to a single phase perturbation (arrow, perturbation strength $\sigma = 10^{-3}$); (b) for inhibitory coupling the system returns to the attractor; (e) for excitatory coupling the system switches from a six-cluster to a five-cluster state. (c,f) Phase differences from the average phase of one cluster (shown in b and e, respectively) in response to the perturbation.

such that the model is meaningful for large N and there is no self-coupling. We focus on excitatory coupling, $\varepsilon > 0$, for which the phenomenon of unstable attractors arises, and briefly compare the results to networks with inhibitory coupling, $\varepsilon < 0$.

For similar classes of pulse-coupled systems, periodic orbits with groups of synchronized units constitute relevant attractors [7–11, 14, 17–19, 21, 53–55, 57, 59–61, 63]. As mentioned above, for the networks of Mirollo-Strogatz oscillators with delayed interactions ($\tau > 0$) considered here, many different cluster-state attractors with several synchronized groups of oscillators (clusters) coexist [17, 18]. After an initial transient, these networks settle down onto such a periodic orbit that displays period-one dynamics with clusters firing successively within each period. Thus, in particular, phase-differences between oscillators are constant at all times when a reference oscillator is reset.

Whereas the noiseless dynamics is seemingly similar for both kinds of coupling, in the presence of noise the collective behavior of excitatorily coupled oscillators strongly differs from that of oscillators coupled inhibitorily. For inhibitory coupling all cluster-state attractors are stable against small phase perturbations. Under the influence of noise the system stays near some periodic orbit that has been reached after a transient from a random initial state (Fig. 4.2a). The dynamics after a small perturbation in an otherwise noiseless sys-

tem confirms this stability property: Perturbations to all clusters decay exponentially and the original attractor is approached again (Fig. 4.2b,c).

In contradistinction, for excitatory coupling, we find (cf. Fig. 4.2d) that, although the system converges towards a periodic orbit from random initial states, small noise is often sufficient to drive the system away from that attractor such that successive switching towards different attractors occurs. In principle, this dynamics might be due to stable attractors located close to the boundaries of their basins of attraction, such that noise drives the trajectory into a neighboring basin. If this explanation were correct, ever smaller perturbations off the attractor would lead to an ever lower probability of leaving its basin. In an otherwise noiseless system we tested this possibility by applying instantaneous, uniformly distributed, independent random perturbations $\delta_i \in [0, \sigma]$ of gradually decreasing strengths (down to $\sigma = 10^{-14}$) to the phases ϕ_i of all oscillators i after the system had settled down to an attractor (see Fig. 4.2e,f). Even for the weakest perturbations applied, *none* of the perturbed states returned to the attractor, but all trajectories separated from the original attractor. We thus hypothesized that the persistent switching dynamics (Fig. 4.2d) is due to attractors that are unstable.

4.3 Stability analysis

In order to verify this hypothesis directly, we analyze a small network of $N = 6$ excitatorily coupled oscillators for which instantaneous phase perturbations lead to a similar switching among attractors. We fix parameters to $\varepsilon = 0.2$, $\tau = 0.15$ and the potential function $U(\phi) = U_3(\phi)$ according to Eq. (3.57). At these parameters the network exhibits a set of periodic orbits with period-one dynamics that are related by a permutation of phases in such a way, that the system may switch among them (cf. Fig. 4.3a, points on the periodic orbits marked in red, yellow, blue). These orbits persist in a neighborhood of these parameters and the function U . Each attractor can be characterized by a list of cluster occupation numbers giving the number of oscillators n_k in the k^{th} cluster, counted in the order of increasing phases at times after a reference oscillator ($i = 1$) has been reset. For instance, the attractor marked in yellow is characterized by the occupation list $[n_1, n_2, n_3, n_4] = [2, 2, 1, 1]$ such that the transitions among the attractors (Fig. 4.3a) are described by the sequence $([1, 2, 2, 1] \text{ (red)} \rightarrow [2, 2, 1, 1] \text{ (yellow)} \rightarrow [2, 1, 1, 2] \text{ (blue)} \rightarrow [1, 2, 2, 1] \text{ (red)})$ for the particular set of perturbations applied. For each of these three attractors there exists another permutation-related attractor with the same occupation list but with the phase values of the two clusters containing only one oscillator interchanged. It turns out that, depending on the perturbation, transitions from one attractor occur to one of only two other attractors that are related through the latter permutation. Thus, once the system has settled down to one of the attractors shown, it may switch within a set of six periodic orbit attractors in response to sufficiently small perturbations.

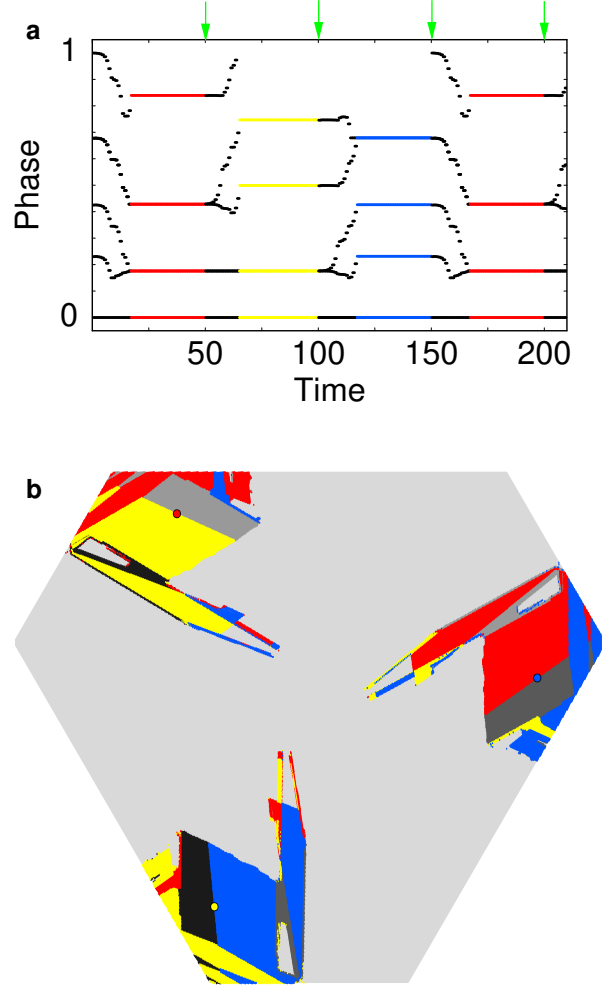


Figure 4.3: Small network ($N = 6$, $\varepsilon = 0.2$, $\tau = 0.15$) exhibiting unstable attractors. (a) Noise-free phase dynamics in response to instantaneous phase perturbations of magnitude $\sigma = 10^{-3}$ (arrows). When an attractor is reached, the phase configuration specifying the current cluster state attractor is marked in color. The perturbations induce a split-up of clusters and a divergence from the attractor such that the network reaches different attractors successively. For the realization of perturbations shown, the attractors marked in red (cluster occupation list $[1, 2, 2, 1]$), yellow ($[2, 2, 1, 1]$), and blue ($[2, 1, 1, 2]$) are visited cyclically. For each of the three attractors there exists another attractor with the same cluster occupation list but with phase values of the two clusters with only one oscillator interchanged. (b) Basin structure of the three attractors color-marked in (a) in two-dimensional planar section through six-dimensional state space. The planar section is defined by one point on each of the three periodic orbit attractors, represented by small red, yellow, and blue disks, respectively. Basins of the three attractors are marked in the same colors. The part of state space within this section is of hexagonal shape. Darker gray areas are basins of the three other permutation-related attractors (cf. (a)) which are located outside the section shown. Lightest gray marks the union of the basins of all other attractors.

Due to their permutation-equivalence these orbits have identical stability properties. The state of the network at time t is specified by $\phi(t) = (\phi_1(t), \dots, \phi_6(t))^T$, such that the orbit marked in yellow in Fig. 4.3a is defined by the initial condition

$$\phi(0) = (0, 0, A, A, B, C)^T \quad (4.3)$$

where

$$A = H_{\hat{\varepsilon}}(\tau) \quad (4.4)$$

$$B = H_{2\hat{\varepsilon}}(1 + 2\tau - a_4) \quad (4.5)$$

$$C = H_{2\hat{\varepsilon}}(H_{\hat{\varepsilon}}(2\tau) + 1 + \tau - a_4) \quad (4.6)$$

and recursively defined

$$a_i = U^{-1}(k_i \hat{\varepsilon} + U(\tau + a_{i-1})) \quad (4.7)$$

for $i \in \{1, \dots, 4\}$, $a_0 = 0$, and $k_1 = k_3 = k_4 = 1$, $k_2 = 2$ (see Appendix A.1 for a detailed derivation of the constants). Here the origin of time, $t = 0$, was chosen such that oscillators 1 and 2 have just sent a signal and have been reset. Moreover, at $t = 0$ only these two signals (and no others) have been sent but not yet received. The numerical values for the particular parameters considered, $A \approx 0.176$, $B \approx 0.499$, $C \approx 0.747$, can be identified in Fig. 4.3a (orbit marked in yellow). This orbit indeed is periodic,

$$\phi(T) = \phi(0), \quad (4.8)$$

and, in particular, period-one, such that each oscillator fires exactly once during one period T .

To perform a stability analysis, we define a return map by choosing oscillator $i = 1$ as a reference: Let

$$\phi_{n,i} := \phi_i(t_n^+) \quad (4.9)$$

be the perturbed phases of the oscillators i at times t_n just after the resets of oscillator $i = 1$,

$$\phi_1(t_n^+) = 0 \quad \text{for } t_n > 0, n \in \mathbb{N}. \quad (4.10)$$

Thus the five-dimensional vector

$$\delta_n = \phi_n - (0, A, A, B, C')^T \quad (4.11)$$

defines the perturbations $\delta_{n,i}$ for $i \in \{2, \dots, 6\}$ where we choose $0 < \delta_{n,2}$ and $\delta_{n,3} < \delta_{n,4}$. Following the derivation in Appendix A.1, we obtain

$$C' = H_{2\hat{\varepsilon}}(H_{\hat{\varepsilon}}(2\tau + H_{\hat{\varepsilon}}(0)) + 1 + \tau - a_4) \quad (4.12)$$

which numerically yields $C' \approx 0.756$. Because after a general perturbation clusters are split up such that in particular $\phi_1 < \phi_2$, oscillator 6 receives the (later) signal from oscillator 1 only after it is reset by the (earlier) signal from oscillator 2 resulting in $C' \neq C$. Thus,

the original orbit is super-unstable, i.e. has infinite expansion rate. At a distance from it there is a “partner orbit” that is obtained in the limit $\delta_n \rightarrow 0$. The stability analysis is performed for the latter orbit (see also Appendix A.1). It is important to note that unstable attractors also exist which do not possess such a “partner orbit” but have a finite expansion rate themselves. For convenience, we here continue considering the above set of orbits which allow a straightforward explanation of the phenomenon of unstable attraction. Following the dynamics, the five-dimensional return map is given by

$$\delta_{n+1} = \mathbf{F}(\delta_n), \quad (4.13)$$

where \mathbf{F} is defined by

$$\begin{aligned} F_2(\delta) &= 0 \\ F_3(\delta) &= L_4 - L_3 + H_{\hat{\varepsilon}}(\tau - L_4 + L_3) - A \\ F_4(\delta) &= H_{\hat{\varepsilon}}(\tau + L_4 - L_3) - A \\ F_5(\delta) &= H_{\hat{\varepsilon}}(H_{\hat{\varepsilon}}(1 + 2\tau - L_4) + L_4 - L_3) - B \\ F_6(\delta) &= H_{\hat{\varepsilon}}(L_4 - L_3 + H_{\hat{\varepsilon}}(\tau + 1 - L_3 + \\ &\quad H_{\hat{\varepsilon}}(2\tau - \delta_2 + H_{\hat{\varepsilon}}(\delta_2)))) - C' \end{aligned} \quad (4.14)$$

with the abbreviations

$$L_i := L_i(\delta) = H_{\hat{\varepsilon}}(\tau + H_{\hat{\varepsilon}}(\tau - \delta_2 + H_{\hat{\varepsilon}}(\delta_2 + H_{\hat{\varepsilon}}(\tau + \delta_i - \delta_2 + H_{\hat{\varepsilon}}(\tau)))) \quad (4.15)$$

for $i \in \{3, 4\}$. Here the difference $L_4 - L_3$, which frequently occurs in Eqs. (4.14), is of order $L_4 - L_3 = \mathcal{O}(\delta)$ where $\mathcal{O}(\delta) = \sum_{i=2}^N \mathcal{O}(\delta_i)$ as all $\delta_i \rightarrow 0$. See Appendix A.1 for a detailed derivation of the map \mathbf{F} .

The linearized dynamics

$$\delta_{n+1} \doteq M\delta_n \quad (4.16)$$

of a slightly perturbed state with split-up clusters is described by the Jacobian matrix

$$M = \left. \frac{\partial \mathbf{F}(\delta)}{\partial \delta} \right|_{\delta=0} = \begin{pmatrix} 0 & 0 & 0 & 0 & 0 \\ 0 & \alpha & -\alpha & 0 & 0 \\ 0 & -\beta & \beta & 0 & 0 \\ * & * & * & 0 & 0 \\ * & * & * & 0 & 0 \end{pmatrix} \quad (4.17)$$

where $\alpha, \beta > 0$ and $*$ denote nonzero real numbers. It has four zero eigenvalues

$$\lambda_i = 0 \text{ for } i \in \{1, 2, 3, 4\} \quad (4.18)$$

implying that a six-dimensional state-space accessed by the random perturbation is contracted onto a two-dimensional manifold. This reflects the fact that suprathreshold input received simultaneously by two or more oscillators (Fig. 4.4) leads to a simultaneous reset

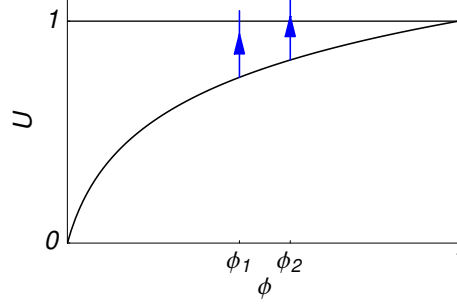


Figure 4.4: Simultaneous suprathreshold excitatory input synchronizes immediately due to the reset at threshold. Sufficiently small but positive phase differences $|\phi_2(t) - \phi_1(t)| > 0$ are reduced to zero such that $\phi_2(t^+) = \phi_1(t^+) = 0$. This is the mechanism of dimensional reduction of effective state space, which is responsible for the attractivity.

and thus a synchronization of these oscillators independent of their precise phases. If a single oscillator is reset by a suprathreshold signal, it instantaneously exhibits a precise lag in firing time $\Delta t = \tau$ compared to the oscillator that has sent this signal.

In particular, the zero eigenvalues (Eq. (4.18)) reflect the following contracting dynamics: (i) Perturbations of phases $\delta_{n,5} \neq 0$ or $\delta_{n,6} \neq 0$ are restored immediately by suprathreshold input pulses received from oscillators $j = 6$ or $j = 1$, respectively. This gives rise to the eigenvalues $\lambda_1 = \lambda_2 = 0$ corresponding to the eigenvectors $\mathbf{v}_1 \propto (0, 0, 0, 1, 0)^\top$ and $\mathbf{v}_2 \propto (0, 0, 0, 0, 1)^\top$. (ii) A splitting of the first cluster, $\delta_{n,2} > 0 \equiv \delta_{n,1}$, corresponding to the vector $\mathbf{v}_3 \propto (1, 0, 0, 0, 0)^\top$, is restored after one period due to one suprathreshold input pulse from oscillator $j = 4$. At the same time, however, this splitting induces a perturbation of oscillators $i = 5$ and $i = 6$ such that $\delta_{n+1,5} \neq 0$ and $\delta_{n+1,6} \neq 0$ which is restored according to (i) in the subsequent period. Taken together, this accounts for the eigenvalue $\lambda_3 = 0$. (iii) As long as $\delta_{n,3} = \delta_{n,4}$, a perturbation vector is mapped onto the subspace spanned by \mathbf{v}_1 and \mathbf{v}_2 (see (i)) within one period and is then mapped onto zero during the next period. As a result, the eigenvalue $\lambda_4 = 0$ corresponds to the direction $\mathbf{v}_4 \propto (0, 1, 1, 0, 0)^\top$. In addition to this analysis, a stability analysis for the subset of states with the cluster $\phi_3(t) \equiv \phi_4(t)$ kept synchronized, results in superstable directions only, as expected.

In contradistinction to this contracting dynamics, the concavity of U implies that simultaneous subthreshold input to two or more oscillators leads to an increase of their phase differences, i.e. a desynchronization of oscillators with similar phases (Fig. 4.5). For the orbits considered here, this is reflected by the only non-zero eigenvalue

$$\lambda_5 = \frac{(2U'(c_0) - U'(a_1))U'(c_1)U'(c_2)U'(c_3)}{U'(a_1)U'(a_2)U'(a_3)U'(a_4)} > 1 \quad (4.19)$$

where

$$c_i = \tau + a_i \quad (4.20)$$

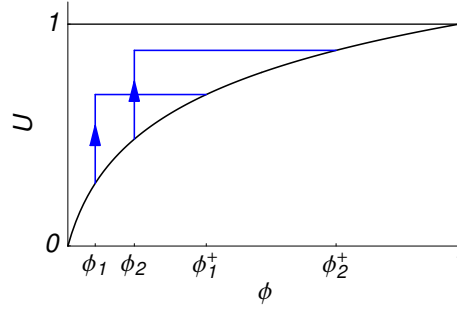


Figure 4.5: Simultaneous subthreshold excitatory input desynchronizes due to the concavity of U . Small phase differences $|\phi_2(t) - \phi_1(t)| > 0$ are increased, $|\phi_2(t^+) - \phi_1(t^+)| > |\phi_2(t) - \phi_1(t)|$, providing the mechanism which creates an instability.

for $i \in \{0, 1, 2, 3\}$ and the a_i are defined in Eq. (4.7). Because $c_i > a_i > c_{i-1}$ for all i and $U' > 0$, $U'' < 0$, this eigenvalue is larger than one, i.e. the periodic orbit is linearly *unstable*. This eigenvalue corresponds to a split-up of the cluster composed of the oscillators $i = 3$ and $i = 4$. Because the Jacobian (4.17) is not symmetric, the eigenvectors are not orthogonal such that the corresponding eigenvector \mathbf{v}_5 is not $\mathbf{v} \propto (0, -1, 1, 0, 0)^T$ but has a component in this direction, $\mathbf{v}_5 \propto (0, -\alpha', \beta', -\gamma', 1)^T$ where $\alpha', \beta', \gamma' > 0$. If there is no homoclinic connection, this instability implies that such an attractor is not surrounded by a positive volume of its own basin of attraction, but is located at a distance from it: Thus, every random perturbation to such an attractor state – no matter how small – leads to a switching towards a different attractor.

4.4 Unstable attractors

The stability analysis presented in the previous section has shown that the periodic orbits considered are unstable. Furthermore, this periodic orbit indeed is an *attractor*: According to the stability analysis, after two firings of the reference oscillator, a trajectory perturbed off a periodic orbit (e.g. the one marked in red in Fig. 4.3a, which is permutation-equivalent to the yellow one) is mapped onto a two-dimensional manifold, re-synchronizing one cluster. The trajectory then evolves towards a neighborhood of another attractor (here: the yellow one) in a lower dimensional effective state space without further dimensional reduction. Here, forming the second cluster, suprathreshold input leads to the last dimensional reduction while the state is mapped directly onto the periodic orbit.

In general, a periodic orbit is *unstable* if, after a random perturbation into its vicinity, one or more clusters are not re-synchronized by simultaneous suprathreshold input but desynchronize due to simultaneous subthreshold input. An unstable *attractor* results if these clusters are formed through synchronization in a region of state space which is located *remote* from the periodic orbit towards which the state then converges.

A remark about the mathematical rigor is appropriate here. Although we adopted an exact formulation, i.e. we used no approximation throughout the derivation, this work can be considered a strong indication for the existence of unstable (minimal Milnor) attractors but not a rigorous mathematical proof. We point out two problems in this regard. First, this is a discontinuous system of such a kind, that there is no ordinary linear stability theory (cf. also Chapter 5). Under a certain class of perturbations, the trajectory jumps from the original orbit towards a “partner orbit” which does not exist in the limit of zero perturbation strength. Second, since the interactions are delayed, the state space is not just a collection of N phases. The entire state space must also contain the times of signals that have been sent but not received at a given instant of time, as well as the possibility of no signal traveling at a certain point in time. Given this additional problem, we chose a subset of perturbations in the full state space. These phase perturbations were added to the phases on a periodic orbit at times at which no signal is traveling. Thus, differences in firing times and, equivalently, temporal positions of traveling signals are induced only after the oscillators reach the threshold the next time. In addition, one can imagine different kinds of perturbations, in particular signal times that are not consistent with the oscillator’s phases as well as additional or missing signals.

A three-dimensional cartoon of the basin structure in a state space of phases may help to gain further insight about how trajectories approach and retreat from an unstable attractor in the presence of noise. Figure 4.6 shows that the basin volume is contracted by creating a cluster in a region of state space located at a distance from the attractor itself. In contrast, near the attractor, the same cluster is unstable against a split-up of the phases of the oscillators it contains. Basically, such an unstable attractor might be viewed as an unstable periodic orbit with a remote basin attached to its stable manifold. The presence of this basin leads to the attractivity property.

It is important to note that for inhibitory coupling we observe that all attractors are stable: An intuitive explanation is that there is only a mechanism of synchronization (Fig. 4.7) due to the concavity of U which contracts state space volume such that all attractors with period-one dynamics are stable. It is instructive to compare Fig. 4.7 to Fig. 4.5 which display how simultaneously incoming subthreshold pulses affect phase differences for inhibition and excitation, respectively. Since a simple mechanism of desynchronization is missing for inhibitory coupling, we expect that the possibility of unstable attractors is excluded for this kind of coupling.

In order to further clarify the structure of state space of networks of excitatorily coupled oscillators, we numerically determined the basins of attraction of the three attractors displayed in Fig. 4.3a in two-dimensional sections of state space. The example shown in Fig. 4.3b reveals that attractors are surrounded by basins of attraction of other attractors as predicted by the above analysis. Because of this basin structure, noise induces repeated attractor switching among unstable attractors. Starting from the orbit defined by (4.3) the system may switch within sets of only six periodic orbit attractors as is apparent from

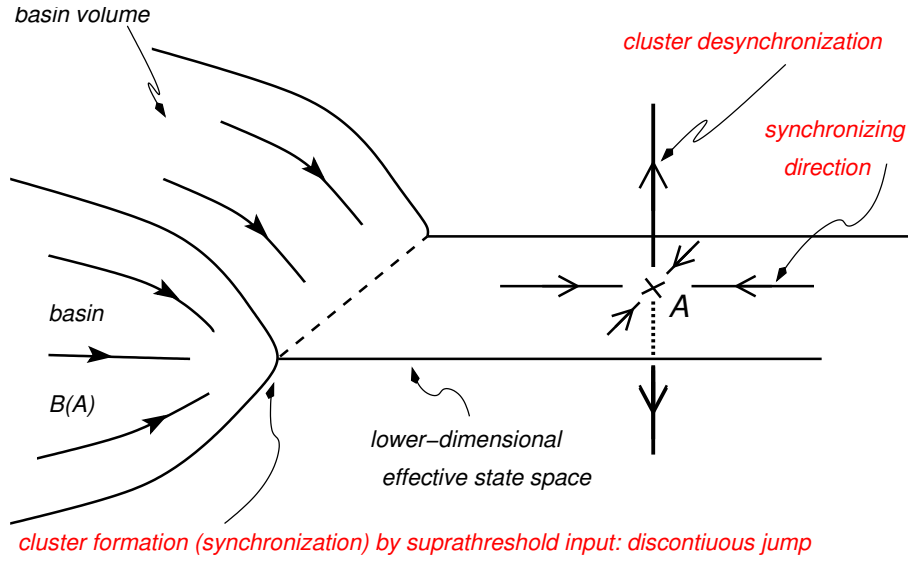


Figure 4.6: Cartoon of the basin structure of an unstable attractor A . First, a positive basin volume $B(A)$ of states is mapped onto a lower-dimensional effective state space. This is achieved by simultaneous suprathreshold input to a group of oscillators, which synchronizes them to form one cluster. Because the attractor is located remote from its own basin volume the same cluster may desynchronize in response to small perturbations near the attractor, where incoming pulses are no longer supra- but subthreshold and thus lead to a desynchronization.

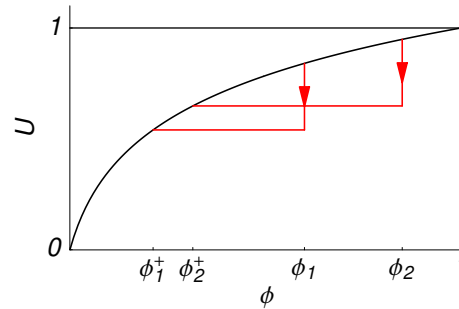


Figure 4.7: Simultaneous inhibitory input synchronizes due to the concavity of U . Contrary to networks of oscillators coupled excitatorily, here the inhibitory interactions allow subthreshold input only and lead to a decrease of phase differences, $|\phi_2(t^+) - \phi_1(t^+)| > |\phi_2(t) - \phi_1(t)|$. Hence, these networks possess a mechanism for synchronization, but there is no simple possibility of desynchronizing a cluster state.

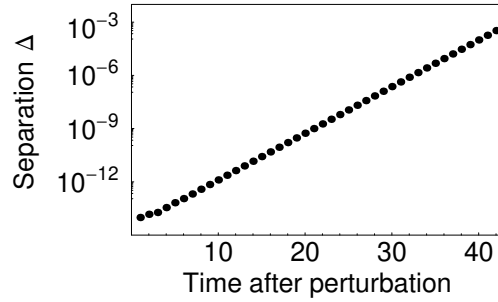


Figure 4.8: Separation of two perturbations off an unstable attractor into the same random direction in a network of $N = 100$ oscillators ($\varepsilon = 0.2$, $\tau = 0.15$). The separation Δ grows exponentially with the time after the perturbation, measured in number of firing events of a reference oscillator.

the basins shown in Fig. 4.3b. However, in larger networks (cf. e.g. Fig. 4.2d) a cluster may split up in a combinatorial number of ways and exponentially many periodic orbit attractors are present among which the system may switch. The larger such networks are, the higher the flexibility they exhibit in visiting different attractors and exploring state space.

4.5 Unstable attractors in large networks

Until now, the analysis has focussed on a small network of $N = 6$ oscillators, for which certain periodic orbits have been demonstrated to be unstable attractors. To study the desynchronization of clusters also observed in larger networks in greater detail, we numerically determined the divergence of small random phase perturbations to an attractor in a network of $N = 100$ oscillators. As an example we chose two perturbations $\delta_1 = \sigma_1 \delta^*$ and $\delta_2 = \sigma_2 \delta^*$ into the same random direction $\delta^* \in [0, 1]^N$, where $\sigma_1 = 10^{-12}$ and $\sigma_2 = \sigma_1 + 10^{-14}$. Figure 4.8 shows that the separation

$$\Delta := \max_i |\delta_{1,i} - \delta_{2,i}| \quad (4.21)$$

between the two perturbed trajectories exponentially increases with time. This indicates that also for large networks, desynchronization is due to a linear instability. Let us remark that, due to the splitting-up of clusters by a general perturbation (cf. Eqs. (4.11) and (4.12)), two perturbations into independent directions might first lead to an additional discontinuous separation, followed by an exponential expansion.

As a second quantity characterizing the dynamics of switching, we consider the time needed by the system to switch from an unstable attractor towards a different attractor after a random perturbation of magnitude σ . The perturbations applied to the attractor are random phase vectors, drawn from a uniform distribution on $[0, \sigma]^N$, with $\sigma \in [10^{-12}, 10^{-2}]$.

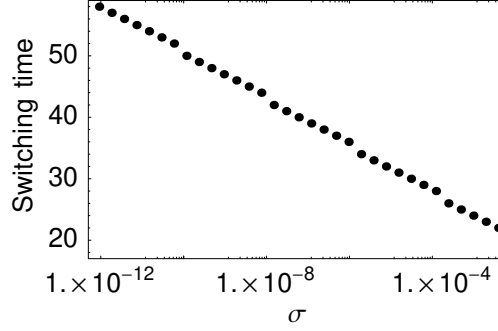


Figure 4.9: Time of switching between two attractors depending on the perturbation strength σ for a large network ($N = 100$, $\varepsilon = 0.2$, $\tau = 0.15$). The switching time increases exponentially with decreasing perturbation strength. The discrete time axis (number of firing events of a reference oscillator) leads to a regular stepping which slightly disrupts the exponential trend.

As displayed in Fig. 4.9, for sufficiently small σ , this switching time clearly increases exponentially with decreasing σ . In particular, this indicates that the attractors found are indeed unstable and do not possess small contracting open neighborhoods. Furthermore, it confirms our observations that the time of switching is mainly determined by the time of divergence from the original unstable attractor. Thus, in the presence of external noise, we expect a similar monotonic increase of an approximate switching time with the amplitude of the noise.

Taken together, this indicates that there exist also unstable attractors in larger networks which are enclosed by basins of other attractors. Thus, these results strongly support the hypothesis that the switching found in large networks in the presence of noise (cf. Fig. 4.2), is also due to unstable attractors. It is important to note that, without a perturbation, numerical noise does not induce a divergence of trajectories from attractors that are unstable: Synchronization occurs by simultaneously resetting the phases of two or more oscillators to zero (cf. Fig. 4.4). Due to the global, homogenous coupling, all signals simultaneously received by these oscillators are of the same size and are exactly synchronous numerically (see Sec. 3.2.2). Thus, although the phase-advance computed for such signals is influenced by numerical round-off errors, such errors are identical for phases of synchronized oscillators and hence do not induce a desynchronization.

4.6 Prevalence and persistence

The preceeding analysis demonstrates the existence of unstable attractors. For excitatory coupling, these unstable attractors coexist with stable attractors. For a cluster-state attractor to be stable, all clusters necessarily receive suprathreshold input once per period which re-synchronizes possibly split-up oscillators. In general, a stable attractor has a

contracting neighborhood in state space from which perturbed trajectories return to the attractor. If an attractor is unstable there are trajectories arbitrarily close to the attractor which diverge from it, such that unstable attractors do not exhibit a contracting neighborhood. In other words, an unstable attractor has to be located on the boundary of its own basin. Therefore, the naïve expectation is that parameters of the system have to be precisely specified in order to keep a periodic orbit simultaneously attracting and unstable. This leads to the question whether the physical parameters of the system, in particular ε , τ , and N , need to be precisely tuned to obtain unstable attractors.

To answer the question, how common unstable attractors actually are, we numerically estimated the fraction

$$p_u(N) \in [0, 1] \quad (4.22)$$

of state space occupied by basins of unstable attractors. To obtain this estimate, we initialized the system with 1000 random initial phase vectors, drawn from the uniform distribution on $[0, 1]^N$. Whenever a period-one orbit was reached, we applied one random phase perturbation δ drawn from the uniform distribution on $[0, \sigma]^N$ where we chose $\sigma = 10^{-6}$, a value well below all scales which are determined by the model parameters, in particular $\sigma \ll \varepsilon/N$ for network sizes up to $N \approx 10^2$. If perturbed trajectories did not return to the original attractor, it was counted unstable. If no period-one orbit was reached from a random initial state but, e.g., orbits of higher period, these were not tested for stability. Thus, the numerical method used estimates a lower bound on $p_u(N)$. As an example, Fig. 4.10a displays such an estimate of $p_u(N)$ for $\varepsilon = 0.2$ and $\tau = 0.15$.

While for these parameters unstable attractors are absent if networks are too small (here $N \leq 4$) and coexist with stable attractors in larger networks, the fraction approaches one for $N \gg 1$. Other parameters ($\varepsilon = 0.2$, $\tau = 0.25$) yield a different dependence on the network size N (Fig. 4.10a). Once again, unstable attractors arise only if the network size is not too small ($N \geq 3$). Yet, the fraction $p_u(N)$ is only substantial for moderate network sizes near $N \approx 10$ and approaches zero for large N . Generally, we observed that unstable attractors are absent in small networks (cf. [17, 18] for the case $N = 2$) and $p_u(N)$ approaches either zero or one in large networks, depending on the parameters. For networks of $N = 100$ oscillators, Fig. 4.11 shows the region of parameter space in which unstable attractors prevail ($p_u(100) > 0.5$, estimated from 100 random initial phase vectors). As this region covers a substantial part of parameter space, precise parameter tuning is not needed to obtain unstable attractors. Furthermore we find the same qualitative behavior independent of the detailed form of $U(\phi)$. This indicates that the occurrence of unstable attractors is a robust collective phenomenon in this model class of networks of excitatorily pulse-coupled oscillators.

It is instructive to note that, on theoretical grounds, a period-one orbit is stable only if the clusters have a difference in firing times of $\Delta t = \tau$, such that its period is an integer multiple of τ . The pulse sent by every single cluster then leads to a suprathreshold input to the following cluster which in response to this input sends a pulse. If these conditions

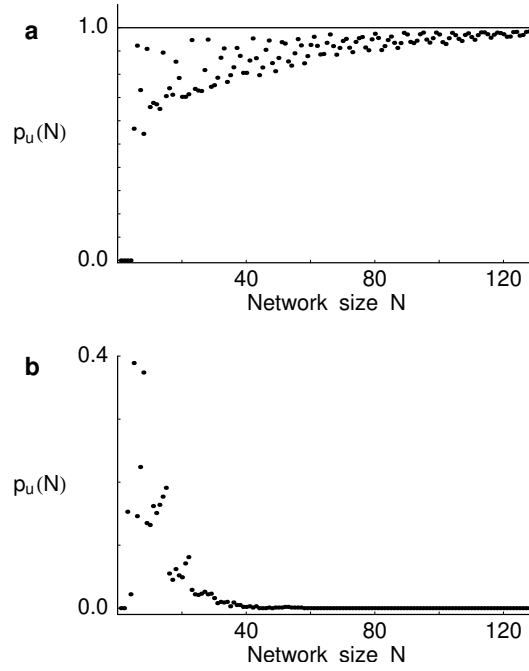


Figure 4.10: Prevalence of unstable attractors in large networks. (a) Unstable attractors prevail for large networks for certain parameters ($\varepsilon = 0.2$, $\tau = 0.15$), but (b) are not important in large networks for other parameters ($\varepsilon = 0.2$, $\tau = 0.25$). The fraction $p_u(N)$ was estimated for every $N \leq 128$ from 1000 random initial phase vectors, drawn from the uniform distribution on $[0, 1]^N$.

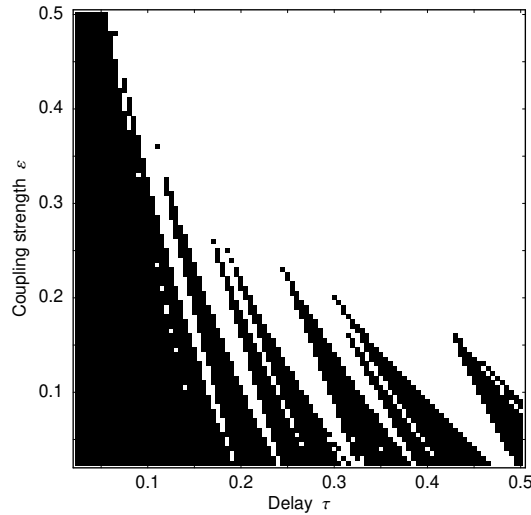


Figure 4.11: Unstable attractors persist in a wide region of parameter space in large networks ($N = 100$). Parameters with $p_u(100) > 0.5$ are marked in black; here $p_u(100)$ was estimated from 100 random initial phase vectors, drawn from the uniform distribution on $[0, 1]^N$, for every set of parameters (resolution $\Delta\tau = \Delta\varepsilon = 0.005$).

are not satisfied for all clusters of a period-one orbit, this orbit is unstable. In particular, it is unstable against a split-up of (at least) one cluster. The same orbit may also be attracting if such a cluster is formed in a region of state space that is located remote from the attractor as exemplified by the analysis in Sec. 4.4.

Whereas the analysis presented above gives some insights into why unstable attractors exist and demonstrates that they prevail under variation of parameters, the precise reasons for their prevalence await discovery in future studies.

4.7 Structural modifications

The occurrence of unstable attractors *per se* is an intriguing phenomenon because it contradicts the common intuition about the stable nature of attracting invariant sets in dynamical systems. Our results suggest, that there are systems of pulse-coupled units in which unstable attractors may be the rule rather than the exception. This leads to the question, which structural modifications of the dynamics of the system conserve the phenomenon of unstable attractors and which are likely to conserve their dynamical consequences of switching in the presence of noise.

Unstable attractors persist under various classes of structural modifications. For instance, preliminary studies on networks with randomly diluted connectivity suggest that a symmetric, all-to-all connectivity is not required [72, 73]. In addition, unstable attractors also arise naturally in networks of inhibitorily coupled oscillators [74, 75], if a lower threshold is introduced and the function U is taken to be convex down, $U''(\phi) > 0$, in a certain range of phase values. This is a model variant motivated by experiments in certain biological neural systems [13].

Moreover, it is expected that every system obtained by a sufficiently small structural perturbation from the one considered here will exhibit a similar set of saddle periodic orbits, because linearly unstable states can generally not be stabilized by such a perturbation. Although, in general, these orbits may no longer be attracting, their dynamical consequences are expected to persist. In particular, a switching along heteroclinic connections may occur in the presence of noisy or deterministic, time-varying signals. As in the original system, the sequence of states reached may be determined by the directions into which such a signal guides the trajectory. By increasing and decreasing the strength of this signal, the time-scale of switching may be decreased and increased, respectively, due to the linear instability.

Furthermore, switching among unstable states also occurs in systems of continuously phase-coupled oscillators [76, 77] which can be obtained from pulse-coupled oscillators in a certain limit of weak coupling [78]. In particular, Hansel, Mato, and Meunier [76] have shown that

a system of phase-coupled oscillators may switch back and forth among pairs of two-cluster states. Working in the limit of infinitely fast response, i.e. discontinuous phase jumps, we have demonstrated that far more complicated switching transitions may occur in large networks if the oscillators are pulse-coupled.

Taken together, whereas unstable attractors will persist under certain classes of structural modifications, their dynamical consequences are expected to persist under all sufficiently small structural perturbations. In particular, it is presumed that in the presence of noise or external, time-varying signals, a similar switching along heteroclinic connections occurs. Interestingly, it has recently been shown that certain models of neural networks may dynamically encode information as trajectories near heteroclinic connections [79].

4.8 Summary and outlook

In summary, we demonstrated that the observation of synchronization and desynchronization in networks of pulse-coupled oscillators is due to an intriguing kind of invariant set – unstable attracting periodic orbits. Applying analytical tools to a specially selected set of periodic orbits in a small network, we presented an exact stability analysis, which not only describes the local dynamics near one orbit, but also illuminates an important part of the dynamics between orbits. Supported by further numerical analysis of the basin structure of these orbits, we derived strong indications that these periodic orbits are minimal Milnor attractors which are unstable. For large networks, we presented numerical evidence that unstable attractors not only exist, but also prevail under variation of the physical parameters.

This is the first analysis of such unstable attractors. The discovery of their existence and prevalence in networks of pulse-coupled oscillators raises a number of challenging questions. For instantaneous interactions ($\tau = 0$) the system exhibits one global attractor such that all oscillators synchronize completely from random initial conditions. For delayed interactions ($\tau > 0$) the system exhibits unstable attracting periodic orbits in a wide range of parameters. What bifurcation scenario underlies this transition? It seems likely that the switching phenomenon found here is related to a similar switching found in networks of phase-coupled oscillators. Is there a bifurcation connecting unstable attracting periodic orbits with unstable non-attracting periodic orbits that are connected by heteroclinic connections? More generally, what are possible classes of bifurcations leading to unstable attractors? From the mathematical point of view, unstable attractors may be useful for the analysis of switching along heteroclinic connections in a certain limit. If such a limit exists, how can this fact be utilized? Furthermore, unstable attractors or related switching phenomena could be used to build systems like artificial neural networks, which perform specific tasks exploiting the combination of attraction and instability. This naturally leads to the question of whether the switching phenomenon based on unstable attractors, could

be implemented in a physical system, and if so, how this can be done in practice. This list could be extensively continued.

In order to fully understand the capabilities of systems exhibiting unstable attractors or unstable periodic orbits linked by heteroclinic connections, and to learn to design such systems for specific functions, it is of major importance to analyze further the requirements for the occurrence of unstable attractors in dynamical systems and the factors which shape their basins. Our results indicate that networks of pulse-coupled oscillators are a promising starting point for such investigations.

Chapter 5

Networks with a complex structure

In this chapter we consider arbitrary connected networks of pulse-coupled oscillators, including regular and random networks as well as networks with a more complex connectivity. We present an exact stability analysis of the synchronous state. It turns out that, as opposed to conventional stability analysis, stability is not determined by a single stability matrix but by a multitude of operators. For generally structured networks, the number of operators increases exponentially with the size of the network. We treat this multi-operator problem analytically. First, using the Gershgorin theorem, we find analytical bounds on the eigenvalues of all operators. Guided by results from the eigenvalue problem, we determine the stability of the synchronous state. For inhibitory interactions the synchronous state is stable, independent of the parameters and the network connectivity. In contrast, in networks of excitatorily coupled oscillators, the synchronous state is unstable. Furthermore, we demonstrate that in random networks of inhibitorily coupled oscillators the stable synchronous state displaying regular, periodic dynamics, coexists with a balanced state exhibiting irregular dynamics. This chapter begins with an introduction to the subject of complex networks and ends with a summary and a brief discussion of further possible applications of our method and implications of our findings.

5.1 Structure and dynamics of complex networks

We are permanently confronted with complex networks, for instance when accessing the internet via our personal computer as well as when reading these lines utilizing the networks of neurons in our brain. In the internet, individual web servers are considered as the vertices of a graph. These are wired together to form a complicated network. Interactions arise if we use this network, for example by searching the world wide web for useful information or by (illegally?) downloading music. This may lead to cooperative (or competitive) phenomena such as congestion of certain web servers which seem interesting to a huge

number of users at a certain instant of time [80]. In a neural network, single neurons are considered as vertices whereas their synaptic connections represent the edges of this directed graph. The interactions in neural networks are the sending and receiving of short-lasting pulses, known as action potentials or spikes. These pulses induce potential changes in the connected postsynaptic neurons (cf. Chapter 3) [81]. As in these two examples, many networks of interacting units are not arranged in regular lattices as atoms are arranged in a solid. Instead, single units form an intricate network of connections that mediate the interactions. In addition, these connections are often directed, meaning that a connection from one unit to another does not imply a connection in the reverse connection.

Recent studies on networks exhibiting a complex connectivity have strongly focussed on their *structure* [82–84]. For instance, it was found that the distribution of degrees of the world wide web pages is a power law [85] such that most pages contain only a relatively small number of outgoing and incoming hyperlinks whereas a few interesting pages, such as search engines, display a huge amount of links. Structural issues are also of major interest in neuroscience because they underly the function of neural networks. As a prototypical model in biology, the topology of the neural network of the nematode worm *Caenorhabditis elegans* has been extensively explored [86]. Quantitative analysis of the wiring diagram [87] shows that the $N \approx 300$ neurons in the network are significantly clustered compared to networks in which the same number of links is randomly and independently chosen. Networks of neurons in the cerebral cortex of mammals (and thus humans) provide an example of where the underlying *structure* is likely to strongly influence the *dynamics* (see e.g. [88,89]). Here, fundamental open questions include how neuronal activity persists and how information is processed depending on the given network structure.

More generally, the *dynamics* on networks exhibiting a complex structure is much less understood than their structure and constitutes a challenging issue of current and future research [7]. Even if the individual vertices of the network are simple dynamical systems, such as limit cycle oscillators, an exact mathematical analysis of their collective dynamics is mostly highly intricate (see also Chapter 1).

As a prototypical class of dynamical systems interacting on networks, pulse-coupled oscillators have received a significant amount of interest in the recent past because of their relevance to diverse natural systems (cf. Chapter 1). Particularly in neuroscience, these models [12] are essential for understanding collective dynamic phenomena such as synchronization or the propagation of sensory signals through extended networks [90–93]. Although biological neural networks, like other networks occurring in the real world, often possess an complex connectivity, most theoretical studies on pulse-coupled oscillators were so far either restricted to networks of globally coupled oscillators and simple regular networks, or work in some mean field limit [8, 11, 14–18, 20–22, 24, 30, 53, 55–59, 62, 64, 66]. This calls for appropriate methods for analyzing the dynamics on networks that exhibit a complex connectivity.

5.2 Structured networks of Mirollo-Strogatz oscillators

We consider a system of N coupled Mirollo-Strogatz oscillators [14,17,18] (cf. also Sec. 3.1.4) which interact on directed graphs by sending and receiving pulses. The structure of this graph is specified by the sets $\text{Pre}(i)$ of presynaptic oscillators that send pulses to oscillator i . For simplicity we assume no self-interactions, $i \notin \text{Pre}(i)$. These sets $\text{Pre}(i)$ determine the sets $\text{Post}(i)$ of postsynaptic oscillators that receive pulses from i . Further graph-theoretical background was introduced in Chapter 2. The coupling strength between oscillator j and oscillator i is given by ε_{ij} such that

$$\begin{aligned} \varepsilon_{ij} &\neq 0 && \text{if } j \in \text{Pre}(i) \\ \varepsilon_{ij} &= 0 && \text{otherwise.} \end{aligned} \quad (5.1)$$

Thus a connection is considered to be present if the connection strength is non-zero. All analytical results presented in this chapter are derived for the general class of interaction functions introduced in Chapter 3.

5.3 Construction of stroboscopic maps

The synchronous state is one of the simplest states a network of pulse-coupled oscillators may assume. We perform a stability analysis of this state

$$\phi_i(t) = \phi_0(t) \quad \text{for all } i \quad (5.2)$$

in which all oscillators display identical phase-dynamics $\phi_0(t)$ on a periodic orbit such that $\phi_0(t+T) = \phi_0(t)$. This synchronous state exists if and only if the coupling strengths are normalized such that

$$\sum_{j \in \text{Pre}(i)} \varepsilon_{ij} = \varepsilon. \quad (5.3)$$

Its period is given by

$$T = \tau + 1 - \alpha \quad (5.4)$$

where

$$\alpha = U^{-1}(U(\tau) + \varepsilon). \quad (5.5)$$

For simplicity, we consider the cases where the total input ε is subthreshold, $U(\tau) + \varepsilon < 1$ such that $\alpha < 1$. A perturbation

$$\boldsymbol{\delta}(0) =: \boldsymbol{\delta} = (\delta_1, \dots, \delta_N) \quad (5.6)$$

to the phases is defined by

$$\delta_i = \phi_i(0) - \phi_0(0). \quad (5.7)$$

If we assume that the perturbation is small in the sense that

$$\max_i \delta_i - \min_i \delta_i < \tau \quad (5.8)$$

this perturbation can be considered to affect the phases of the oscillators at some time just after all signals have been received, i.e. after a time $t > t_0 + \tau$ if all oscillators have fired at $t = t_0$. Such a perturbation will affect the time of the next firing events because the larger the perturbed phase of an oscillator is, the earlier this oscillator reaches threshold and sends a signal. In principle, there may be other perturbations, in which, for instance, a signal is added or removed at a certain time. For simplicity, we do not consider such perturbations here.

To construct a stroboscopic period- T map, δ is ordered according to the rank order $\text{rank}(\delta)$ of the δ_i : For each oscillator i we label the perturbations δ_j of its presynaptic oscillators $j \in \text{Pre}(i)$ (for which $\varepsilon_{ij} \neq 0$) according to their size

$$\Delta_{i,1} \geq \Delta_{i,2} \geq \dots \geq \Delta_{i,k_i} \quad (5.9)$$

where

$$k_i := |\text{Pre}(i)| \quad (5.10)$$

is the number of its presynaptic oscillators, called in-degree in graph theory (see Chapter 2). The index $n \in \{1, \dots, k_i\}$ counts the signals that arrive successively. Thus, if $j_n \equiv j_n(i) \in \text{Pre}(i)$ labels the presynaptic oscillator from which i receives its n^{th} signal during the period considered, we have

$$\Delta_{i,n} = \delta_{j_n(i)}. \quad (5.11)$$

In addition, we define

$$\Delta_{i,0} = \delta_i. \quad (5.12)$$

For illustration, let us assume that an oscillator i has exactly two presynaptic oscillators j and j' such that $\text{Pre}(i) = \{j, j'\}$ and $k_i = 2$ (Fig. 5.1a,d). For certain perturbations, oscillator i first receives a signal from oscillator j' and slightly later from oscillator j . This determines the rank order, $\delta_{j'} > \delta_j$, and hence $\Delta_{i,1} = \delta_{j'}$ and $\Delta_{i,2} = \delta_j$ (Fig. 5.1a). Perturbations with the opposite rank order, $\delta_j > \delta_{j'}$, lead to the opposite labeling, $\Delta_{i,1} = \delta_j$ and $\Delta_{i,2} = \delta_{j'}$ (Fig. 5.1d).

We now consider a fixed, arbitrary, perturbation, the rank order of which determines the $\Delta_{i,n}$ according to the inequalities (5.9). Using the phase shift function $H_\varepsilon(\phi)$ (see Eq. (3.18)) and denoting

$$D_{i,n} := \Delta_{i,n-1} - \Delta_{i,n} \quad (5.13)$$

for $n \in \{1, \dots, k_i\}$ we calculate the time evolution of phase-perturbations δ_i satisfying (5.8), starting near $\phi_0(0) = \tau/2$ without loss of generality. The stroboscopic time- T map of the perturbations, $\delta_i \mapsto \delta_i(T)$, is obtained from the scheme given in Table 5.1. The time

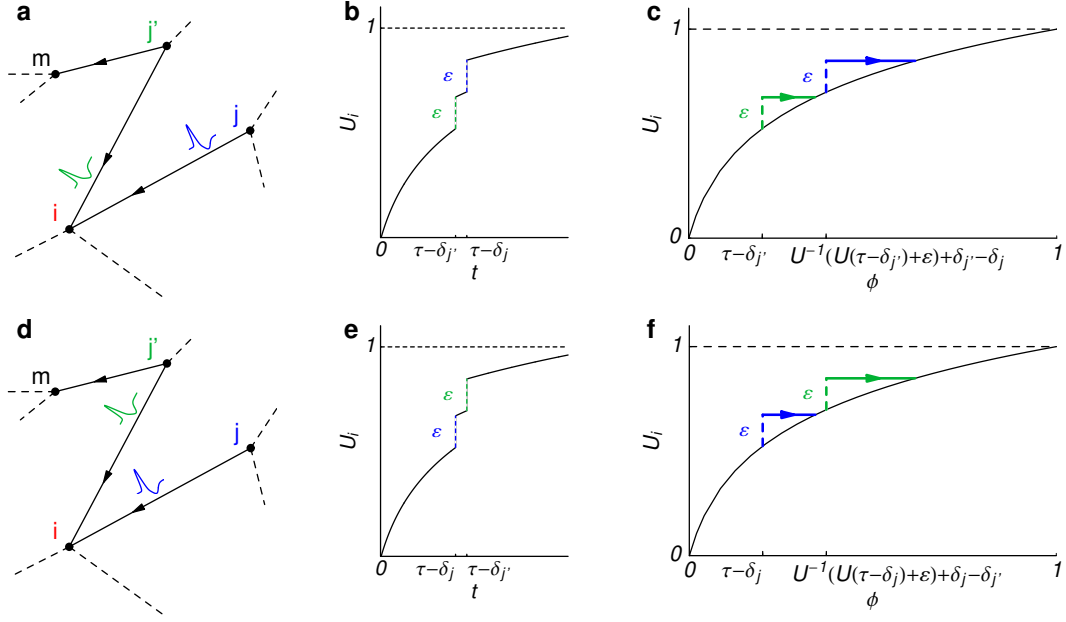


Figure 5.1: Two signals arriving almost simultaneously induce different phase changes, depending on their rank order. The figure illustrates a simple case where $\text{Pre}(i) = \{j, j'\}$ and $\delta_i = 0$, (a)–(c) for $\delta_{j'} > \delta_j$ and (d)–(f) for $\delta_j > \delta_{j'}$. (a), (d) Local patch of the network displaying the reception times of signals that are received by oscillator i . Whereas in (a) the signal from j' arrives before the signal of j , the situation in (d) is reversed. (b), (e) Identical coupling strengths induce identical jumps of the *potential* U but (c), (f) the *phase* jumps these signals induce are different and depend on the order of the incoming signals. For small $|\delta_i| \ll 1$, individual phase jumps are encoded by the $p_{i,n}$, see Eq. (5.18).

| t | $\phi_i(t)$ |
|---|--|
| 0 | $\frac{\tau}{2} + \delta_i =: \frac{\tau}{2} + \Delta_{i,0}$ |
| $\frac{\tau}{2} - \Delta_{i,1}$ | $U^{-1}(U(\tau + D_{i,1}) + \varepsilon_{ij_1}) =: \beta_{i,1}$ |
| $\frac{\tau}{2} - \Delta_{i,2}$ | $U^{-1}(U(\beta_{i,1} + D_{i,2}) + \varepsilon_{ij_2}) =: \beta_{i,2}$ |
| \vdots | \vdots |
| $\frac{\tau}{2} - \Delta_{i,k_i}$ | $U^{-1}(U(\beta_{i,k_i-1} + D_{i,k_i}) + \varepsilon_{ij_{k_i}}) =: \beta_{i,k_i}$ |
| $\frac{\tau}{2} - \Delta_{i,k_i} + 1 - \beta_{i,k_i}$ | reset: $1 \mapsto 0$ |

Table 5.1: Time evolution of oscillator i in response to k_i successively incoming signals from its presynaptic oscillators j_n , $n \in \{1, \dots, k_i\}$, from which i receives the n^{th} signal during this period. The right column gives the phases $\phi_i(t)$ at times t given in the left column. The time evolution is shown for a part of one period ranging from $\phi_i \approx \tau/2$ to reset, $1 \rightarrow 0$, such that $\phi_i = 0$ in the last row. The first row gives the initial condition $\phi_i(0) = \tau/2 + \delta_i$. The following rows describe the reception of the k_i signals during this period whereby the phases are mapped to $\beta_{i,n}$ after the n^{th} signal has been received. The last row describes the reset at threshold such that the respective time $T_i^{(0)} = \tau/2 - \Delta_{i,k_i} + 1 - \beta_{i,k_i}$ gives the time to threshold of oscillator i .

to threshold of oscillator i , which is given in the lower left of the scheme,

$$T_i^{(0)} := \frac{\tau}{2} - \Delta_{i,k_i} + 1 - \beta_{i,k_i} \quad (5.14)$$

is about $\phi_0(0) = \tau/2$ smaller than the period T . Hence the period- T map of the perturbation can be expressed as

$$\delta_i(T) = T - T_i^{(0)} - \frac{\tau}{2} = \beta_{i,k_i} - \alpha + \Delta_{i,k_i} \quad (5.15)$$

where α is given by (5.5).

Equation (5.15) defines a map of one particular perturbation. In general the perturbations of all k_i presynaptic oscillators of oscillator i lead to $k_i!$ different possibilities of ordering. Thus the number of possible maps, μ , is bounded by

$$\max_i k_i! \leq \mu \leq N!. \quad (5.16)$$

Here the minimum is assumed, $\mu = \max_i k_i!$, if only one oscillator has exactly μ presynaptic oscillators and all other oscillators have exactly one presynaptic oscillator. The maximum, $\mu = N!$, is assumed if the oscillators are coupled all-to-all such that all connections are present, $\varepsilon_{ij} \neq 0$ for all i and $j \neq i$. If the coupling is all-to-all and in addition homogeneous, $\varepsilon_{ij} = \varepsilon/N$ for all i and $j \neq i$, all maps are equivalent in the sense that for any pair of maps there is a permutation of oscillator indices that transforms one map onto the other. For general network connectivities, however, there is no such permutation symmetry. For instance, in random networks with N vertices and edges that are independently chosen with identical probability p , the number of maps increases strongly with N .

5.4 First order operators

In order to perform a local stability analysis, we consider the first order approximations of the maps derived in the previous section. Expanding β_{i,k_i} for small $D_{i,n} \ll 1$ one can proof by induction (see Appendix A.2) that to first order

$$\beta_{i,k_i} \doteq \alpha + \sum_{n=1}^{k_i} p_{i,n-1} D_{i,n} \quad (5.17)$$

where

$$p_{i,n} := \frac{U'(U^{-1}(U(\tau) + \sum_{m=1}^n \varepsilon_{ij_m}))}{U'(U^{-1}(U(\tau) + \varepsilon))} \quad (5.18)$$

for $n \in \{0, 1, \dots, k_i\}$ encodes the effect of an individual incoming signal of strength ε_{ij_n} . The statement $x \doteq y$ means that $x = y + \sum_{i,n} \mathcal{O}(D_{i,n}^2)$ as all $D_{i,n} \rightarrow 0$. Substituting the

first order approximation (5.17) into (5.15) using (5.13) leads to

$$\delta_i(T) \doteq \sum_{n=1}^{k_i} p_{i,n-1}(\Delta_{i,n-1} - \Delta_{i,n}) + \Delta_{i,k_i} \quad (5.19)$$

such that after rewriting

$$\delta_i(T) \doteq p_{i,0}\Delta_{i,0} + \sum_{n=1}^{k_i} (p_{i,n} - p_{i,n-1})\Delta_{i,n} \quad (5.20)$$

to first order in all $\Delta_{i,n}$. Since $\Delta_{i,n} = \delta_{j_n(i)}$ for $n \in \{1, \dots, k_i\}$ and $\Delta_{i,0} = \delta_i$ according to (5.11) and (5.12), this results in a first order map

$$\boldsymbol{\delta}(T) \doteq A\boldsymbol{\delta} \quad (5.21)$$

where the elements of the matrix A are given by

$$A_{ij} = \begin{cases} p_{i,n} - p_{i,n-1} & \text{if } j = j_n \in \text{Pre}(i) \\ p_{i,0} & \text{if } j = i \\ 0 & \text{if } j \notin \text{Pre}(i) \cup \{i\}. \end{cases} \quad (5.22)$$

Because j_n in (5.22) identifies the n^{th} pulse received during this period by oscillator i , the first order operator depends on the rank order of the perturbations, $A = A(\text{rank}(\boldsymbol{\delta}))$. The map $A\boldsymbol{\delta}$ consists of a number of linear operators, the domains of which depend on the rank order of the specific perturbation. Thus $A\boldsymbol{\delta}$ is piecewise linear in $\boldsymbol{\delta}$. It is straightforwardly shown that this map is continuous but in general not differentiable at the domain boundaries where $\delta_i = \delta_j$ for at least one pair i and j of oscillators. In general, signals received at similar times by the same oscillator induce different phase changes: For the above example of an oscillator i with exactly two presynaptic oscillators j and j' and equal coupling strengths, $\varepsilon_{i,j} = \varepsilon_{i,j'}$, the first of the two received signals has a larger effect than the second, by virtue of the concavity of $U(\phi)$. For small $|\delta_i| \ll 1$, this effect is encoded by the $p_{i,n}$ (see Eq. (5.18) and Appendix A.2 for details). Since the matrix elements (5.22) are differences of these $p_{i,n}$ the respective matrix elements $A_{i,j}$ and $A_{i,j'}$ have in general different values depending on which signal is received first. This is induced by the structure of the network together with the jump-like interactions. For networks with homogeneous, global coupling different matrices A can be identified by an appropriate permutation of the oscillator indices. In general, however, this is impossible.

5.5 Bounds on the eigenvalues

In this stability problem, given a network structure, we have to deal with an in general large number of operators instead of a single stability matrix. We treat all these operators simultaneously. To get an intuition about the stability properties of the synchronous state depending on the parameters and the network structure, we study bounds on the eigenvalues of these operators.

5.5.1 General properties of matrix elements

The matrix elements defined in Eqs. (5.21) and (5.22) are normalized row-wise,

$$\sum_{j=1}^N A_{ij} = A_{ii} + \sum_{\substack{j=1 \\ j \neq i}}^N A_{ij} \quad (5.23)$$

$$= A_{ii} + \sum_{n=1}^{k_i} A_{ij_n} \quad (5.24)$$

$$= p_{i,0} + \sum_{n=1}^{k_i} (p_{i,n} - p_{i,n-1}) \quad (5.25)$$

$$= p_{i,k_i} \quad (5.26)$$

$$= 1 \quad (5.27)$$

for all i . Here the second last equality holds because the telescope sum equals $p_{i,k_i} - p_{i,0}$. Therefore, every matrix A has the trivial eigenvalue

$$\lambda_1 = 1 \quad (5.28)$$

corresponding to the eigenvector

$$v_1 = (1, 1, \dots, 1)^\top \quad (5.29)$$

that reflects the time-translation invariance of the system. In addition, we note that the diagonal elements

$$A_{ii} = p_{i,0} = \frac{U'(\tau)}{U'(U^{-1}(U(\tau) + \varepsilon))} =: A_0 \quad (5.30)$$

are identical for all i . Since U is monotonically increasing, $U'(\phi) > 0$ for all ϕ , the diagonal elements are positive,

$$A_0 > 0. \quad (5.31)$$

It is important to note that A has the properties (5.23)–(5.31) independent of the parameters, the network connectivity, and the specific perturbation considered. Due to the above properties of the stability matrices, bounds on the eigenvalues of a specific matrix A can be obtained from the Gershgorin theorem [94] (see also [95]).

Theorem 5.5.1 (Gershgorin). *Given an $N \times N$ matrix $A = (A_{ij})$ and disks*

$$K_i := \{z \in \mathbb{C} \mid |z - A_{ii}| \leq \sum_{\substack{j=1 \\ j \neq i}}^N |A_{ij}|\} \quad (5.32)$$

for $i \in \{1, \dots, N\}$. Then the union

$$K := \bigcup_{i=1}^N K_i \quad (5.33)$$

contains all eigenvalues of A .

Let us remark that for real matrices A the disks K_i in the complex plane are centered on the real axis at $A_{ii} = A_0$.

5.5.2 Eigenvalues for inhibitory coupling

As an example application of this theorem to the above eigenvalue problem, we consider the class of networks of inhibitorily coupled oscillators, where all $\varepsilon_{ij} \leq 0$ and $\varepsilon < 0$. In these cases, all nonzero matrix elements A_{ij} are positive: Since $U(\phi)$ is monotonically increasing, $U' > 0$, and concave (down), $U'' < 0$, its derivative U' is positive and monotonically decreasing. Thus all $p_{i,n}$ (Eq. (5.18)) are positive, bounded above by one,

$$0 < p_{i,n} \leq 1, \quad (5.34)$$

and increase with n ,

$$p_{i,n-1} < p_{i,n}. \quad (5.35)$$

Hence the nonzero off-diagonal elements are positive, $A_{ij} = p_{i,n} - p_{i,n-1} > 0$ such that

$$A_{ij} \geq 0 \quad (5.36)$$

for all $i, j \in \{1, \dots, N\}$ and

$$0 < A_0 < 1. \quad (5.37)$$

As a consequence, for inhibitorily coupled oscillators,

$$\sum_{\substack{j=1 \\ j \neq i}}^N |A_{ij}| = \sum_{j=1}^N A_{ij} - A_{ii} = 1 - A_0 \quad (5.38)$$

such that all Gershgorin disks K_i are identical and the disk

$$K_i = K = \{z \in \mathbb{C} \mid |z - A_0| \leq 1 - A_0\} \quad (5.39)$$

contains all eigenvalues of A . This disk K contacts the unit disk from the inside at the trivial eigenvalue $z = \lambda_1 = 1$ (Fig. 5.2).

A stronger result can be derived for strongly connected networks. If the network is strongly connected, the resulting stability matrix A is irreducible such that the Perron-Frobenius theorem [96–99] (see also [100, 101]) is applicable.

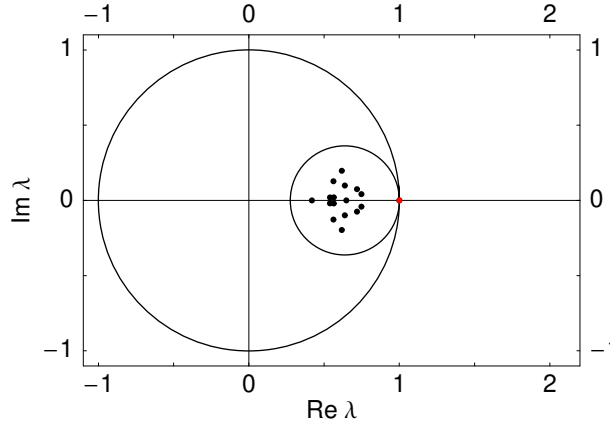


Figure 5.2: Eigenvalues in the complex plane for inhibitory coupling. The Gershgorin disk, that contacts the unit disk from the inside, contains all eigenvalues of the stability matrices A . Black dots show eigenvalues of a specific stability matrix for a network of $N = 16$ oscillators (in which every connection is present with probability $p = 0.25$) with coupling strengths $\varepsilon_{ij} = \varepsilon/k_i$, $\varepsilon = -0.2$, $\tau = 0.15$, and a particular rank order of the perturbation.

Theorem 5.5.2 (Perron-Frobenius). *Let A be an $N \times N$ irreducible matrix with all its elements real and non-negative. Then*

1. *A has a real positive eigenvalue λ_{max} , the maximal eigenvalue, which is simple and such that all eigenvalues λ_i of A satisfy $|\lambda_i| \leq \lambda_{max}$.*
2. *The eigenvector corresponding to λ_{max} has all its components real and positive.*
3. *If A has k eigenvalues $\lambda_1 = \lambda_{max}, \lambda_2, \dots, \lambda_k$ of modulus $|\lambda_i| = \lambda_{max}$ for $i \in \{1, \dots, k\}$ then these eigenvalues are the distinct roots of $\lambda_{max}^k = \lambda_i^k$.*
4. *Under the condition of (3.), the set of eigenvalues $\Lambda = \{\lambda_1, \dots, \lambda_N\}$ of A is invariant under a phase shift of $e^{2\pi i/k}$, i.e. $e^{2\pi i/k}\Lambda = \Lambda$.*
5. *If any element of A is increased, then λ_{max} is increased.*

Part 1 of the Perron-Frobenius theorem implies, that the eigenvalue that is largest in absolute value, here $\lambda_1 = 1$, is unique for strongly connected networks. The Gershgorin theorem guarantees that eigenvalues λ of modulus one are degenerate at one, $\lambda = \lambda_1 = 1$. Taken together, for strongly connected networks, the non-trivial eigenvalues λ_i satisfy

$$|\lambda_i| < 1 \quad (5.40)$$

for $i \in \{2, \dots, N\}$. This indicates that the synchronous state is stable for inhibitory couplings. The proof of stability, however, requires further careful analysis, that is given in Sec. 5.6.

5.5.3 Eigenvalues for excitatory coupling

Let us briefly discuss excitatorily coupled oscillators, where all $\varepsilon_{ij} \geq 0$ and $\varepsilon > 0$. Here the analysis proceeds similar to the case of inhibitory coupling. Due to the monotonicity and concavity of $U(\phi)$, we obtain

$$p_{i,n} \geq 1 \quad (5.41)$$

as well as a decrease with n ,

$$p_{i,n-1} > p_{i,n}, \quad (5.42)$$

such that $A_{i,jn} = p_{i,n} - p_{i,n-1} < 0$ and thus

$$A_{ij} \leq 0 \quad (5.43)$$

for $i \in \{1, \dots, N\}$ and $j \neq i$ and

$$A_{ii} = A_0 > 1. \quad (5.44)$$

Consequently, for excitatorily coupled oscillators,

$$\sum_{\substack{j=1 \\ j \neq i}}^N |A_{ij}| = - \sum_{\substack{j=1 \\ j \neq i}}^N A_{ij} = A_0 - 1 \quad (5.45)$$

such that again all Gershgorin disks K_i are identical and

$$K_i = K = \{z \in \mathbb{C} \mid |z - A_0| \leq A_0 - 1\}. \quad (5.46)$$

Since $A_0 > 1$, the disk K contacts the unit disk from the outside at $z = \lambda_1 = 1$ (Fig. 5.3). If the network is strongly connected, $\lambda_1 = 1$ is again unique by the Perron-Frobenius theorem for irreducible matrices because it is the largest eigenvalue (in absolute value) of the inverse A^{-1} of A , if the inverse exists. This result indicates that the fully synchronous state is unstable for excitatory couplings, but care has to be taken, as in the case of inhibitory couplings.

5.6 Stability and instability

In Sec. 5.5, we found analytical bounds on the eigenvalues of the stability matrices. However, even if only eigenvalues λ with $|\lambda| \leq 1$ are present, a growth of perturbations might seem to be possible because (i) the eigenspaces of the (asymmetric) matrices A cannot be guaranteed to be orthogonal, and (ii) in general, different matrices A are successively applied to a given perturbation. Due to the non-orthogonality (i) the length $\|\delta\|$ of a given perturbation vector δ might increase during one period. Since the stability matrix and the set of eigenvectors may change due to (ii), the length of the perturbation vector

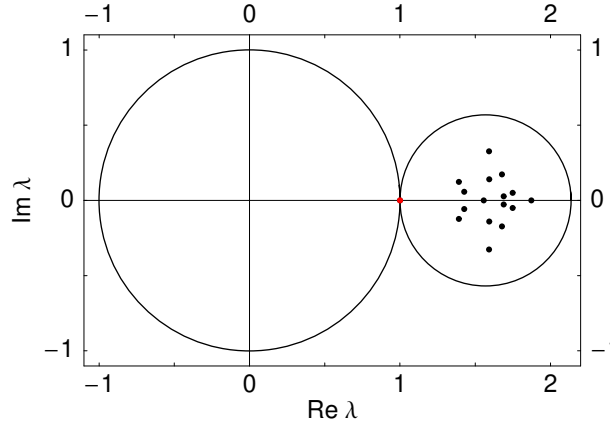


Figure 5.3: Eigenvalues in the complex plane for excitatory coupling. Gershgorin disk, that contacts the unit disk from the outside, contains all eigenvalues of the stability matrices A . Black dots show eigenvalues of a specific stability matrix for a network of $N = 16$ oscillators (in which every connection is present with probability $p = 0.25$) with coupling strength $\varepsilon_{ij} = \varepsilon/k_i$, $\varepsilon = 0.2$, $\tau = 0.15$) and a particular rank order of the perturbation.

might increase in the subsequent period as well. Since this procedure may be iterated, the eigenvalues λ_i of the stability matrices, although satisfying $|\lambda_i| < 1$ for $i \in \{2, \dots, N\}$ and $\lambda_1 = 1$, might not be sufficient for the stability of the synchronous state.

Thus, the eigenvalues of the dynamically changing stability matrices guide the intuition about the stability of the synchronous state as well as about the speed of convergence (in case of stability) or divergence (in case of instability). Nevertheless, stability cannot be directly inferred from the set of eigenvalues. In the following we illustrate the final proof of stability in the simple case of inhibitory coupling where all $A_{ij} \geq 0$ (5.36). We complete this section by a brief outline of the proof of instability for excitatory coupling where $A_{ii} > 1$ but $A_{ij} \leq 0$ for all $j \neq i$.

5.6.1 Stability for inhibitory coupling

The proof of plain (non-asymptotic) stability is simple. Given the fact that for inhibition $\sum_{j=1}^N A_{ij} = 1$ and $A_{ij} \geq 0$, the synchronous state is stable because a given perturbation $\delta = \delta(0)$ satisfies

$$\|\boldsymbol{\delta}(T)\| := \max_i |\delta_i(T)| \quad (5.47)$$

$$= \max_i \left| \sum_{j=1}^N A_{ij} \delta_j \right| \quad (5.48)$$

$$\leq \max_i \sum_j |A_{ij}| |\delta_j| \quad (5.49)$$

$$\leq \max_i \sum_j |A_{ij}| \max_k |\delta_k| \quad (5.50)$$

$$= \max_i \sum_j A_{ij} \max_k |\delta_k| \quad (5.51)$$

$$= \max_k |\delta_k| \quad (5.52)$$

$$= \|\boldsymbol{\delta}\|. \quad (5.53)$$

In this section, we use the vector norm

$$\|\boldsymbol{\delta}\| := \max_i \delta_i. \quad (5.54)$$

Thus the length of a perturbation vector does not increase during one period implying that it does not increase for an arbitrary long time. This result is independent of the connectivity structure of the network, the special choice of parameters, $\varepsilon_{ij} \leq 0$, $\tau > 0$, the potential function $U(\phi)$, and the rank order of the perturbation.

5.6.2 Asymptotic stability for inhibitory coupling

In the following, we present an analysis of asymptotic stability for networks of inhibitorily coupled oscillators assuming that the network satisfies the condition of strong connectivity. We assume here that the directed graph is strongly connected meaning that every vertex can be reached from every other vertex by only following the directed connections. Thus a network is strongly connected, if every oscillator can communicate with every other at least indirectly (cf. also Chapter 2). It is clear that in a disconnected network only the connected components may synchronize completely in the long-term, but these components may not be synchronized among each other. In the proof given below, we do not consider networks that are disconnected. We do also not consider networks that are weakly connected such as two globally coupled sub-networks which are linked by unidirectional connections from one sub-network to the other. Here we prove asymptotic stability for strongly connected networks, a class of networks that are relevant for many applications.

The synchronous state is characterized by a perturbation $\boldsymbol{\delta} \equiv \boldsymbol{\delta}(0)$ that represents a uniform phase shift,

$$\boldsymbol{\delta} = c_1 \mathbf{v}_1 = c_1 (1, 1, \dots, 1)^T \quad (5.55)$$

where $c_1 \in \mathbb{R}$, $|c_1| \ll 1$, and \mathbf{v}_1 is the eigenvector of A corresponding to the eigenvalue $\lambda_1 = 1$ (5.29). Such a perturbation satisfies

$$\boldsymbol{\delta}(T) = A\boldsymbol{\delta} = \boldsymbol{\delta} \quad (5.56)$$

for all matrices $A = A(\text{rank}(\boldsymbol{\delta}))$ independent of the rank order $\text{rank}(\boldsymbol{\delta})$ and thus

$$\|\boldsymbol{\delta}(T)\| = \|\boldsymbol{\delta}\|. \quad (5.57)$$

Now suppose that $\boldsymbol{\delta}$ does not represent the synchronous state or a uniform phase shift,

$$\boldsymbol{\delta} \neq c_1 \mathbf{v}_1 \quad (5.58)$$

for all $c_1 \in \mathbb{R}$. Then one might guess that

$$\|\boldsymbol{\delta}(T)\| < \|\boldsymbol{\delta}\|. \quad (5.59)$$

We assume that (i) $\boldsymbol{\delta}$ is not the synchronous state (5.58) and that (ii) all single-oscillator perturbations are non-negative, $\delta_i \geq 0$. The latter assumption is made without loss of generality, because otherwise a vector proportional to \mathbf{v}_1 can be added such that $\delta_i \geq 0$ is satisfied. The assumption (ii) has the consequence that the components of the perturbation stay non-negative for all times, because $\delta_i(T) = \sum_{j=1}^N A_{ij} \delta_j \geq 0$ for all i such that $\delta_i(lT) \geq 0$ for all i and all $l \in \mathbb{N}$.

For convenience, we define the largest component of the perturbation

$$\delta_M := \max_i \delta_i \quad (5.60)$$

and the second largest component

$$\delta_m := \max\{\delta_i \mid \delta_i < \delta_M\} \quad (5.61)$$

such that $\delta_m < \delta_M$. We also define the index set of maximal components

$$\mathbb{M} := \{j \in \{1, \dots, N\} \mid \delta_j = \delta_M\} \quad (5.62)$$

which is always non-empty. We write $j \notin \mathbb{M}$ if $j \in \{1, \dots, N\} \setminus \mathbb{M}$. With these definitions

we find

$$\delta_i(T) = \sum_{j=1}^N A_{ij} \delta_j \quad (5.63)$$

$$= \sum_{j \in \mathbb{M}} A_{ij} \delta_j + \sum_{j \notin \mathbb{M}} A_{ij} \delta_j \quad (5.64)$$

$$\leq \sum_{j \in \mathbb{M}} A_{ij} \delta_M + \sum_{j \notin \mathbb{M}} A_{ij} \delta_m \quad (5.65)$$

$$+ \sum_{j \notin \mathbb{M}} A_{ij} \delta_M - \sum_{j \notin \mathbb{M}} A_{ij} \delta_M \quad (5.66)$$

$$= \delta_M \sum_{j=1}^N A_{ij} - (\delta_M - \delta_m) \sum_{j \notin \mathbb{M}} A_{ij} \quad (5.67)$$

$$= \delta_M - (\delta_M - \delta_m) \sum_{j \notin \mathbb{M}} A_{ij}. \quad (5.68)$$

Hence if $\sum_{j \notin \mathbb{M}} A_{ij} > 0$ the norm of the perturbation vector *decreases* in one period,

$$\|\boldsymbol{\delta}(T)\| = \max_i \delta_i(T) < \delta_M = \max_i \delta_i = \|\boldsymbol{\delta}\|. \quad (5.69)$$

There are, however, also perturbations that imply $A_{ij} = 0$ for (at least) one specific i and all $j \notin \mathbb{M}$ such that $\sum_{j \notin \mathbb{M}} A_{ij} = 0$. This is the case if and only if there is an oscillator i that receives input only from oscillators j with maximal components, $\delta_j = \delta_M$, and itself has maximal component, $\delta_i = \delta_M$. So suppose that

$$\exists i \in \{1, \dots, N\} \forall j \in \text{Pre}(i) \cup \{i\} : \delta_j = \delta_M, \quad (5.70)$$

i.e. $\text{Pre}(i) \cup \{i\} \subset \mathbb{M}$. Then $\delta_i(T) = \delta_M$ for this oscillator i and hence

$$\max_i \delta_i(T) = \delta_M \quad (5.71)$$

such that the norm of the perturbation vector does *not decrease* within one period.

Nevertheless, if the network is strongly connected, the norm of the perturbation vector is reduced in at most $N - 1$ periods: We know that if and only if there is no oscillator i satisfying (5.70), the norm will be reduced (5.69) because $\sum_{j \notin \mathbb{M}} A_{ij} > 0$ for all i by (5.68). So to have $\max_i \delta_i(T) = \delta_M$ one needs one oscillator i that satisfies (5.70), i.e. i and $\text{Pre}(i)$ have to have maximal components. If the vector norm stays maximal another period,

$$\max_i \delta_i(2T) = \delta_M, \quad (5.72)$$

not only all $j \in \{i\} \cup \text{Pre}(i)$ but also all $j \in \text{Pre}(\text{Pre}(i))$ have to have maximal components, $\delta_j = \delta_M$. Iterating this l times, leads to the condition

$$\begin{aligned} \max_i \delta_i(lT) = \delta_M &\Leftrightarrow \\ \exists i \forall j \in \{i\} \cup \text{Pre}(i) \cup \text{Pre}^{(2)}(i) \cup \dots \cup \text{Pre}^{(l)}(i) : \delta_j = \delta_M \end{aligned} \quad (5.73)$$

where

$$\text{Pre}^{(l)}(i) := \underbrace{\text{Pre} \circ \text{Pre} \circ \dots \circ \text{Pre}}_{l \text{ times}}(i) \quad (5.74)$$

is the set of oscillators, that is connected to oscillator i via a sequence of exactly l directed connections.

Since for a strongly connected network the union of all presynaptic oscillators and their respective presynaptic oscillators is the set of all oscillators

$$\{i\} \cup \text{Pre}(i) \cup \text{Pre}^{(2)}(i) \cup \dots \cup \text{Pre}^{(l)}(i) = \{1, \dots, N\} \quad (5.75)$$

for $l \geq N - 1$, this leads to the conclusion that

$$\max_i \delta_i((N - 1)T) = \delta_M \Rightarrow \forall j : \delta_j = \delta_M \quad (5.76)$$

such that

$$\boldsymbol{\delta} = \delta_M \mathbf{v}_1 \quad (5.77)$$

contrary to the assumption (5.58). Note that for a given network connectivity, (5.75) is satisfied for any $l \geq l_c$ where l_c is the diameter of the underlying network (see Chapter 2), the longest directed connection path between any two oscillators in the network. The diameter is maximal, $l_c = N - 1$, only for the ring of N oscillators.

Hence, after at most l_c periods, the norm of the perturbation vector decreases,

$$\|\boldsymbol{\delta}(lT)\| < \|\boldsymbol{\delta}\| \quad (5.78)$$

for $l \geq l_c$. Since $\|\boldsymbol{\delta}(ml_c T)\|$ is strictly monotonically decreasing with $m \in \mathbb{N}$ and bounded below by zero, the limit

$$\boldsymbol{\delta}^\infty := \lim_{m \rightarrow \infty} \boldsymbol{\delta}(ml_c T) \quad (5.79)$$

exists. If $\boldsymbol{\delta}^\infty \neq c_1 \mathbf{v}_1$ the vector norm would be reduced as implied by the above considerations. Thus we find that

$$\boldsymbol{\delta}^\infty = c_1 \mathbf{v}_1 \quad (5.80)$$

because the uniform components $c_1 \mathbf{v}_1$ of the original perturbation $\boldsymbol{\delta}$ does not change under the dynamics (see Eq. (5.56)). Hence the synchronous state is asymptotically stable for any strongly connected network of inhibitorily coupled oscillators. This completes the proof.

5.6.3 Instability for excitatory coupling

The synchronous state is unstable for excitatory coupling, where $\varepsilon_{ij} \geq 0$. Let us briefly outline the proof. For excitatory coupling the diagonal element is larger than one, $A_{ii} = A_0 > 1$, and all off-diagonal elements are non-positive, $A_{ij} \leq 0$ for $i \neq j$. We choose a perturbation $\boldsymbol{\delta} = \boldsymbol{\delta}(0)$ such that

$$\sum_{i=1}^N \delta_i = 0. \quad (5.81)$$

This choice is made without loss of generality because one can always add a uniform component vector $c_1 \mathbf{v}_1$ (5.55), that will not change under the dynamics. In particular, it follows

$$\|\boldsymbol{\delta}(T)\| := \max_i |\delta_i(T)| \quad (5.82)$$

$$= \max_i \left| \sum_{j=1}^N A_{ij} \delta_j \right| \quad (5.83)$$

$$\geq \max_i \sum_{j=1}^N A_{ij} \delta_j \quad (5.84)$$

$$= \max_i A_0 \delta_i + \sum_{\substack{j=1 \\ j \neq i}}^N A_{ij} \delta_j \quad (5.85)$$

$$\geq A_0 \delta_M + \sum_{\substack{j=1 \\ j \neq i^*}}^N A_{i^*j} \delta_j \quad (5.86)$$

$$\geq A_0 \delta_M + \delta_M \sum_{\substack{j=1 \\ j \neq i^*}}^N A_{i^*j} \quad (5.87)$$

$$= \delta_M \quad (5.88)$$

$$= \|\boldsymbol{\delta}\| \quad (5.89)$$

This derivation proceeds in several steps. The first inequality (5.84) arises because an expression is smaller or equal to its absolute value, $x \leq |x|$. The second inequality (5.86) is achieved by choosing a specific oscillator i^* the phase of which is maximal, $\delta_{i^*} = \delta_M$ and noting that $\max_i x_i \geq x_{i^*}$ for arbitrary expressions x_i and any i^* . The third inequality (5.87) is caused by the fact that $A_{ij} \leq 0$ for all $j \neq i$. Finally, the maximal component of the perturbation is positive, $\delta_M > 0$, because otherwise it would be zero, $\delta_M = 0$, such that all components would be zero given the condition (5.81). Thus the last equality (5.89) holds, $\delta_M = \|\boldsymbol{\delta}\|$. This proves that the norm of the perturbation vector does not decrease with time. Note that the third inequality used above is strict if not all oscillators $j \in \text{Pre}(i^*)$

satisfy $\delta_j = \delta_M$. Similar to the proof of the asymptotic stability for inhibitory coupling, this argumentation may be iterated for strongly connected networks to $\text{Pre}(\text{Pre}(i^*))$ etc., such that the norm of any non-uniform perturbation increases after at most $N - 1$ periods, rendering the synchronous state unstable for excitatory coupling.

5.7 Coexistence of regular and irregular dynamics

The analysis of the previous section shows that for inhibitory coupling the synchronous state is stable, independent of the parameters and the network structure. In networks of various structures, this synchronous state, which displays regular dynamics, is not the only attractor. In the following, we show the coexistence with another state that exhibits irregular dynamics and persists in random networks with strong inhibitory interactions.

To be specific, we consider integrate-and-fire oscillators where $U(\phi) = U_{\text{IF}}(\phi) = I(1 - e^{-\phi T_{\text{IF}}})$ and $T_{\text{IF}} = \ln(I/(I - 1))$, setting $\gamma = 1$ in Eq. (3.32). Numerical simulations of networks of different structures demonstrate that for a network at given parameters the synchronous state often coexists with one or more other attractors. For instance, we have seen in Chapter 4, Fig. 4.2, that it coexists with cluster states in globally, homogeneously coupled networks. A particularly important example of an attractor, which occurs in randomly connected networks with strong interactions, is a balanced state (cf. [28–30]) that exhibits irregular dynamics. In this balanced state, found originally in binary neural networks [28, 29], inhibitory and excitatory inputs cancel each other on average but fluctuations lead to a variability of the membrane potential and a high irregularity in firing times (see also [30]). Figures 5.4a,b display sample trajectories of the potentials $U(\phi_i)$ of three oscillators for the same random network, making obvious the two distinct kinds of coexisting dynamics. Whereas in the synchronous state all oscillators display identical periodic dynamics, in the balanced state oscillators fire irregularly, asynchronous, and in addition differ in their firing rates.

The latter dynamical difference is quantified by a histogram p_ν of oscillator rates (Fig. 5.4c)

$$\nu_i = (\langle t_{i,n+1} - t_{i,n} \rangle_n)^{-1}, \quad (5.90)$$

the reciprocal values of the time averaged inter-spike intervals. Here the $t_{i,n}$ are the times when oscillator i fires the n^{th} time. The temporal irregularity of the firing-sequence of single oscillators i is measured by the coefficient of variation

$$CV_i = (\nu_i^2 \langle (t_{i,n+1} - t_{i,n})^2 \rangle_n - 1)^{\frac{1}{2}}, \quad (5.91)$$

defined as the ratio of the standard deviation of the inter-spike intervals and their average. A histogram p_{CV} of the CV_i (Fig. 5.4d) shows that the irregular state exhibits coefficients

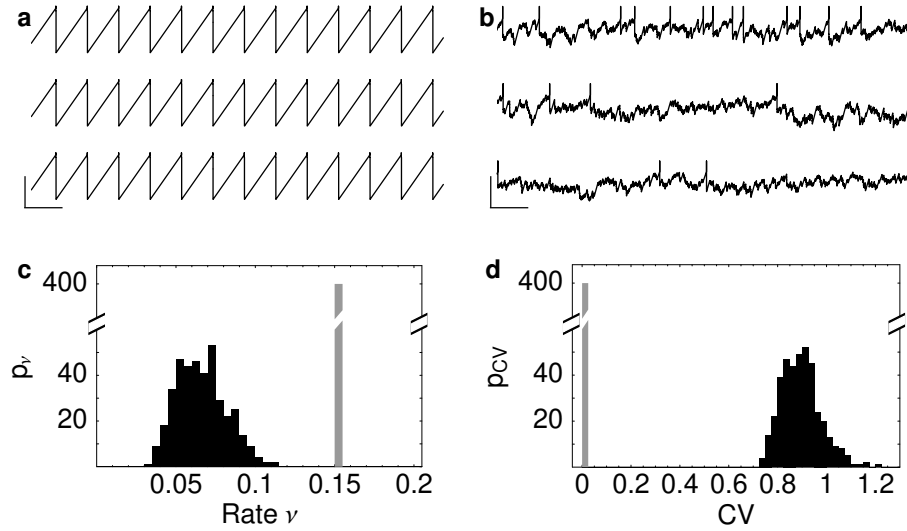


Figure 5.4: Coexistence of (a) synchronous and (b) irregular dynamics in a random network ($N = 400$, $p = 0.2$, $I = 4.0$, $\varepsilon = 16.0$, $\tau = 0.035$). (a),(b): Trajectories of the potential $U(\phi_i)$ of three oscillators (angular bars: time scale (horizontal) $\Delta t = 8$; potential scales (vertical) (a) $\Delta U = 8$, (b) $\Delta U = 2$; spikes of height $\Delta U = 1$ added at firing times). (c),(d): Distributions (c) p_ν of rates and (d) p_{CV} of the coefficient of variation, displayed for the irregular (dark gray) and synchronous (light gray) dynamics.

of variation near one, the coefficient of variation of a Poisson process. Such irregular states occur robustly when changing parameters and network topology.

The coexistence of two qualitatively different kinds of dynamics leads to the question how regular dynamics can be induced when the system currently is in an irregular state and vice versa. A simple mechanism to synchronize oscillators that are in a state of irregular firing is the delivery of two sufficiently strong external excitatory (phase-advancing) *pulses* that are separated by a time $\Delta t \in (\tau, 1)$, cf. Fig. 5.5. The first pulse then leads to a synchronization of phases due to simultaneous suprathreshold input (cf. Eq. (3.18)). If there are traveling signals that have been sent but not received at the time of the first pulse, a second pulse after a time $\Delta t > \tau$ is needed that synchronizes the phases after all internal signals have been received. This synchronous state is not affected by *small random perturbations*, whereas *large random perturbations* lead back to irregular dynamics (Fig. 5.5). Mechanisms for both directions of switching may be realized in biological neural networks by external neuronal populations: While strong external pulses may be generated by external neurons that are highly synchronized, a random perturbation can be realized by neurons which fire irregularly.

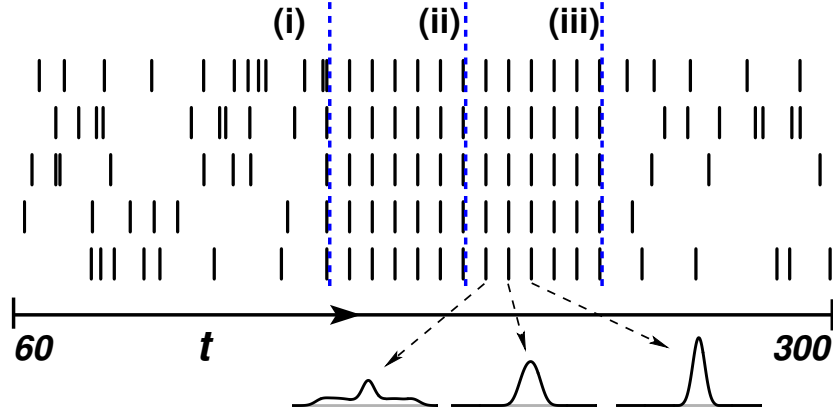


Figure 5.5: Switching between irregular and synchronous dynamics ($N = 400$, $p = 0.2$, $I = 4.0$, $\varepsilon = 16.0$, $\tau = 0.14$). Firing times of five oscillators are shown in a time window $\Delta t = 240$. Vertical dashed lines mark external perturbations: (i) large excitatory pulses lead to synchronous state, (ii) a small random perturbation ($|\Delta\phi_i| \leq 0.18$) is restored, (iii) a sufficiently large random perturbation ($|\Delta\phi_i| \leq 0.36$) leads to an irregular state. Bottom: Time evolution of the spread of the spike times after perturbation (ii), total length $\Delta t = 0.25$ each.

5.8 Summary and discussion

In summary, we analyzed the stability of synchronous states in arbitrary connected networks of pulse-coupled oscillators. For generally structured networks, the exciting problem of multiple stability operators arises (cf. also [62]). We analyzed this multi-operator problem exactly. For both inhibitory and excitatory couplings, we determined analytical bounds on the eigenvalues of all operators at once. Given the multi-operator property, stability does not follow directly from the considerations of the eigenvalues. We therefore completed the stability analysis for two examples. For networks with inhibitory couplings ($\varepsilon_{ij} \leq 0$) we found that the synchronous state is stable and, under mild constraints (strong connectivity of the underlying network), also asymptotically stable, independent of the parameters and the connectivity structure. For excitatory couplings ($\varepsilon_{ij} \geq 0$), the synchronous state was shown to be unstable, at least for strongly connected networks. Furthermore, we presented the first demonstration that in random networks with strong inhibitory interactions, states exhibiting two qualitatively different dynamics, a synchronous state exhibiting regular and a balanced state exhibiting irregular dynamics, coexist at the same parameters. We proposed simple mechanisms to switch between these two states.

The stability results obtained in this chapter are valid for finite networks with a general connectivity. In contrast to ordinary stability problems, the eigenvalues of the first order operators do not directly determine the stability here, because different linear operators may act subsequently on a given perturbation vector. Thus the eigenvalues and eigenvectors of an individual matrix alone do not define the local dynamics of the system. This

raises the questions of what determines the asymptotic speed of synchronization and what are necessary conditions for the robustness of the synchronous state against structural perturbations, i.e. conditions necessary to ensure that the local dynamics stays qualitatively similar if the time evolution of the model is slightly modified. For important cases of the model considered here, these issues are considered in the next chapter.

Most previous studies on the dynamics of networks of pulse-coupled units focussed on regular networks or worked in some mean field limit [8, 11, 14, 16–18, 20–22, 24, 30, 53, 55–59, 62, 64, 66]. Moreover, these studies often relied on the analysis of bifurcations from one state to another as an external parameter is changed, see in particular Refs. [21, 24, 60, 63]. Based on the stability analysis developed here, that applies to networks with general connectivity, we have demonstrated that regular synchronous dynamics may coexist with irregular dynamics in sufficiently complex networks. The coexistence of qualitatively different states at identical parameters indicates that bifurcation approaches may often not give a complete picture of the network dynamics, if the network structure is too complex. This fact may well apply not only to networks of pulse-coupled units but also to the dynamics of many other complex networks. In addition, our results emphasize that in complex networks of pulse-coupled units the occurrence of temporally regular and irregular firing patterns may typically reflect the collective state of the network rather than the dynamics of individual units.

It has been hypothesized (see e.g. [61, 88]) that the experimentally observed precisely timed firing patterns in otherwise irregular neural activity might be generated dynamically by the cerebral cortex. Our results provide the first theoretical demonstration that states in which units fire in a temporally highly regular fashion and states with irregular asynchronous activity may be coexisting attractors of a recurrent network. This already applies for random networks. More specifically structured networks may possess a large variety of dynamical states in which firing times are precisely coordinated. A promising direction for future research is thus to adopt the methods developed here for investigating the stability of such states. In particular, these methods may be applied to networks for which the coupling strengths are not normalized and precise temporal firing patterns occur in place of a synchronous state [74].

Chapter 6

Robust synchronization

In the previous chapter we analyzed the stability of the synchronous state in arbitrary connected networks of pulse-coupled oscillators. Due to the network structure, a multi-operator problem arises such that the dynamics in the vicinity of the synchronous state is in general described by a sequence of a large number of different linear operators. As a consequence, the location of the eigenvalues of a single stability matrix does not provide a criterion for stability. Moreover, it remained an open problem whether a generalization beyond the specific class of models considered is possible.

In order to explore these questions, we consider networks of inhibitorily coupled oscillators. In this chapter, we study conditions required if the results obtained in the previous chapter are to be valid for models obtained by a structural perturbation of the original dynamics. We focus on specific models of oscillators from the general class analyzed in Chapter 5. We show that there is a subclass of potential functions in which all operators are degenerate. Interestingly, this subclass is defined by standard leaky integrate-and-fire oscillators if the coupling strengths are suitably chosen. Within this subclass, the local dynamics in the vicinity of the synchronous state is determined by the eigenvalues and eigenvectors of a single matrix. Thus, in contrast to the general multi-operator problem, the eigensystem of this matrix directly characterizes the stability of the synchronous state and the asymptotic speed of synchronization. The eigenvalues also provide necessary conditions for the robustness of the fully synchronous state under small changes of the model dynamics. For symmetric networks, the convergence towards the synchronous state is shown to be equivalent to the convergence of a diffusion process towards its equilibrium. Proceeding from these results, we investigate large random networks of integrate-and-fire oscillators. First, we present numerical evidence that the eigenvalues of a stability matrix for sufficiently large random networks are located in a disk in the complex plane such that there is a gap between that disk and the unit circle. Second, the location and radius of this disk is estimated using the theory of asymmetric Gaussian random matrices. Third, a comparison with numerically determined eigenvalue distributions yields excellent agreement with our

theoretical estimate for a wide range of parameters and network sizes. The chapter ends with a brief summary and an outlook.

6.1 Equivalence of synchronization and diffusion

From the general class of concave potential functions, we specialize to a subclass of potential functions satisfying the condition that all multiple operators derived in Chapter 5 degenerate to a single stability matrix if the coupling strength are suitably chosen. Interestingly, it turns out that the class of standard leaky integrate-and-fire oscillators provides potential functions consistent with this condition.

We start from the class of models used in Chapter 5. A general potential function U that is monotonically increasing, $U'(\phi) > 0$, and concave (down), $U''(\phi) < 0$, yielded stability operators A in the first order map (5.21)

$$\delta(T) \doteq A\delta(0) \quad (6.1)$$

that are defined by (5.22)

$$A_{ij} = \begin{cases} p_{i,n} - p_{i,n-1} & \text{if } j = j_n \in \text{Pre}(i) \\ p_{i,0} & \text{if } j = i \\ 0 & \text{if } j \notin \text{Pre}(i) \cup \{i\}. \end{cases} \quad (6.2)$$

where (5.18)

$$p_{i,n} := \frac{U'(U^{-1}(U(\tau) + \sum_{m=1}^n \varepsilon_{ij_m}))}{U'(U^{-1}(U(\tau) + \varepsilon))} \quad (6.3)$$

describe the effect of the n^{th} signal received by oscillator i within the period considered. Thus, the actual operator applied depends on the rank order of the incoming signals.

Can the multiple operators be made degenerate? Consider a network for which the coupling strengths of all presynaptic oscillators $j \in \text{Pre}(i)$ are identical,

$$\varepsilon_{ij} = \frac{\varepsilon}{k_i} \quad (6.4)$$

for each oscillator i . For such a network, two matrix elements are interchanged at the boundary of the domains of definition of an individual operator. For instance, assume that an oscillator i has exactly two presynaptic oscillators j and j' . If a perturbation is changed such that $\delta_j > \delta_{j'}$ is turned into $\delta_j < \delta_{j'}$, the operator A will change from $A = A^{(1)}$ to $A = A^{(2)}$ where the non-zero off-diagonal elements of row i read

$$A_{ij}^{(1)} = A_{ij_1} = p_{i,1} - p_{i,0} \quad \text{and} \quad A_{ij'}^{(1)} = A_{ij_2} = p_{i,2} - p_{i,1}, \quad (6.5)$$

$$A_{ij}^{(2)} = A_{ij_2} = p_{i,2} - p_{i,1} \quad \text{and} \quad A_{ij'}^{(2)} = A_{ij_1} = p_{i,1} - p_{i,0}, \quad (6.6)$$

respectively. As above, j_1 labels the oscillator presynaptic to i that has sent the first signal to i during the period considered, and j_2 labels the presynaptic oscillator that has sent the second one such that

$$j_1 = j \text{ and } j_2 = j' \quad \Leftrightarrow \quad \delta_j > \delta_{j'}, \quad (6.7)$$

$$j_1 = j' \text{ and } j_2 = j \quad \Leftrightarrow \quad \delta_{j'} > \delta_j. \quad (6.8)$$

Degeneracy of these two, in general distinct, cases requires that

$$A_{ij}^{(k)} \stackrel{!}{=} A_{ij}^{(l)} \quad (6.9)$$

for $k, l \in \{1, 2\}$ or, equivalently,

$$p_{i,2} - p_{i,1} \stackrel{!}{=} p_{i,1} - p_{i,0}. \quad (6.10)$$

If every oscillator $i \in \{1, \dots, N\}$ in the network has k_i presynaptic oscillators, the degeneracy condition is easily generalized to (6.9) with k and l running over all different stability matrices that occur for all possible differently ordered perturbations. Expressed in terms of the $p_{i,n}$, which describe the effect of individual incoming pulses, we obtain

$$p_{i,n} - p_{i,n-1} \stackrel{!}{=} p_{i,m} - p_{i,m-1} \quad (6.11)$$

for all $i \in \{1, \dots, N\}$ and all $n, m \in \{1, \dots, k_i\}$.

If we define

$$q(x_{i,n}) := p_{i,n} = \frac{U'(U^{-1}(U(\tau) + x_{i,n}))}{U'(U^{-1}(U(\tau) + \varepsilon))} \quad (6.12)$$

where

$$x_{i,n} = \sum_{m=1}^n \varepsilon_{ij_m} = \frac{n\varepsilon}{k_i} \quad (6.13)$$

for $n \leq k_i$, the requirement (6.11) is satisfied if

$$q'(x) = \text{const} \quad (6.14)$$

in the relevant interval $x \in [\varepsilon, 0]$. Note that $\varepsilon < 0$ because we consider inhibitory coupling. The first derivative of $q(x)$ satisfies

$$q'(x) \propto \frac{U''(U^{-1}(U(\tau) + x))}{U'(U^{-1}(U(\tau) + x))} =: \frac{U''(h(x))}{U'(h(x))} \quad (6.15)$$

where $h(x) = H_x(\tau) = U^{-1}(U(\tau) + x)$ (see Eq. (3.18)) is an invertible function of x . Together with (6.14) this leads to a differential equation

$$U'' = cU' \quad (6.16)$$

where $c \in \mathbb{R}$ is a constant. The solution $U(\phi) = a + be^{c\phi}$ with constants $a, b, c \in \mathbb{R}$ together with the normalization $U(0) = 0$, $U(1) = 1$, and the monotonicity requirement $U'(\phi) > 0$ yields the one-parameter family of solutions in integrate-and-fire form

$$U(\phi) = U_{\text{IF}}(\phi) = I(1 - e^{-\phi T_{\text{IF}}}) \quad (6.17)$$

where $I > 1$ and $T_{\text{IF}} = \ln(I/(I - 1)) > 0$ (see Eq. (3.32)). This leads to

$$U'_{\text{IF}}(\phi) = IT_{\text{IF}}e^{-\phi T_{\text{IF}}}, \quad (6.18)$$

$$U_{\text{IF}}^{-1}(y) = \frac{1}{T_{\text{IF}}} \ln \left(1 - \frac{y}{I} \right)^{-1}, \quad (6.19)$$

and

$$U_{\text{IF}}^{-1}(U_{\text{IF}}(\phi) + \varepsilon) = \frac{1}{T_{\text{IF}}} \ln \left(e^{-\phi T_{\text{IF}}} - \frac{\varepsilon}{I} \right)^{-1} \quad (6.20)$$

such that

$$U'_{\text{IF}}(U_{\text{IF}}^{-1}(U(\phi) + \varepsilon)) = T_{\text{IF}} (Ie^{-\phi T_{\text{IF}}} - \varepsilon) \quad (6.21)$$

and

$$p_{i,n} = \frac{U'_{\text{IF}}(U_{\text{IF}}^{-1}(U_{\text{IF}}(\tau) + \sum_{m=1}^n \varepsilon_{ij_m}))}{U'_{\text{IF}}(U_{\text{IF}}^{-1}(U_{\text{IF}}(\tau) + \varepsilon))} \quad (6.22)$$

$$= \frac{Ie^{-\tau T_{\text{IF}}} - \sum_{m=1}^n \varepsilon_{ij_m}}{Ie^{-\tau T_{\text{IF}}} - \varepsilon} \quad (6.23)$$

Thus, by construction, if we substitute $\varepsilon_{ij_n} = \varepsilon/k_i$ all non-zero off-diagonal elements

$$A_{ij_n} = p_{i,n} - p_{i,n-1} = \frac{1}{Ie^{-\tau T_{\text{IF}}} - \varepsilon} \frac{\varepsilon}{k_i} \quad (6.24)$$

in one row i of the stability matrix are identical,

$$A_{ij_n} = A_{ij_m}, \quad (6.25)$$

for all $n, m \in \{1, \dots, k_i\}$.

One should note that, given the coupling strengths satisfy (6.4), the condition (6.14) is sufficient but not necessary for degeneracy of all operators. At given parameters and a given network connectivity, one can construct potential functions that fulfill condition (6.14) only on (local) average such that the requirement for identical (non-zero) off-diagonal matrix elements in each row (6.11) is still satisfied. If we do not a priori fix the parameters and the network structure, however, the potential function U_{IF} uniquely leads to operator degeneracy within the class of concave down, increasing functions.

This degeneracy has important consequences: Whereas for the multi-operator problem, the dynamics in the vicinity of the synchronous state is determined by an (unknown but

deterministic) sequence of different linear operators, the dynamics in case of degeneracy is determined by the eigenvectors and eigenvalues of a single matrix A . In particular, the second largest eigenvalue

$$\lambda_m := \max\{|\lambda_i| : |\lambda_i| < 1\} \quad (6.26)$$

of this matrix A determines the asymptotic speed of convergence towards the synchronous state,

$$|\delta((n+l)T)| \sim \lambda_m^n |\delta(lT)| \quad (6.27)$$

for $n \gg 1$ and all $l \in \mathbb{N}$.

Interestingly, the derivation of a condition for degeneracy led to the standard leaky integrate-and-fire model as a subclass of models that imply degeneracy for suitably chosen coupling strengths. A further restriction to networks with symmetric connections yields another remarkable result: Convergence towards the synchronous state is equivalent to convergence towards the equilibrium of a diffusion process.

Due to the normalization of matrix elements, $\sum_j A_{ij} = 1$ for all i , a symmetric stability matrix, where $\sum_i A_{ij} = 1$ for all j , constitutes a stochastic matrix. A symmetric matrix can be achieved by choosing $k_i = k$ for all i and $\varepsilon_{ij} = \varepsilon_{ji} = \varepsilon/k$ for all connections present. For symmetric networks of integrate-and-fire oscillators, the time evolution of a perturbation δ from the synchronous state thus follows the dynamics

$$\delta((n+1)T) = A\delta(nT) \quad (6.28)$$

with a constant, perturbation-independent matrix A .

Since A is a fixed stochastic symmetric matrix, Eq. (6.28) also exactly describes the dynamics of a diffusion process, i.e. a random walk on the network. In this interpretation, $\delta_i(nT)$ is the probability of a walker to be at site i after n steps. The (non-negative) matrix elements $A_{ij} \geq 0$ define the transition probabilities between the sites j and i . The positive diagonal elements $A_{ii} > 0$ model a positive probability of staying at the presently occupied site.

We have thus established complete equivalence between the convergence towards the synchronous state of a network of pulse-coupled oscillators and convergence towards the equilibrium state of a diffusion process, i.e. a random walk, on a network that exhibits the same structure.

6.2 Location of eigenvalues in large random networks

In this section, we present examples for the distribution of eigenvalues of stability matrices describing the dynamics of large asymmetric random networks of integrate-and-fire oscillators in the vicinity of the synchronous state. From the previous chapter (Eq. (5.39)), we

know that all eigenvalues must be located in a Gershgorin disk K in the complex plane that is centered at $A_0 < 1$ (Eq. (5.37)) and has radius $1 - A_0$ such that it contacts the unit circle at $z = 1$ from the inside. In the following, we consider oscillators that interact inhibitorily on two classes of random networks (defined in Subsections 6.2.1 and 6.2.2). The potential functions of the oscillators are of the integrate-and-fire form $U(\phi) = U_{\text{IF}}(\phi) = I(1 - e^{-\phi T_{\text{IF}}})$, where $T_{\text{IF}} = \ln(I/(I - 1))$ setting $\gamma = 1$ in Eq. (3.32). The non-zero coupling strength are chosen according to $\varepsilon_{ij} = \varepsilon/k_i$. We consider only sparsely connected networks which lead to sparse stability matrices where we term a matrix “sparse” if at least a positive fraction of its entries is zero in the limit of large N .

6.2.1 Networks with constant in-degree

The first class of networks is given by random networks in which all oscillators i have the same number $k_i = k$ of presynaptic oscillators which are independently drawn from the set of all other oscillators with uniform probability. When increasing the network size N , the number of connections k per oscillator is kept fixed. We numerically determined the eigenvalues of different stability matrices changing the network size $N \in \{2^6, \dots, 2^{14}\}$, the in-degree $k \in \{2, \dots, 2^8\}$, and the dynamical parameters ε , τ , and I such that $A_0 \in [0.6, 0.9]$. In general, we find that, for sufficiently large N and sufficiently large k , the non-trivial eigenvalues resemble a disk in the complex plane that is centered at about A_0 but has a radius r that is smaller than the upper bound given by the Gershgorin theorem,

$$r < 1 - A_0. \quad (6.29)$$

Note that, due to the time-translation invariance of the system, there is always a trivial eigenvalue $\lambda_1 = 1$ (see Eq. (5.28), Chapter 5). As an example, the eigenvalue distributions in the complex plane are displayed in Fig. 6.1 for specific parameters and differently sized networks.

6.2.2 Networks with constant connection probability

The second class of networks is given by random networks for which every connection between every oscillator i and every other oscillator $j \neq i$ is present with given probability p . When increasing N , this probability is kept fixed such that the number of connections per oscillator is proportional to N . As for the other class of random networks, we find numerically that the distribution of non-trivial eigenvalues resemble disks in the complex plane that are smaller than the Gershgorin disk (6.29) but centered at about the same point A_0 . We numerically determined the distribution of eigenvalues for $N \in \{2^8, \dots, 2^{14}\}$, $p \in [0.01, 0.2]$, and the dynamical parameters ε , τ , and I such that $A_0 \in [0.6, 0.9]$. Figure 6.2 displays examples of eigenvalue distributions for differently sized networks at the same parameters.

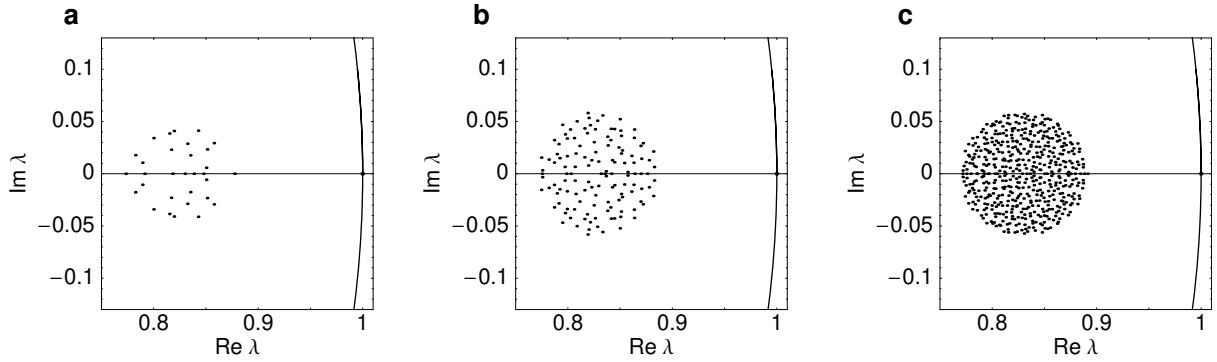


Figure 6.1: Distribution of eigenvalues λ_i in the complex plane for networks of fixed in-degree $k = 8$ and different sizes (a) $N = 32$, (b) $N = 128$, (c) $N = 512$. For large networks, the non-trivial eigenvalues seem to be distributed uniformly on a disk in the complex plane. The arc through the trivial eigenvalue (dot at $z = \lambda_1 = 1$) is a sector of the unit circle. Parameters of integrate-and-fire oscillators are $I = 1.1$, $\varepsilon = -0.2$, $\tau = 0.05$.

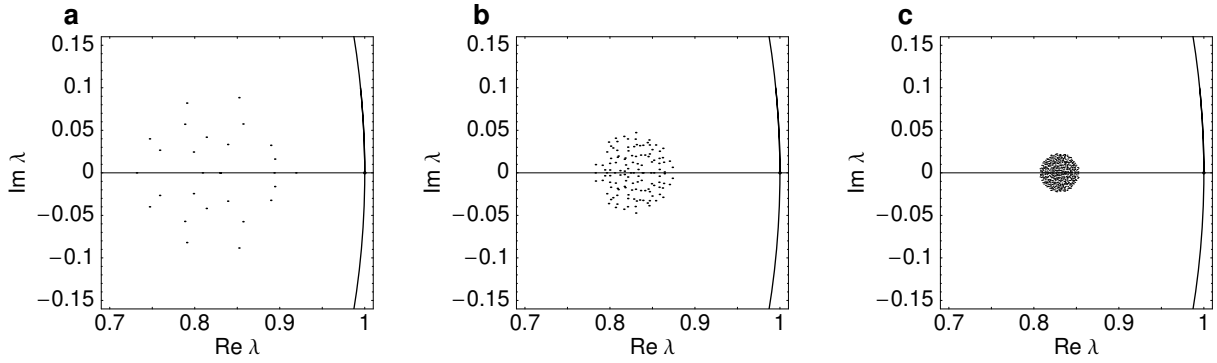


Figure 6.2: Distribution of eigenvalues λ_i in the complex plane for networks of fixed connection probability $p = 0.1$ and different sizes (a) $N = 32$, (b) $N = 128$, (c) $N = 512$. For large networks, the non-trivial eigenvalues seem to be distributed uniformly on a disk in the complex plane, the radius of which shrinks with increasing network size. The arc through the trivial eigenvalue (dot at $z = \lambda_1 = 1$) is a sector of the unit circle. Parameters of integrate-and-fire oscillators are $I = 1.1$, $\varepsilon = -0.2$, $\tau = 0.05$.

6.3 Estimates from random matrix theory

The results of the previous section indicate that the eigenvalues of stability matrices for large asymmetric random networks of integrate-and-fire oscillators are located in disks in the complex plane if the network size N is sufficiently large. If this could be demonstrated independent of specific parameters, it would be guaranteed that all non-trivial eigenvalues are separated from the unit circle. Thus the main condition required for the robustness of the stable synchronous state under a structural perturbation to the dynamics of the system would be satisfied.

How can we estimate the location of the eigenvalues? Since we are considering random networks, a natural starting point is the theory of large random matrices. Random matrix theory has been investigated intensively since the early 1950s [102] (see also [103, 104]) and is nowadays accepted as a valuable tool for both qualitative and quantitative description of spectral properties of complex systems. For instance, it describes level correlations in nuclear physics [105] as well as quantum mechanical aspects of chaos [106, 107]. In applications of random matrix theory to physical problems, it is generally assumed that the details of the physical system are less important for many statistical properties of interest. Often it turns out that important statistical properties such as the distribution of spacings of energy levels in quantum systems are well described by the respective properties of random matrices that respect the same symmetries as the physical system. Both theoretical investigations and applications of random matrix theory have focussed on symmetric matrices. Asymmetric matrices are less well understood and found only limited applicability. In the following, we will evaluate the applicability of random matrix theory for estimating distributions of eigenvalues of asymmetric stability matrices.

6.3.1 Ensembles of symmetric and asymmetric random matrices

For the case of real *symmetric* random $N \times N$ -matrices $J = J^T$ with independent, identically distributed components $J_{ij} = J_{ji}$, it is believed [108, 109] that there are exactly two universality classes. Every ensemble of matrices within one of these universality classes exhibits the same distribution of eigenvalues in the limit of large matrices, $N \rightarrow \infty$ but the eigenvalue distributions are in general different for the two classes. Both universality classes are characterized by specific ensembles of matrices the elements of which are distributed according to a simple probability distribution. The class of sparse matrices is represented by the probability distribution

$$p_{\text{sparse}}(J_{ij}) = \frac{k}{N} \delta\left(J_{ij} - \frac{1}{k}\right) + \left(1 - \frac{k}{N}\right) \delta(J_{ij}) \quad (6.30)$$

where k is the (finite) average number of entries in any row i and $\delta(\cdot)$ is the Dirac delta distribution. The class of Gaussian random matrices is exemplified by a Gaussian distribution of matrix elements

$$p_{\text{Gauss}}(J_{ij}) = (2\pi s^2)^{-\frac{1}{2}} \exp\left(-\frac{N J_{ij}^2}{2s^2}\right). \quad (6.31)$$

To obtain symmetric matrices, one chooses $J_{ij} = J_{ji}$ and $J_{ii} = 0$ for both ensembles. Thus the arithmetic mean of the eigenvalues is zero,

$$[\lambda_i]_i := \frac{1}{N} \sum_{i=1}^N \lambda_i = \frac{1}{N} \sum_{i=1}^N J_{ii} = 0, \quad (6.32)$$

the ensemble average of the matrix elements is zero,

$$\langle J_{ij} \rangle := \int_{-\infty}^{\infty} J p(J) dJ = 0, \quad (6.33)$$

and the variances scale like

$$\sigma^2 = \langle J_{ij}^2 \rangle \doteq \frac{r^2}{N} \quad (6.34)$$

for $N \gg 1$. For the Gaussian symmetric ensemble, it is known [102, 104] that the distribution of eigenvalues $\rho_{\text{Gauss}}^s(\lambda)$ in the limit $N \rightarrow \infty$ is given by Wigner's semicircle law

$$\rho_{\text{Gauss}}^s(\lambda) = \begin{cases} \frac{1}{2\pi r^2} (4r^2 - \lambda^2)^{\frac{1}{2}} & \text{if } |\lambda| \leq 2r \\ 0 & \text{otherwise.} \end{cases} \quad (6.35)$$

The ensemble of sparse matrices [108–111] exhibits a different eigenvalue distribution $\rho_{\text{sparse}}^s(\lambda)$ that depends on the finite number k of nonzero entries per row and approaches the distribution $\rho_{\text{Gauss}}^s(\lambda)$ in the limit of large k such that

$$\lim_{k \rightarrow \infty} \rho_{\text{sparse}}^s(\lambda) = \rho_{\text{Gauss}}^s(\lambda). \quad (6.36)$$

It is important to note that in the limit of large N the distributions ρ_{sparse}^s and ρ_{Gauss}^s eigenvalues depend only on the one parameter r , that is derived from the variance of the matrix elements (6.34).

For real, *asymmetric* matrices (independent J_{ij} and J_{ji}), there are no analytical results for the case of sparse matrices but only for the case of Gaussian random matrices. The Gaussian asymmetric ensemble (e.g. (6.31) with independent J_{ij} and J_{ji}) yields the distribution of complex eigenvalues in a disk in the complex plane [112, 113]

$$\rho_{\text{Gauss}}^a(\lambda) = \begin{cases} (\pi r^2)^{-1} & \text{if } |\lambda| \leq r \\ 0 & \text{otherwise} \end{cases} \quad (6.37)$$

where r from (6.34) is the radius of the disk that is centered at zero. Like in the case of symmetric matrices, this distribution also depends only on one parameter r , that is derived from the variance of the matrix elements.

6.3.2 Stability matrices and the Gaussian asymmetric ensemble

In the numerical studies of stability matrices for random networks (Sec. 6.2), we observed that all non-trivial eigenvalues of sparse stability matrices A are located on or near a disk in the complex plane (Figures 6.1 and 6.2). Since this is also predicted by the theory of asymmetric Gaussian random matrices, let us compare these predictions to numerical results. If the distribution of eigenvalues of sparse asymmetric random matrices ρ_{sparse}^a for $k \gg 1$ is approximately equal to the distribution of Gaussian asymmetric matrices,

$\rho_{\text{sparse}}^a(\lambda) \approx \rho_{\text{Gauss}}^a(\lambda)$, in analogy to the case of symmetric matrices (6.36), and random matrix theory is applicable to the stability matrices at all, we can obtain an analytical estimate for the radii of the disks of eigenvalues.

The elements of the original stability matrix A have an average

$$[A_{ij}] = \frac{1}{N} \sum_{j=1}^N A_{ij} = \frac{1}{N} \quad (6.38)$$

and a second moment

$$[A_{ij}^2] = \frac{1}{N} \sum_{j=1}^N A_{ij}^2 = \frac{1}{N} \left(A_0^2 + \sum_{\substack{j=1 \\ j \neq i}}^N A_{ij}^2 \right) \quad (6.39)$$

where the off-diagonal sum is bounded above and below by

$$\frac{(1 - A_0)^2}{\max_i k_i} \leq \sum_{\substack{j=1 \\ j \neq i}}^N A_{ij}^2 \leq (1 - A_0)^2 \quad (6.40)$$

due to the normalization (5.23).

The variance $\sigma_A^2 = [A_{ij}^2] - [A_{ij}]^2$ given by

$$\sigma_A^2 = \frac{A_0^2}{N} + \frac{\sum_{j \neq i} A_{ij}^2}{N} - \frac{1}{N^2} \quad (6.41)$$

is thus also bounded

$$\frac{A_0^2}{N} + \frac{(1 - A_0)^2}{N(N-1)} - \frac{1}{N^2} \leq \sigma_A^2 \leq \frac{A_0^2 + (1 - A_0)^2}{N} - \frac{1}{N^2} \quad (6.42)$$

because $\max_i k_i \leq N - 1$. The eigenvalues of the original matrix A have the average value

$$[\lambda_i] := \frac{1}{N} \sum_{i=1}^N \lambda_i = \frac{1}{N} \sum_{i=1}^N A_{ii} = A_0. \quad (6.43)$$

To directly compare the ensemble of the stability matrices considered here to random matrices with zero average eigenvalue, $\langle \lambda_i \rangle = 0$, and given variance (6.34), we transform the stability matrix A to

$$A'_{ij} = A_{ij} - A_0 \delta_{ij} \quad (6.44)$$

for $i \in \{1, \dots, N\}$. Here δ_{ij} denotes the Kronecker delta, $\delta_{ij} = 1$ if $i = j$ and $\delta_{ij} = 0$ if $i \neq j$. The transformation to A' shifts all eigenvalues by $-A_0$ and hence the average value of the eigenvalues to

$$[\lambda'_i] = 0. \quad (6.45)$$

In addition

$$[A'_{ij}] = [A_{ij}] - \frac{A_0}{N} = \frac{(1 - A_0)}{N} \quad (6.46)$$

and

$$[A'^2_{ij}] = [A^2_{ij}] - \frac{A_0^2}{N} \quad (6.47)$$

such that the variance is

$$\sigma_{A'}^2 = \sigma_A^2 - \frac{A_0^2}{N} + \frac{2A_0}{N^2} - \frac{A_0^2}{N^2} \quad (6.48)$$

$$= \frac{1}{N} \left(\sum_{\substack{j=1 \\ j \neq i}}^N A_{ij}^2 - \frac{(1 - A_0)^2}{N} \right). \quad (6.49)$$

The eigenvalue distribution of this ensemble of rescaled stability matrices A' for random networks may be compared to the Gaussian asymmetric ensemble with zero average eigenvalue and variance $\sigma_{A'}^2$. In such a comparison, the additional eigenvalue $\lambda_1 = 1$ of A , is neglected. This should not matter for large networks ($N \gg 1$).

It is important to note that we compare the location of eigenvalues of a *sparse* matrix with deterministic non-zero entries at certain random positions with the eigenvalue distribution of the *Gaussian* ensemble, which consists of fully occupied matrices with purely random entries.

If we assume that the eigenvalue distributions for these two ensembles of networks with fixed in-degree and networks with a fixed connection probability are similar to those for random matrices, we obtain an estimate

$$r^2 \approx N\sigma_{A'}^2 \quad (6.50)$$

for the radius of the disk of eigenvalues from Eq. (6.34). For further investigations, we consider the two exemplary classes of large random networks of integrate-and-fire oscillators discussed in Sec. 6.2. If we assume that the stability matrix A has *exactly* k non-zero off-diagonal elements per row and identical coupling strength $\varepsilon_{ij} = \varepsilon/k$ between the integrate-and-fire oscillators, the off-diagonal sum is exactly equal to

$$\sum_{n=1}^k A_{ij_n}^2 = \frac{(1 - A_0)^2}{k}. \quad (6.51)$$

such that the variance of A equals

$$\sigma_A^2 = \frac{A_0^2}{N} + \frac{(1 - A_0)^2}{Nk} - \frac{1}{N^2} \quad (6.52)$$

and the variance of A' is given by

$$\sigma_{A'}^2 = \frac{1}{N}(1 - A_0)^2 \left(\frac{1}{k} - \frac{1}{N} \right). \quad (6.53)$$

If we now take the estimate from random matrix theory r_{RMT} for the radius r of the disk of eigenvalues of the stability matrices, we obtain

$$r_{\text{RMT}} = N^{\frac{1}{2}} \sigma_{A'} = (1 - A_0) \left(\frac{1}{k} - \frac{1}{N} \right)^{\frac{1}{2}}. \quad (6.54)$$

In random networks where all oscillators have *exactly* k presynaptic oscillators, the estimate for the variance of A (and thus of A') is exact. If the random network is constructed by choosing every connection independently with probability p , the variance (6.52) is only an approximation because we replaced $[k_i^{-1}]_i$ by k^{-1} which gives the order of magnitude of the number of connections as a function of N .

6.4 Numerical tests of eigenvalue estimates

We verified this scaling law for different parameters A_0 determined by different I , ε , and τ and found good agreement with numerically determined eigenvalue distributions. We compared the theoretical estimate (6.54) to the numerical data for both ensembles considered in Sec. 6.2.

6.4.1 Networks with constant in-degree

At a given network connectivity and given parameters, we obtained all eigenvalues of the stability matrix A for several network sizes N and in-degrees k . We find that the estimate obtained from random matrix theory well describes the numerically determined eigenvalues. Examples of eigenvalue distributions for matrices at fixed k and three different N are shown in Fig. 6.3.

There are several ways to numerically estimate the radius of the disk of eigenvalues. For illustration, we use three different estimators here. The real part estimator

$$r_{\text{Re}} := \frac{1}{2} \left(\max_{i \neq 1} \text{Re}(\lambda_i) - \min_{i \neq 1} \text{Re}(\lambda_i) \right) \quad (6.55)$$

estimates the radius from the maximum spread of eigenvalues parallel to the real axis. Typically, r_{Re} should give an estimate that is too low compared to the radius obtained

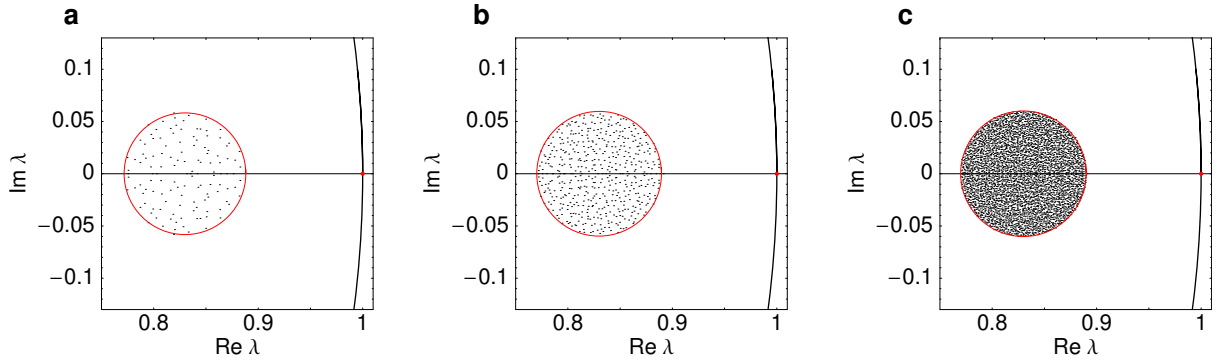


Figure 6.3: Distribution of eigenvalues in the complex plane for networks with fixed in-degree $k = 8$ for different network sizes (a) $N = 128$, (b) $N = 512$, (c) $N = 4096$. The disks are centered at A_0 and have radius r_{RMT} , the estimate obtained from random matrix theory. The arc through the trivial eigenvalue $z = \lambda_1 = 1$ is a sector of the unit circle. Parameters of integrate-and-fire oscillators are $I = 1.1$, $\varepsilon = -0.2$, $\tau = 0.05$.

from the eigenvalues of an ensemble of matrices because it measures the maximal spread in one direction only. This is circumvented by the radial estimator

$$r_{\text{rad}} := \max_{i \neq 1} |\lambda_i - (A_0 - (1 - A_0)N^{-1})| \quad (6.56)$$

that finds the maximum distance of any non-trivial eigenvalues from the average of the non-trivial eigenvalues, $\langle \lambda_i \rangle_{i \neq 1} = A_0 - (1 - A_0)N^{-1} + \mathcal{O}(N^{-2})$. This estimator should yield an approximation that may be too large compared to the respective ensemble average. The average estimator

$$r_{\text{av}} := \frac{3}{2} \frac{1}{N-1} \sum_{i=2}^N |\lambda_i - (A_0 - (1 - A_0)N^{-1})| \quad (6.57)$$

estimates the radius r of a circle from the average distance $\langle d \rangle$ of eigenvalues from its center, because

$$\langle d \rangle = \int_0^{2\pi} \int_0^r r'^2 \rho(r') dr' d\varphi = \frac{2}{3} r \quad (6.58)$$

if we assume a uniform $\rho(r') = 1/(\pi r^2)$ for $r' < r$ and $\rho(r') = 0$ otherwise (6.37). This estimate has the advantage, that it contains information from all eigenvalues in contradistinction to the two other estimators. Its disadvantage is that one has to assume a priori a uniform distribution of non-trivial eigenvalues. As displayed in Fig. 6.4, all three estimators converge towards the radius predicted by the random matrix model for large N and given in-degree k . Varying the in-degree k at fixed N also yields excellent agreement between the numerical data and the theoretical predictions for sufficiently large N and k . An example is displayed in Fig. 6.5.

For both, networks of fixed k and networks of fixed p , there are deviations for small and even for intermediate N , because the estimate r_{RMT} was obtained from random matrix

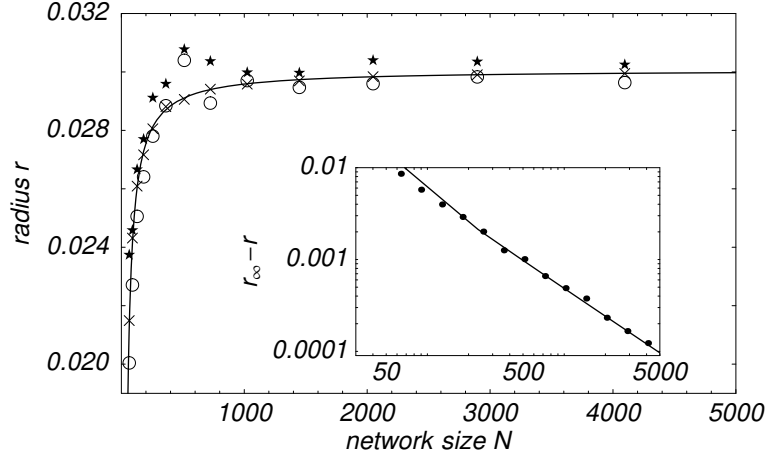


Figure 6.4: Scaling of the radius r of the disk of non-trivial eigenvalues with the network size N at fixed in-degree $k = 32$ ($I = 1.1$, $\varepsilon = -0.2$, $\tau = 0.05$). Main panel displays the radius r as a function of network size N . Symbols display r_{rad} (\star), r_{av} (\times) and r_{Re} (\circ). Inset displays $r_{\infty} - r$ as a function of N on a doubly logarithmic scale, where $r_{\infty} = (1 - A_0)k^{-1/2}$. Dots display numerical data of r_{av} . In the main panel and the inset, lines are the theoretical estimate $r_{\text{RMT}} = (1 - A_0)(1/k - 1/N)^{1/2}$.

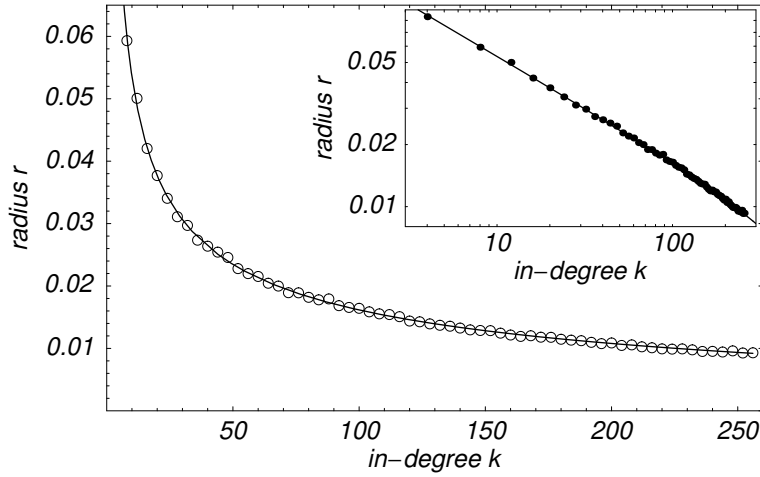


Figure 6.5: Scaling of the radius r of the disk of non-trivial eigenvalues with the in-degree k for random networks of $N = 1024$ oscillators ($I = 1.1$, $\varepsilon = -0.2$, $\tau = 0.05$). Main panel displays the radius r as a function of in-degree k . Inset displays the same data on a doubly logarithmic scale. Symbols display numerical results, using the average estimator r_{av} , lines are the theoretical estimate $r_{\text{RMT}} = (1 - A_0)(1/k - 1/N)^{1/2}$.

theory that is exact only in the limit $N \rightarrow \infty$, and the finite-size scaling of r_{RMT} was assumed to resemble the scaling of the variance of finite matrices. Furthermore, as discussed above, the numerical estimators of the radius rely on assumptions that are fulfilled only approximately. For sufficiently large networks, however, the theoretical estimate agrees well with the numerical data.

Thus there is a gap of size

$$\Delta = 1 - A_0 - r_\infty \quad (6.59)$$

between the non-trivial eigenvalues for large networks and the unit circle, where

$$r_\infty := \lim_{N \rightarrow \infty} r_{\text{RMT}} = (1 - A_0)k^{-1/2}. \quad (6.60)$$

This indicates that the stability of the synchronous state in the model system considered is robust, i.e., sufficiently small perturbations to the systems dynamics will not alter the stability results.

Nevertheless, there is an important restriction to these results. Given a fixed in-degree k , the limit $N \rightarrow \infty$ is *not* described by the theory derived in the previous section, because the structure of the network considered and thus the structure of the stability matrices is only well defined if the network is not connected in the sense that every oscillator has at least one presynaptic oscillator. However, the probability that at least one oscillator is disconnected from the remaining network approaches one with increasing network size. Thus eigenvalue estimates of stability matrices of networks with fixed in-degree k are only reasonably described for network sizes that are large, $N \gg 1$, but not in the limit $N \rightarrow \infty$.

6.4.2 Networks with constant connection probability

If we assume that every connection is present with a constant probability p , the network will be connected with probability one in the limit $N \rightarrow \infty$ because the number of presynaptic oscillators k_i follows a binomial distribution with average pN and standard deviation $(p(1-p)N)^{1/2}$. In this limit, the radius of the disk of eigenvalues decreases with increasing network size N , see Fig. 6.6.

In order to verify the scaling behavior of the radius of the eigenvalue disk for large stability matrices A , we numerically determined the eigenvalues (6.26)

$$\lambda_m = \{|\lambda_i| : |\lambda_i| < 1\} \quad (6.61)$$

that are second largest in absolute value. For sufficiently large N , the theoretical estimate $\lambda_m \approx A_0 + r_{\text{RMT}}$ agrees well with the numerical data (Fig. 6.7). The radius approaches zero for large networks such that the eigenvalue second largest in absolute value converges towards the center A_0 of the disk. In conclusion, for large networks, all non-trivial eigenvalues are located near A_0 and are thus bounded away from the unit circle. This implies that

the speed of synchronization that is determined by λ_m increases with increasing network size. Moreover, the condition necessary for robustness against structural perturbations of the systems dynamics is satisfied.

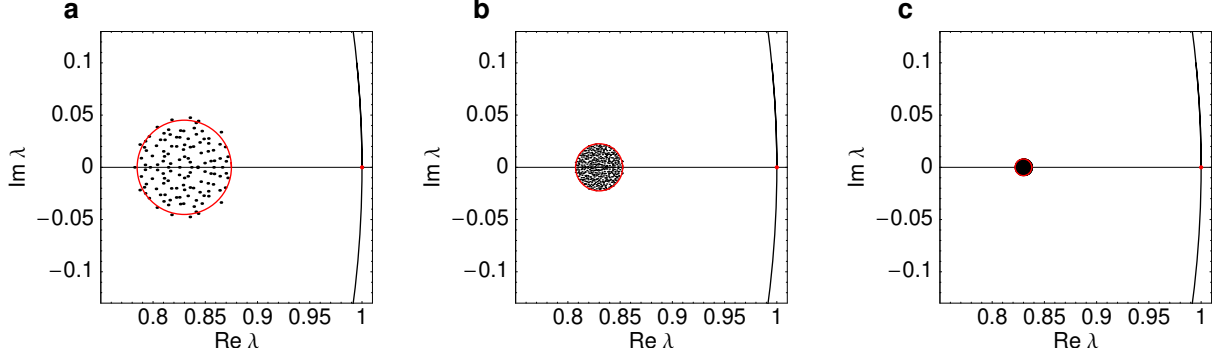


Figure 6.6: Distribution of eigenvalues in the complex plane for networks with fixed connection probability $p = 0.1$ for different network sizes (a) $N = 128$, (b) $N = 512$, (c) $N = 4096$. The disks are centered at A_0 and have radius r_{RMT} , the estimate obtained from random matrix theory. Note that the disk of non-trivial eigenvalues shrinks towards the point A_0 in the limit $N \rightarrow \infty$. The arc through the trivial eigenvalue $z = \lambda_1 = 1$ is a sector of the unit circle. Parameters of integrate-and-fire oscillators are $I = 1.1$, $\varepsilon = -0.2$, $\tau = 0.05$.

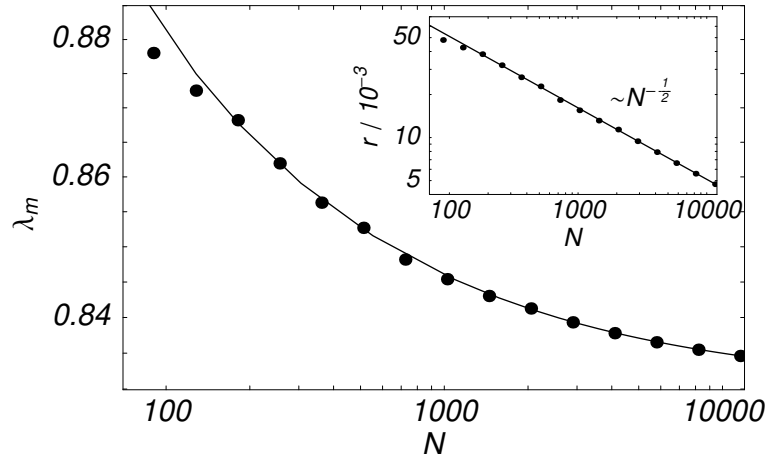


Figure 6.7: Maximum non-trivial eigenvalue and the radius of the eigenvalue distribution for random networks (same parameters as in Fig. 6.6). Main panel displays the maximal non-trivial eigenvalue $\lambda_m \approx A_0 + r$ as a function of network size N . The maximal non-trivial eigenvalue converges to $A_0 \approx 0.83$ as $N \rightarrow \infty$. Inset displays the radius r of the disk of eigenvalues as a function of N . Dots display numerical results based on $r = r_{\text{rad}}$ (Eq. (6.56)), lines are the theoretical estimate for both, the radius r and the maximal non-trivial eigenvalue λ_m .

6.5 Summary and outlook

In this chapter, we investigated conditions that are required for robustness of the stable synchronous state in large networks of pulse-coupled oscillators against structural perturbations of the model dynamics studied in Chapter 5.

We have first derived a class of networks for which the original multi-operator problem reduces to a single operator problem. Interestingly, in this class of models, the potential function is determined by the standard leaky integrate-and-fire oscillator if the coupling strengths are suitably chosen. The reduction to one stability matrix implies that the dynamics in the vicinity of the synchronous state is completely described by the eigenvalues and eigenvectors of that matrix. In particular, the eigenvalue second largest in modulus determines the asymptotic speed of synchronization. For the subclass of symmetric networks we established equivalence between the convergence towards the synchronous state in networks of integrate-and-fire oscillators and the convergence of a diffusion process towards its equilibrium on the same network. In the case of one stability operator the second largest eigenvalue is also an indicator for robustness against structural perturbations. Furthermore, we numerically studied the location of eigenvalues for two classes of large sparse asymmetric random matrices. An estimate of the location of eigenvalues obtained from the theory of large Gaussian asymmetric matrices agrees well with our numerical results. This indicates that for a large class of random networks of integrate-and-fire oscillators, the second largest eigenvalue is separated from the unit circle by a gap. The eigenvalues of a matrix only change smoothly with the entries of that matrix. Hence, sufficiently small structural perturbations to the linear dynamics cannot cause any eigenvalue to cross the unit circle and become larger than one in modulus. It is thus strongly suggested that the stability results obtained for complex networks of Mirollo-Strogatz oscillators in Chapter 5 are robust against structural perturbations of the model dynamics.

Chapter 7

Conclusions

In this thesis, we studied aspects of the collective dynamics of networks of oscillators with delayed pulse-interactions. Individual vertices of these networks are modelled by single-variable Mirollo-Strogatz oscillators. Therefore the dynamical systems considered are idealizations of naturally occurring systems of pulse-coupled units such as neural networks. We focussed on two challenges which arise in the study of pulse-coupled dynamical systems: delayed interactions and a complex network structure.

In the first part of the thesis (Chapter 3), we analyzed the basic advantages of the Mirollo-Strogatz model. The limit of infinitely fast response together with the description by a phase variable allows to explore analytically the nonlinear dynamics of interacting oscillators and to perform exact numerical simulations.

In the second part (Chapter 4), the behavior of networks of oscillators with global, excitatory, delayed pulse-coupling was presented and analyzed. This class of networks provides the first example of a dynamical system in which unstable attracting periodic orbits exist and prevail under variation of the parameters of the system. There is evidence that such unstable attractors also occur in randomly diluted networks [72] as well as in networks with inhibitory interactions, convex down potential functions and a lower potential threshold [74]. More generally, it will be a challenging task to analyze which properties are required from a dynamical system to exhibit non-trivial unstable attractors.

The third part of the thesis (Chapters 5 and 6) is devoted to networks with a complex structure. We exploited the advantages of the Mirollo-Strogatz model to study the existence and stability of the synchronous state in complex networks of pulse-coupled oscillators. A novel analytical approach of pre-sorting a given perturbation led to an exact stability analysis for arbitrary network structures, in which a multioperator problem arises. Solving this problem, we found that the synchronous state is stable for inhibitory coupling and unstable for excitatory coupling. Furthermore, we showed that for strong inhibitory inter-

actions, the synchronous state, in which all oscillators display identical, periodic dynamics, coexists with a state of highly irregular dynamics in random networks.

In order to study the robustness of the stable synchronous state to structural perturbations of the model dynamics, we reduced the multioperator stability problem to a one-operator problem by specializing to a subclass of networks. Interestingly, we found that networks in this subclass consist of standard leaky integrate-and-fire oscillators if the coupling strengths are suitably chosen. In this simplified stability problem, the eigenvalues and eigenvectors of a single matrix describe the dynamics in the vicinity of the synchronous state. For symmetric networks, we established complete mathematical equivalence of the convergence towards the synchronous state in networks of pulse-coupled oscillators and the convergence towards equilibrium of a diffusion process on the same network. For large asymmetric random networks, we demonstrated that the second largest eigenvalue is separated from the unit circle indicating that the stable synchronous state is robust in the limit of infinitely large networks. We obtained these results by comparison between numerically determined eigenvalues of large sparse asymmetric stability matrices and an estimate obtained from the theory of large Gaussian asymmetric random matrices. This comparison between numerics and theory yielded excellent agreement.

Extensions of the work presented in this thesis open further novel perspectives about the dynamics of networks of pulse-coupled oscillators. A generalization [74] of our original stability analysis for complex networks to almost synchronous states provides theoretical insights to a challenging problem of current research: how can precisely timed spike patterns of neurons be generated by a recurrent neural network? Furthermore, it has been found [72] that randomly diluted networks of excitatorily pulse-coupled oscillators, where the synchronous state is unstable, provide an intriguing kind of dynamics: long chaotic transients which significantly delay the convergence towards periodic orbits.

Many complex networks are neither globally coupled nor purely random. For instance, an important class of networks is provided by small-world networks which interpolate between random and regular connectivities [114]. Since the structure of complex networks is likely to influence their dynamics, it will be an interesting future task to study the dynamics on additional real-world network topologies.

Our results demonstrate that the dynamics in certain complex networks can be revealed by considering the vertices as units with simple dynamical properties, e.g. intrinsic oscillators. Such systems provide a promising starting point for future studies addressing the *dynamics* on networks [7], now that important aspects of their *complex structure* have been understood [82–84].

When the science of complex systems was in its infancy, concepts from mathematics and theoretical physics were applied to problems of interdisciplinary character with foundations in all areas of science, including physics, biology, ecology, economics, and social sciences. In this thesis, we also adapted well-known methods to attack questions about networks of

pulse-coupled oscillators, a particular kind of complex network. As large parts of this thesis illustrate, ideas are also gained in exchange from the investigations of those systems. For example, the concept of unstable yet attracting periodic orbits emerged from the investigation of a switching phenomenon (Chapter 4) and a mathematically novel multioperator problem and methods for its solution were found through the analysis of synchronization mechanisms in complex networks (Chapter 5). In the future, such kinds of ideas gained from interdisciplinary research may become increasingly valuable to physicists and applied mathematicians as well as researchers from other areas. We hope that we contributed a small part to the puzzle that is created by the exciting new phenomena emerging when many units of a complex system interact.

Appendix A

Two exact derivations

A.1 Return map of unstable attracting periodic orbit

In Chapter 4 we used a nonlinear return map $\mathbf{F}(\boldsymbol{\delta})$ of perturbations $\boldsymbol{\delta}$ to the unstable attracting periodic orbits in a network of $N = 6$ oscillators (Eq. (4.13)). Here we give a complete derivation of this return map. The periodic orbits considered have two clusters of two synchronized oscillators each and two clusters of only one oscillator each. There are $\binom{6}{2} \times \binom{4}{2} \times \binom{2}{1} \times \binom{1}{1} = 180$ such periodic orbits which are related by a permutation of oscillator indices and thus have identical stability properties. As a representative example, we analyze the orbit $\phi(t)$ that is marked in yellow in Fig. 4.3 of Chapter 4. We choose $\phi_1(t_0) = 0$ where $t_0 = 0$ without loss of generality and consider the five-dimensional return map from the five-dimensional plane defined by $\phi_1 = 0$ to itself. The following analysis applies for the parameters $\varepsilon = 0.2$, $\tau = 0.15$, and the function $U = U_b$ (Eq. (3.57)) where $b = 3.0$ and a neighborhood thereof. In Chapter 2 (Eq. (3.18)) we introduced the transfer function

$$H_\varepsilon(\phi) = U^{-1}(U(\phi) + \varepsilon) \quad (\text{A.1})$$

that mediates the action of an incoming pulse of strength ε on the phase ϕ . We will use it extensively in the following.

A.1.1 Periodic orbit dynamics

First we determine the dynamics of the unperturbed orbit (Table A.1). We show that it indeed is periodic with period

$$T = 4\tau + 1 - p_{3,4} \quad (\text{A.2})$$

given by the time in the lowest row of Table A.1 where

$$p_{3,4} = H_{\hat{\varepsilon}}(H_{\hat{\varepsilon}}(H_{2\hat{\varepsilon}}(A + \tau) + \tau) + \tau) \quad (\text{A.3})$$

and $A = H_{\hat{\varepsilon}}(\tau)$ was defined in Chapter 4 (Eq. (4.4)) and will be derived below (see Eq. (A.15)). Here we use the abbreviation $\hat{\varepsilon} = \varepsilon/(N - 1)$.

Table A.1 displays the time evolution on the periodic orbit event by event. The left column gives the sequence of events, labeled s_i if oscillator i sends a signal and r_i if the signal from oscillator i is received by all other oscillators. The second left column gives the time of occurrence of these events. The right four columns give the phases of oscillators $i \in \{1, \dots, 6\}$ right after the events have occurred, where oscillators in the same clusters have identical phases, $\phi_1(t) \equiv \phi_2(t)$ and $\phi_3(t) \equiv \phi_4(t)$. The first row gives the initial condition at $t = 0$, just after the signals of oscillators $i = 1$ and $i = 2$ have been sent, s_1, s_2 . The initial phases

$$\phi(0) = (0, 0, A, A, B, C)^T \quad (\text{A.4})$$

are obtained from the first column with constants defined in Chapter 4 (Equations 4.4–4.6) and derived below. Throughout the table, the phases after each event are labeled $p_{i,k}$ where the first index labels the oscillator $i \in \{1, 3, 5, 6\}$ and the second index counts the events k occurring for a *perturbed* trajectory (see Table A.2 below) starting with $k = 0$ for the initial condition (first row of Table A.1). Since the second oscillators $i = 2$ and $i = 4$ in the two clusters have the same phases as the oscillators $i = 1$ and $i = 3$, respectively, we define

$$p_{2,k} := p_{1,k} \text{ and } p_{4,k} := p_{3,k} \quad (\text{A.5})$$

for all k .

In general, the time interval to the next event is given by the minimal distance of any phase to threshold, $\Delta t = \min\{1 - \phi_i(t) \mid i \in \{1, \dots, 6\}\}$, or by the time $\Delta t \leq \tau$ until the next signal arrives, depending on which time interval is smallest at a given time t .

As an example of the event-based dynamics, consider the event $k = 2$ at time $t = \tau$. This event contains the reception of signals sent by oscillators $i = 1$ and $i = 2$ at time $t = 0$, r_1 and r_2 . Since there are no self-connections, these oscillators receive only one signal each such that their phases are shifted according to

$$p_{i,2} = H_{\hat{\varepsilon}}(p_{i,0} + \tau) \quad (\text{A.6})$$

for $i \in \{1, 2\}$. All other oscillators receive two signals of total strength $2\hat{\varepsilon}$. For the three oscillators $i \in \{3, 4, 5\}$, these incoming signals are subthreshold, $U(p_{i,0} + \tau) + 2\hat{\varepsilon} < 1$, such that

$$p_{i,2} = H_{2\hat{\varepsilon}}(p_{i,0} + \tau). \quad (\text{A.7})$$

Since for the oscillator $i = 6$ these incoming signals are suprathreshold,

$$U(p_{6,0} + \tau) + 2\hat{\varepsilon} > 1, \quad (\text{A.8})$$

| event | t | $\phi_1(t) \equiv \phi_2(t)$ | $\phi_3(t) \equiv \phi_4(t)$ | $\phi_5(t)$ | $\phi_6(t)$ |
|----------------------|-----------------------|---|---|--|---|
| s_1, s_2 | 0 | 0 =: $p_{1,0}$ | A =: $p_{3,0}$ | B =: $p_{5,0}$ | C =: $p_{6,0}$ |
| r_1, r_2, s_6 | τ | $H_{\hat{\varepsilon}}(p_{1,0} + \tau)$ =: $p_{1,2}$ | $H_{2\hat{\varepsilon}}(p_{3,0} + \tau)$ =: $p_{3,2}$ | $H_{2\hat{\varepsilon}}(p_{5,0} + \tau)$ =: $p_{5,2}$ | $U(p_{6,0} + \tau) + 2\hat{\varepsilon} > 1$ $1 \rightarrow 0$ $0 =: p_{6,2}$ |
| r_6, s_5 | 2τ | $H_{\hat{\varepsilon}}(p_{1,2} + \tau)$ =: $p_{1,3}$ | $H_{\hat{\varepsilon}}(p_{3,2} + \tau)$ =: $p_{3,3}$ | $U(p_{5,2} + \tau) + \hat{\varepsilon} > 1$ $1 \rightarrow 0$ $0 =: p_{5,3}$ | $p_{6,2} + \tau$ =: $p_{6,3}$ |
| r_5 | 3τ | $H_{\hat{\varepsilon}}(p_{1,3} + \tau)$ =: $p_{1,4}$ | $H_{\hat{\varepsilon}}(p_{3,3} + \tau)$ =: $p_{3,4}$ | $p_{5,3} + \tau$ =: $p_{5,4}$ | $H_{\hat{\varepsilon}}(p_{6,3} + \tau)$ =: $p_{6,4}$ |
| s_3, s_4 | $3\tau + 1 - p_{3,4}$ | $p_{1,4} + 1 - p_{3,4}$ =: $p_{1,6}$ | $1 \rightarrow 0$ $0 =: p_{3,6}$ | $p_{5,4} + 1 - p_{3,4}$ =: $p_{5,6}$ | $p_{6,4} + 1 - p_{3,4}$ =: $p_{6,6}$ |
| r_3, r_4, s_1, s_2 | $4\tau + 1 - p_{3,4}$ | $U(p_{1,6} + \tau) + 2\hat{\varepsilon} > 1$ $1 \rightarrow 0$ $0 =: p_{1,8}$ | $H_{\hat{\varepsilon}}(p_{3,6} + \tau)$ =: $p_{3,8}$ $\vdash A$ | $H_{2\hat{\varepsilon}}(p_{5,6} + \tau)$ =: $p_{5,8}$ $\vdash B$ | $H_{2\hat{\varepsilon}}(p_{6,6} + \tau)$ =: $p_{6,8}$ $\vdash C$ |

Table A.1: Time evolution on the periodic orbit event by event. See text for explanation.

this oscillator is reset and generates a signal, denoted $1 \rightarrow 0$, such that

$$p_{6,2} = 0. \quad (\text{A.9})$$

Here, one incoming signal would have been sufficient to reach the threshold,

$$U(p_{6,0} + \tau) + \hat{\varepsilon} > 1, \quad (\text{A.10})$$

such that this oscillator reacts differently to the reception of signals from two oscillators with phases that are not identical. This will be seen below (Sec. A.1.2) in the discussion of the dynamics of the perturbations to the periodic orbit.

There are two other kinds of events: First, there are input signals that are subthreshold to all oscillators, i.e. no oscillator is reset and sends a signal upon reception. Here, the only example of such an event is the reception r_5 (fourth row) of the signal sent by oscillator $i = 5$. The third kind of event is the sending of a signal that is not induced by a simultaneous reception of another signal, as exemplified by s_3 and s_4 (fifth row). Here all phases are just shifted by a constant amount, $\Delta\phi_i = 1 - p_{3,4}$, and the oscillators $i = 3$ and $i = 4$ which reach threshold are reset ($1 \rightarrow 0$), and generate a signal.

Going through the table row by row, the phases proceed (with time) from event to event. The last row gives the phases when the first oscillator has been reset again,

$$\phi_1(T) = p_{1,8} = 0, \quad (\text{A.11})$$

after period $T = 4\tau - 1 + p_{3,4}$. The actual parameter dependence of the constants A , B , and C are then determined from the conditions

$$p_{3,8} \stackrel{!}{=} A \quad (\text{A.12})$$

$$p_{5,8} \stackrel{!}{=} B \quad (\text{A.13})$$

$$p_{6,8} \stackrel{!}{=} C \quad (\text{A.14})$$

arising from the requirement that the orbit is closed. They lead to

$$A = H_{\hat{\varepsilon}}(\tau) \quad (\text{A.15})$$

$$B = H_{2\hat{\varepsilon}}(1 + 2\tau - a_4) \quad (\text{A.16})$$

$$C = H_{2\hat{\varepsilon}}(H_{\hat{\varepsilon}}(2\tau) + 1 + \tau - a_4) \quad (\text{A.17})$$

with recursively defined

$$a_i = U^{-1}(k_i \hat{\varepsilon} + U(\tau + a_{i-1})) \quad (\text{A.18})$$

for $i \in \{1, \dots, 4\}$, $a_0 = 0$, and $k_1 = k_3 = k_4 = 1$, $k_2 = 2$ as in Chapter 4, Eqs. (4.4)–(4.7).

A.1.2 Dynamics of a general perturbation to the periodic orbit

Here we consider the dynamics of a general perturbation applied to the periodic orbit studied above. By general perturbation we mean that both clusters occupied by two oscillators are split up such that $\phi_1(0) \neq \phi_2(0)$ and $\phi_3(0) \neq \phi_4(0)$. To be specific we assume $\delta_2 > \delta_1 = 0$ and $\delta_4 > \delta_3$. This assumption is made without loss of generality because of the permutation symmetry. The changes of the phases due to single events are obtained from Table A.2. If we denote $\boldsymbol{\delta} = (\delta_2, \delta_3, \delta_4, \delta_5, \delta_6)^\top$, the return map

$$\boldsymbol{\delta}' = \mathbf{F}(\boldsymbol{\delta}) \quad (\text{A.19})$$

from the five-dimensional plane defined by $\phi_1 = 0$ to itself is obtained after all oscillators have fired exactly once (last row of Table A.2).

Table A.2 displays the time evolution of a general perturbation event by event. As for the unperturbed orbit described above, the left column gives the sequence of events. The second left column gives the time of these events. The right six columns give the phases of oscillators $i \in \{1, \dots, 6\}$ right after an event has occurred. The first row gives the initial condition at $t = 0$, just after the signal has been sent, s_1 , by oscillator $i = 1$. Before, at time $t = -\delta_2 < 0$, the signal of oscillator $i = 2$ has been sent, denoted (s_2); this signal will travel until time $t = \tau - \delta_2$. The initial phases

$$\boldsymbol{\phi}(0) = (0, 0, A, A, B, C')^\top + (\delta_1, \delta_2, \delta_3, \delta_4, \delta_5, \delta_6)^\top \quad (\text{A.20})$$

are displayed in the first column. Here $\delta_1 = 0$ by definition. Throughout the table, the phases after each event are labeled $\varphi_{i,k}$ where the first index labels the oscillator i and the second index counts the events k starting with $k = 0$ for the initial condition.

For instance, the first event (after the initial condition), $k = 1$, at time $t = \tau - \delta_2$ is the reception r_2 of the signal sent by oscillator $i = 2$. This signal is suprathreshold to oscillator $i = 6$ that consequentially fires, s_6 . Since there are no self-interactions, the phase of oscillator $i = 2$ is only shifted in time,

$$\varphi_{2,1} = \delta_2 + (\tau - \delta_2) = \tau. \quad (\text{A.21})$$

The phases of the oscillators $i \in \{1, 3, 4, 5\}$ additionally jump because of the incoming subthreshold signal,

$$\varphi_{i,1} = H_{\hat{\varepsilon}}(\varphi_{i,0} + (\tau - \delta_2)). \quad (\text{A.22})$$

Since to oscillator $i = 6$ this signal is not subthreshold but suprathreshold,

$$U(\varphi_{6,0} + (\tau - \delta_2)) + \hat{\varepsilon} > 1, \quad (\text{A.23})$$

it is instantaneously reset, $1 \rightarrow 0$, such that its phase after this event is

$$\varphi_{6,1} = 0. \quad (\text{A.24})$$

| event | t | $\phi_1(t)$ | $\phi_2(t)$ | $\phi_3(t)$ | $\phi_4(t)$ | $\phi_5(t)$ | $\phi_6(t)$ |
|-----------------|--|---|---|--|---|---|--|
| $s_1, (s_2)$ | 0 | 0 =: $\varphi_{1,0}$ | δ_2 =: $\varphi_{2,0}$ | $A + \delta_3$ =: $\varphi_{3,0}$ | $A + \delta_4$ =: $\varphi_{4,0}$ | $B + \delta_5$ =: $\varphi_{5,0}$ | $C' + \delta_6$ =: $\varphi_{6,0}$ |
| r_2, s_6 | $\tau - \delta_2$ | $H_{\bar{\varepsilon}}(\varphi_{1,0} + \tau - \delta_2)$ =: $\varphi_{1,1}$ | τ =: $\varphi_{2,1}$ | $H_{\bar{\varepsilon}}(\varphi_{3,0} + \tau - \delta_2)$ =: $\varphi_{3,1}$ | $H_{\bar{\varepsilon}}(\varphi_{4,0} + \tau - \delta_2)$ =: $\varphi_{4,1}$ | $H_{\bar{\varepsilon}}(\varphi_{5,0} + \tau - \delta_2)$ =: $\varphi_{5,1}$ | $U(\varphi_{6,0} + \tau - \delta_2)$ $+ \hat{\varepsilon} > 1$ $1 \rightarrow 0$ $0 =: \varphi_{6,1}$ |
| r_1 | τ | $\varphi_{1,1} + \delta_2$ =: $\varphi_{1,2}$ | $H_{\bar{\varepsilon}}(\varphi_{2,1} + \delta_2)$ =: $\varphi_{2,2}$ | $H_{\bar{\varepsilon}}(\varphi_{3,1} + \delta_2)$ =: $\varphi_{3,2}$ | $H_{\bar{\varepsilon}}(\varphi_{4,1} + \delta_2)$ =: $\varphi_{4,2}$ | $H_{\bar{\varepsilon}}(\varphi_{5,1} + \delta_2)$ =: $\varphi_{5,2}$ | $H_{\bar{\varepsilon}}(\varphi_{6,1} + \delta_2)$ =: $\varphi_{6,2}$ |
| r_6, s_5 | $2\tau - \delta_2$ | $H_{\bar{\varepsilon}}(\varphi_{1,2} + \tau - \delta_2)$ =: $\varphi_{1,3}$ | $H_{\bar{\varepsilon}}(\varphi_{2,2} + \tau - \delta_2)$ =: $\varphi_{2,3}$ | $H_{\bar{\varepsilon}}(\varphi_{3,2} + \tau - \delta_2)$ =: $\varphi_{3,3}$ | $H_{\bar{\varepsilon}}(\varphi_{4,2} + \tau - \delta_2)$ =: $\varphi_{4,3}$ | $U(\varphi_{5,2} + \tau - \delta_2)$ $+ \hat{\varepsilon} > 1$ $1 \rightarrow 0$ $0 =: \varphi_{5,3}$ | $\varphi_{6,2} + \tau - \delta_2$ =: $\varphi_{6,3}$ |
| r_5 | $3\tau - \delta_2$ | $H_{\bar{\varepsilon}}(\varphi_{1,3} + \tau)$ =: $\varphi_{1,4}$ | $H_{\bar{\varepsilon}}(\varphi_{2,3} + \tau)$ =: $\varphi_{2,4}$ | $H_{\bar{\varepsilon}}(\varphi_{3,3} + \tau)$ =: $\varphi_{3,4}$ | $H_{\bar{\varepsilon}}(\varphi_{4,3} + \tau)$ =: $\varphi_{4,4}$ | τ =: $\varphi_{5,4}$ | $H_{\bar{\varepsilon}}(\varphi_{6,3} + \tau)$ =: $\varphi_{6,4}$ |
| s_4 | $3\tau + 1 - \varphi_{4,4} - \delta_2$ | $\varphi_{1,4} + 1 - \varphi_{4,4}$ =: $\varphi_{1,5}$ | $\varphi_{2,4} + 1 - \varphi_{4,4}$ =: $\varphi_{2,5}$ | $\varphi_{3,4} + 1 - \varphi_{4,4}$ =: $\varphi_{3,5}$ | $1 \rightarrow 0$ $0 =: \varphi_{4,5}$ | $\varphi_{5,4} + 1 - \varphi_{4,4}$ =: $\varphi_{5,5}$ | $\varphi_{6,4} + 1 - \varphi_{4,4}$ =: $\varphi_{6,5}$ |
| s_3 | $3\tau + 1 - \varphi_{3,4} - \delta_2$ | $\varphi_{1,5} + \varphi_{4,4} - \varphi_{3,4}$ =: $\varphi_{1,6}$ | $\varphi_{2,5} + \varphi_{4,4} - \varphi_{3,4}$ =: $\varphi_{2,6}$ | $1 \rightarrow 0$ $0 =: \varphi_{3,6}$ | $\varphi_{4,4} - \varphi_{3,4}$ =: $\varphi_{4,6}$ | $\varphi_{5,5} + \varphi_{4,4} - \varphi_{3,4}$ =: $\varphi_{5,6}$ | $\varphi_{6,5} + \varphi_{4,4} - \varphi_{3,4}$ =: $\varphi_{6,6}$ |
| r_4 | $4\tau + 1 - \varphi_{4,4} - \delta_2$ | $H_{\bar{\varepsilon}}(\varphi_{1,5} + \tau)$ =: $\varphi_{1,7}$ | $H_{\bar{\varepsilon}}(\varphi_{2,5} + \tau)$ =: $\varphi_{2,7}$ | $\tau - \varphi_{4,4} + \varphi_{3,4}$ =: $\varphi_{3,7}$ | τ =: $\varphi_{4,7}$ | $H_{\bar{\varepsilon}}(\varphi_{5,5} + \tau)$ =: $\varphi_{5,7}$ | $H_{\bar{\varepsilon}}(\varphi_{6,5} + \tau)$ =: $\varphi_{6,7}$ |
| r_3, s_1, s_2 | $4\tau + 1 - \varphi_{3,4} - \delta_2$ | $U(\varphi_{1,7} + \varphi_{4,4} - \varphi_{3,4})$ $+ \hat{\varepsilon} > 1$ $1 \rightarrow 0$ $0 =: \varphi_{1,8}$ $= \delta'_1$ | $U(\varphi_{2,7} + \varphi_{4,4} - \varphi_{3,4})$ $+ \hat{\varepsilon} > 1$ $1 \rightarrow 0$ $0 =: \varphi_{2,8}$ $= \delta'_2$ | $\varphi_{3,7} + \varphi_{4,4} - \varphi_{3,4}$ =: $\varphi_{3,8}$ $= A + \delta'_3$ | $H_{\bar{\varepsilon}}(\varphi_{4,7} + \varphi_{4,4} - \varphi_{3,4})$ =: $\varphi_{4,8}$ $= A + \delta'_4$ | $H_{\bar{\varepsilon}}(\varphi_{5,7} + \varphi_{4,4} - \varphi_{3,4})$ =: $\varphi_{5,8}$ $= B + \delta'_5$ | $H_{\bar{\varepsilon}}(\varphi_{6,7} + \varphi_{4,4} - \varphi_{3,4})$ =: $\varphi_{6,8}$ $= C' + \delta'_6$ |

Table A.2: Time evolution of a general perturbation event by event. A general perturbation that splits up both clusters, $\delta_2 > \delta_1 \equiv 0$ and $\delta_4 > \delta_3$. For explanation see text.

Again, as for the unperturbed dynamics, going through the table row by row, the phases are calculated event by event. The phases $\varphi_{i,k}$ for $i \in \{1, \dots, 5\}$ right after the events are approximated by the unperturbed phases $p_{i,k}$ defined in Table A.1,

$$\varphi_{i,k} = p_{i,k} + \mathcal{O}(\boldsymbol{\delta}) \quad (\text{A.25})$$

for all k for which the $p_{i,k}$ are defined, $k \in \{0, 2, 3, 4, 6, 8\}$. Here $\mathcal{O}(\boldsymbol{\delta})$ symbolizes a function of all δ_i , $i \in \{2, \dots, 6\}$, that approaches zero at least linearly if all $\delta_i \rightarrow 0$, i.e. $\mathcal{O}(\boldsymbol{\delta}) := \sum_{i=2}^N \mathcal{O}(\delta_i)$. The phases $\varphi_{6,k}$ are not approximated in this way because of the splitting of the first cluster, $\phi_2(0) \neq \phi_1(0)$. In the unperturbed case, oscillator $i = 6$ is reset by the simultaneous reception of the two signals sent by oscillators $i = 1$ and $i = 2$ (Eqs. (A.8) and (A.9)). If there is a perturbation that splits up the first cluster, $\delta_2 > \delta_1$, oscillator $i = 6$ is reset by the reception of the signal sent by oscillator $i = 2$ alone (Eqs. (A.23) and (A.24)); only after this reset, the signal of oscillator $i = 1$ arrives and causes an additional phase shift such that $\phi_6 \approx C'$ where $C' > C$. Hence the offset of the phase of oscillator $i = 6$ is changed. The actual expression of C' is obtained from the limiting case

$$C' \stackrel{!}{=} \lim_{\text{all } \delta_i \rightarrow 0} \varphi_{6,8} \quad (\text{A.26})$$

where the directed limit is taken on some path satisfying $\delta_2 > 0$ if any $\delta_i \neq 0$. This leads to

$$C' = H_{2\hat{\varepsilon}}(H_{\hat{\varepsilon}}(2\tau + H_{\hat{\varepsilon}}(0)) + 1 + \tau - a_4) \quad (\text{A.27})$$

where a_4 is defined above (A.18).

Having determined C' , the return map

$$\mathbf{F}(\boldsymbol{\delta}) = \boldsymbol{\delta}' \quad (\text{A.28})$$

$$= (\delta'_2, \delta'_3, \delta'_4, \delta'_5, \delta'_6)^\top \quad (\text{A.29})$$

$$= (0, \varphi_{3,8} - A, \varphi_{4,8} - A, \varphi_{5,8} - B, \varphi_{6,8} - C')^\top \quad (\text{A.30})$$

is obtained from the last row of the table. Here the $\varphi_{i,8}$ again depend on the original perturbation vector $\boldsymbol{\delta}$. From this identification we obtain the components

$$\begin{aligned} F_2(\boldsymbol{\delta}) &= 0 \\ F_3(\boldsymbol{\delta}) &= L_4 - L_3 + H_{\hat{\varepsilon}}(\tau - L_4 + L_3) - A \\ F_4(\boldsymbol{\delta}) &= H_{\hat{\varepsilon}}(\tau + L_4 - L_3) - A \\ F_5(\boldsymbol{\delta}) &= H_{\hat{\varepsilon}}(H_{\hat{\varepsilon}}(1 + 2\tau - L_4) + L_4 - L_3) - B \\ F_6(\boldsymbol{\delta}) &= H_{\hat{\varepsilon}}(L_4 - L_3 + H_{\hat{\varepsilon}}(\tau + 1 - L_3 + \\ &\quad H_{\hat{\varepsilon}}(2\tau - \delta_2 + H_{\hat{\varepsilon}}(\delta_2)))) - C' \end{aligned} \quad (\text{A.31})$$

with the abbreviations

$$L_i := L_i(\boldsymbol{\delta}) = H_{\hat{\varepsilon}}(\tau + H_{\hat{\varepsilon}}(\tau - \delta_2 + H_{\hat{\varepsilon}}(\delta_2 + H_{\hat{\varepsilon}}(\tau + \delta_i - \delta_2 + H_{\hat{\varepsilon}}(\tau)))) \quad (\text{A.32})$$

for $i \in \{3, 4\}$ as defined in Chapter 4. Here the difference $L_4 - L_3$ in Eqs. (A.31) is of order $L_4 - L_3 = \mathcal{O}(\delta)$.

It is important to note that the nonlinear analysis results in $\delta'_2 = \delta'_1 = 0$ such that after two cycles we again have $\phi_6 \approx C$. The dynamics of all other phases is not affected by this change because no phase $\varphi_{6,k}$ enters the phase dynamics $\phi_i(t)$ for all $i \in \{1, \dots, 5\}$. Thus, the dynamics for $\delta_2 = \delta_1 = 0$ is obtained from Table A.2 by substituting C' by C in the initial condition $\varphi_{6,0}$ and setting $\varphi_{6,2} = 0$ because the two signals from $i = 1$ and $i = 2$ arrive simultaneously (see Eq. (A.8)). The case $\delta_3 = \delta_4$ is captured by the nonlinear analysis presented here. Such initial phases obviously result in $\delta'_3 = \delta'_4$ because synchronized oscillators stay synchronized.

A.2 Derivation of the expansion (5.17)

We prove a generalization of the first order expansion (5.17) used in Chapter 5,

$$\beta_{i,m} \doteq \alpha_{i,m} + \sum_{n=1}^m p_{i,n-1,m} D_{i,n} \quad \text{for } m \in \{1, \dots, k_i\}, \quad (\text{A.33})$$

by induction over m for arbitrary fixed $i \in \{1, \dots, N\}$. As in the main text, here the statement $x \doteq y$ means that $x = y + \sum_{i,n} \mathcal{O}(D_{i,n}^2)$ as all $D_{i,n} \rightarrow 0$. The quantities $\beta_{i,m}$ were defined in Table 5.1 of Chapter 5. The quantities (A.33) appear in the derivation of the map (5.15) for $m = k_i$. As an extension of the notation in Sec. 5.3, we denote here

$$\alpha_{i,m} = U^{-1} \left(U(\tau) + \sum_{n=1}^m \varepsilon_{ij_n} \right) \quad \text{for } m \in \{0, \dots, k_i\}, \quad (\text{A.34})$$

$$D_{i,n} = \Delta_{i,n-1} - \Delta_{i,n} \quad \text{for } n \in \{1, \dots, k_i\}, \quad (\text{A.35})$$

and

$$p_{i,n,m} = \frac{U'(\alpha_{i,n})}{U'(\alpha_{i,m})} \quad \text{for } 0 \leq n \leq m \leq k_i. \quad (\text{A.36})$$

Here the prime denotes the derivative of the potential function U with respect to its argument. The latter definition implies the identity

$$p_{i,n,l} p_{i,l,m} = p_{i,n,m}. \quad (\text{A.37})$$

For the case $m = 1$, the induction basis, expression (A.33) holds because

$$\beta_{i,1} = U^{-1}(U(\tau + D_{i,1}) + \varepsilon_{ij_1}) \quad (\text{A.38})$$

$$\doteq U^{-1}(U(\tau) + \varepsilon_{ij_1}) \quad (\text{A.39})$$

$$\begin{aligned} &+ \left[\frac{\partial}{\partial D} U^{-1}(U(\tau + D) + \varepsilon_{ij_1}) \right]_{D=0} D_{i,1} \\ &= \alpha_{i,1} + \frac{U'(\tau)}{U'(U^{-1}(U(\tau) + \varepsilon_{ij_1}))} D_{i,1} \end{aligned} \quad (\text{A.40})$$

$$= \alpha_{i,1} + \frac{U'(\alpha_{i,0})}{U'(\alpha_{i,1})} D_{i,1} \quad (\text{A.41})$$

$$= \alpha_{i,1} + p_{i,0,1} D_{i,1} \quad (\text{A.42})$$

where the third last equality holds because the derivatives of inverse functions are given by $\partial/\partial x U^{-1}(x) = 1/U'(U^{-1}(x))$. The induction step, $m \mapsto m+1$, is proven by

$$\beta_{i,m+1} = U^{-1}(U(\beta_{i,m} + D_{i,m+1}) + \varepsilon_{ij_{m+1}}) \quad (\text{A.43})$$

$$\doteq U^{-1} \left(U \left(\alpha_{i,m} + \sum_{n=1}^m p_{i,n-1,m} D_{i,n} + D_{i,m+1} \right) + \varepsilon_{ij_{m+1}} \right) \quad (\text{A.44})$$

$$\doteq U^{-1} (U(\alpha_{i,m}) + \varepsilon_{ij_{m+1}}) \quad (\text{A.45})$$

$$\begin{aligned} &+ \left[\frac{\partial}{\partial D} U^{-1}(U(\alpha_{i,m} + D) + \varepsilon_{ij_{m+1}}) \right]_{D=0} \left(\sum_{n=1}^m p_{i,n-1,m} D_{i,n} + D_{i,m+1} \right) \\ &= U^{-1} (U(\alpha_{i,m}) + \varepsilon_{ij_{m+1}}) + \frac{U'(\alpha_{i,m})}{U'(\alpha_{i,m+1})} \left(\sum_{n=1}^m p_{i,n-1,m} D_{i,n} + D_{i,m+1} \right) \end{aligned} \quad (\text{A.46})$$

$$= \alpha_{i,m+1} + p_{i,m,m+1} \left(\sum_{n=1}^m p_{i,n-1,m} D_{i,n} + D_{i,m+1} \right) \quad (\text{A.47})$$

$$= \alpha_{i,m+1} + \sum_{n=1}^{m+1} p_{i,n-1,m+1} D_{i,n} \quad (\text{A.48})$$

where we used $U(\alpha_{i,m}) + \varepsilon_{ij_{m+1}} = U(\alpha_{i,m+1})$ in the second last step and the identity (A.37) in the last step. This completes the proof of the first order expansion (A.33).

Note that because of the normalization $\sum_{n=1}^{k_i} \varepsilon_{ij_n} = \sum_{j=1}^N \varepsilon_{ij} = \varepsilon$ for all i , the quantity $\alpha_{i,k_i} = U^{-1}(U(\tau) + \varepsilon) = \alpha$ is independent of i . In addition, $p_{i,n,k_i} = p_{i,n}$ for all i and all n . Hence, theorem (A.33) in the case $m = k_i$ yields expression (5.17).

Bibliography

- [1] *Nature Insight: Complex Systems*, edited by K. Ziemelis (Nature, London, 2001), Vol. 410, pp. 241–284.
- [2] R. Badii and A. Politi, *Complexity* (Cambridge University Press, Cambridge, England, 1997).
- [3] T. Vicsek, The bigger picture, *Nature* **418**, 131 (2002).
- [4] T. Vicsek, A question of scale, *Nature* **411**, 421 (2001).
- [5] K. Huang, *Statistical Mechanics*, 2 ed. (Wiley, New York, 1987).
- [6] L. Reichl, *A Modern Course in Statistical Physics*, 2 ed. (Wiley-Interscience, New York, 1998).
- [7] S. H. Strogatz, Exploring complex networks, *Nature* **410**, 268 (2001).
- [8] A. V. Herz and J. J. Hopfield, Earthquake Cycles and Neural Revertebrations: Collective Oscillations in Systems with Pulse-Coupled Threshold Elements, *Phys. Rev. Lett.* **75**, 1222 (1995).
- [9] J. Buck and E. Buck, Synchronous Fireflies, *Sc. American* **234**, 74 (1976).
- [10] J. Buck, Synchronous Rythmic Flashing of Fireflies. II., *Quart. Rev. Biol.* **63**, 265 (1988).
- [11] C. Peskin, *Mathematical Aspects of Heart Physiology* (Courant Institute of Mathematical Sciences, New York University, 1984), pp. 268.
- [12] *Pulsed Neural Networks*, edited by W. Maass and C. M. Bishop (MIT Press, Cambridge, Massachusetts, 1999).
- [13] D. Johnston and S. M.-S. Wu, *Foundations of Cellular Neurophysiology* (MIT Press, Cambridge, Massachusetts, 1995).
- [14] R. E. Mirollo and S. H. Strogatz, Synchronization of Pulse-Coupled Biological Oscillators, *SIAM J. Appl. Math.* **50**, 1645 (1990).

- [15] C.-C. Chen, Threshold effects on synchronization of pulse-coupled oscillators, *Phys. Rev. E* **49**, 2668 (1994).
- [16] W. Senn and R. Urbanczik, Similar non-leaky integrate-and-fire neurons with instantaneous couplings always synchronize, *SIAM J. Appl. Math.* **61**, 1143 (2001).
- [17] U. Ernst, K. Pawelzik, and T. Geisel, Synchronization Induced by Temporal Delays in Pulse-Coupled Oscillators, *Phys. Rev. Lett.* **74**, 1570 (1995).
- [18] U. Ernst, K. Pawelzik, and T. Geisel, Delay-Induced multistable synchronization of biological oscillators, *Phys. Rev. E* **57**, 2150 (1998).
- [19] W. Gerstner, Rapid Phase Locking in Systems of Pulse-Coupled Oscillators with Delay, *Phys. Rev. Lett.* **76**, 1755 (1996).
- [20] L. Abbott and C. van Vreeswijk, Asynchronous states in networks of pulse-coupled oscillators, *Phys. Rev. E* **48**, 1483 (1993).
- [21] C. van Vreeswijk, Partial synchronization in populations of pulse-coupled oscillators, *Phys. Rev. E* **54**, 5522 (1996).
- [22] C. van Vreeswijk, Analysis of the Asynchronous State in Networks of Strongly Coupled Oscillators, *Phys. Rev. Lett.* **84**, 5110 (2000).
- [23] P. Bressloff and S. Coombes, Spike Train Dynamics Underlying Pattern Formation in Integrate-and-Fire Oscillators, *Phys. Rev. Lett.* **81**, 2384 (1998).
- [24] P. Bressloff and S. Coombes, Travelling Waves in a Chain of Pulse-Coupled Oscillators, *Phys. Rev. Lett.* **80**, 4815 (1998).
- [25] L. Glass and M. Mackey, *From Clocks to Chaos, The Rhythms of Life* (Princeton University Press, Princeton, New Jersey, 1988).
- [26] D. R. Reddy, A. Sen, and G. Johnston, Time Delay Induced Death in Coupled Limit Cycle Oscillators, *Phys. Rev. Lett.* **80**, 5109 (1998).
- [27] S. H. Strogatz, Death by delay, *Nature* **394**, 316 (1998).
- [28] C. van Vreeswijk and H. Sompolinsky, Chaos in Neuronal Networks with Balanced Excitatory and Inhibitory Activity, *Science* **274**, 1724 (1996).
- [29] C. van Vreeswijk and H. Sompolinsky, Chaotic Balanced State in a Model of Cortical Circuits, *Neural Comput.* **10**, 1321 (1998).
- [30] N. Brunel and V. Hakim, Fast Global Oscillations in Networks of Integrate-and-Fire Neurons with Low Firing Rates, *Neural Comput.* **11**, 1621 (1999).

- [31] M. Timme, F. Wolf, and T. Geisel, Prevalence of Unstable Attractors in Networks of Pulse-Coupled Oscillators, *Phys. Rev. Lett.* **89**, 154105 (2002).
- [32] M. Timme, F. Wolf, and T. Geisel, Unstable attractors induce perpetual synchronization and desynchronization, *Chaos* **13**, (2003), in press.
- [33] M. Timme, F. Wolf, and T. Geisel, Coexistence of Regular and Irregular Dynamics in Complex Networks of Pulse-Coupled Oscillators, *Phys. Rev. Lett.* (2002), accepted.
- [34] B. Bollobás, *Modern Graph Theory, Graduate Texts in Mathematics* (Springer, New York, 1998).
- [35] G. Chartrand and L. Lesniak, *Graphs and Digraphs*, 3 ed. (Chapman and Hall, Boca Raton, Florida, 1996).
- [36] R. Diestel, *Graph Theory, Graduate Texts in Mathematics*, 2 ed. (Springer, New York, 2000).
- [37] R. J. Wilson, *Graph Theory*, 4 ed. (Prentice Hall, Harlow, England, 1996).
- [38] J. Milnor, On the Concept of Attractor, *Comm. Math. Phys.* **99**, 177 (1985).
- [39] J. Milnor, On the Concept of Attractor: Correction and Remarks, *Comm. Math. Phys.* **102**, 517 (1985).
- [40] J. Buescu, *Exotic Attractors* (Birkhäuser, Basel, Switzerland, 1997).
- [41] P. Ashwin and J. R. Terry, On riddling and weak attractors, *Physica D* **142**, 87 (2000).
- [42] D. K. Arrowsmith and C. M. Place, *An introduction to dynamical systems* (Cambridge University Press, Cambridge, England, 1990).
- [43] J. Guckenheimer and P. Holmes, *Nonlinear Oscillations, Dynamical Systems, and Bifurcations of Vector Fields* (Springer, New York, 1983).
- [44] A. Katok and B. Hasselblatt, *Introduction to the Modern Theory of Dynamical Systems* (Cambridge University Press, Cambridge, England, 1995).
- [45] A. Lichtenberg and M. A. Lieberman, *Regular and Chaotic Dynamics, Applied Mathematical Sciences* (Springer, New York, 1992).
- [46] S. H. Strogatz, *Nonlinear Dynamics and Chaos* (Perseus Publ., Cambridge, Massachusetts, 2000).
- [47] B. S. Gutkin and G. B. Ermentrout, Dynamics of Membrane Excitability Determine Interspike Interval Variability: A Link Between Spike Generation Mechanisms and Cortical Spike Train Statistics, *Neural Comput.* **10**, 1047 (1998).

- [48] D. Hansel, G. Mato, C. Meunier, and L. Neltner, On Numerical Simulations of Integrate-and-Fire Neural Networks, *Neural Comput.* **10**, 467 (1998).
- [49] S. Rotter and M. Diesmann, Exact digital simulation of time-invariant linear systems with applications to neuronal modeling, *Biol. Cybern.* **81**, 381 (1999).
- [50] J. J. Hopfield, Neural Networks and Physical Systems with Emergent Collective Computational Abilities, *Proc. Natl. Acad. Sci. U. S. A.* **79**, 2554 (1982).
- [51] J. A. Hertz, A. Krogh, and R. Palmer, *Introduction to the Theory of Neural Computation* (Perseus Publ., Cambridge, Massachusetts, 1991).
- [52] D. J. Amit, *Modeling Brain Function* (Cambridge University Press, Cambridge, England, 1992).
- [53] M. Tsodyks, I. Mitkov, and H. Sompolinsky, Pattern of Synchrony in Inhomogeneous Networks of Oscillators with Pulse Interactions, *Phys. Rev. Lett.* **71**, 1280 (1993).
- [54] W. Gerstner and J. L. van Hemmen, Coherence and Incoherence in a Globally Coupled Ensemble of Pulse-Emitting Units, *Phys. Rev. Lett.* **71**, 312 (1993).
- [55] C. van Vreeswijk, L. F. Abbott, and G. B. Ermentrout, When Inhibition not Excitation Synchronizes Neural Firing, *J. Comp. Neurosci.* **1**, 313 (1994).
- [56] Á. Corral, C. J. Pérez, A. Díaz-Guilera, and A. Arenas, Synchronization in a Lattice Model of Pulse-Coupled Oscillators, *Phys. Rev. Lett.* **75**, 3697 (1995).
- [57] W. Gerstner, J. L. van Hemmen, and J. D. Cowan, What Matters in Neuronal Locking?, *Neural Comput.* **8**, 1653 (1996).
- [58] P. Bressloff, S. Coombes, and B. de Souza, Dynamics of a Ring of Pulse-Coupled Oscillators: Group Theoretic Approach, *Phys. Rev. Lett.* **79**, 2791 (1997).
- [59] P. Bressloff and S. Coombes, Synchrony in an Array of Integrate-and-Fire Neurons with Dendritic Structure, *Phys. Rev. Lett.* **78**, 4665 (1997).
- [60] P. Bressloff and S. Coombes, Desynchronization, Mode Locking, and Bursting in Strongly Coupled Integrate-and-Fire Oscillators, *Phys. Rev. Lett.* **81**, 2168 (1998).
- [61] M. Diesmann, M.-O. Gewaltig, and A. Aertsen, Stable propagation of synchronous spiking in cortical neural networks, *Nature* **402**, 529 (1999).
- [62] R. O. Dror, C. C. Canavier, R. J. Butera, J. W. Clark, and J. H. Byrne, A mathematical criterion based on phase response curves for stability in a ring of coupled oscillators, *Biol. Cybern* **80**, 11 (1999).
- [63] P. C. Bressloff, Dynamics of Strongly Coupled Spiking Neurons, *Neural Comput.* **12**, 91 (2000).

- [64] D. Golomb and D. Hansel, The Number of Synaptic Inputs and the Synchrony of Large Sparse Neuronal Networks, *Neural Comput.* **12**, 1095 (2000).
- [65] M. Diesmann, M.-O. Gewaltig, S. Rotter, and A. Aertsen, State space analysis of synchronous spiking in cortical neural networks, *Neurocomputing* **38–40**, 565 (2001).
- [66] D. Hansel and G. Mato, Existence and Stability of Persistent States in Large Neuronal Networks, *Phys. Rev. Lett.* **86**, 4175 (2001).
- [67] J.-P. Eckmann, Roads to turbulence in dissipative dynamical systems, *Rev. Mod. Phys.* **53**, 643 (1981).
- [68] J. Alexander, J. A. Yorke, and Z. You, Riddled Basins, *Int. J. Bifurc. Chaos* **2**, 795 (1992).
- [69] J. C. Sommerer and E. Ott, A physical system with qualitatively uncertain dynamics, *Nature* **365**, 138 (1993).
- [70] K. Kaneko, Dominance of Milnor Attractors and Noise-Induced Selection in a Multia attractor System, *Phys. Rev. Lett.* **78**, 2736 (1997).
- [71] H. Yang, Milnor strange non-chaotic attractor with complex basin of attraction, *Phys. Rev. E* **63**, 036208 (2001).
- [72] A. Zumdick, Dynamik von Zufallsnetzen pulsgekoppelter Modellneurone, Diploma thesis, Department of Physics, University of Göttingen, 2002.
- [73] A. Zumdick, M. Timme, F. Wolf, and T. Geisel, in preparation.
- [74] M. Denker, Complex networks of spiking neurons with a generalized rise function, Diploma thesis, Department of Physics, University of Göttingen, 2002.
- [75] M. Denker, M. Timme, M. Diesmann, and T. Geisel, in preparation.
- [76] D. Hansel, G. Mato, and C. Meunier, Clustering and slow switching in globally coupled phase oscillators, *Phys. Rev. E* **48**, 3470 (1993).
- [77] H. Kori and Y. Kuramoto, Slow switching in globally coupled oscillators: robustness and occurrence through delayed coupling, *Phys. Rev. E* **63**, 046214 (2001).
- [78] Y. Kuramoto, Collective Synchronization of pulse-coupled oscillators and excitable units, *Physica D* **50**, 15 (1991).
- [79] M. Rabinovich, A. Volkovskii, P. Lecanda, R. Huerta, H. D. I. Abarbanel, and G. Laurent, Dynamical Encoding by Networks of Competing Neuron Groups: Winnerless Competition, *Phys. Rev. Lett.* **87**, 068102 (2001).

- [80] B. A. Huberman and R. M. Lukose, Social dilemmas and Internet congestion, *Science* **277**, 535 (1997).
- [81] F. Rieke, D. Warland, and W. Bialek, *Spikes: Exploring the Neural Code* (MIT Press, Cambridge, Massachusetts, 1999).
- [82] *Handbook on Graphs and Networks*, edited by S. Bornholdt and H. G. Schuster (Wiley-VCH, Weinheim, Germany, 2002).
- [83] R. Albert and A.-L. Barabási, Statistical mechanics of complex networks, *Rev. Mod. Phys.* **74**, 47 (2002).
- [84] S. Dorogovtsev and J. F. F. Mendes, Evolution of Networks, *Adv. Phys.* **51**, 1079 (2002).
- [85] A. Albert, H. Jeong, and A.-L. Barabási, Diameter of the World Wide Web, *Nature* **401**, 130 (1999).
- [86] *AY's Neuroanatomy of C. elegans for Computation*, edited by T. B. Achacoso and W. S. Yamamoto (CRC Press, Boca Raton, Florida, 1992).
- [87] D. J. Watts and S. H. Strogatz, Collective dynamics of 'small-world' networks, *Nature* **393**, 440 (1998).
- [88] M. Abeles, *Corticonics: Neural circuits for the cerebral cortex* (Cambridge University Press, Cambridge, England, 1991).
- [89] M. A. Arbib, P. Erdi, and J. Szentagothai, *Neural Organization: Structure, Function, and Dynamics* (MIT Press, Cambridge, Massachusetts, 1997).
- [90] R. Eckhorn, R. Bauer, W. Jordan, M. Brosch, W. Kruse, M. Munk, and H. J. Reitboeck, Coherent oscillations: A mechanism of feature linking in the visual cortex?, *Biol. Cybern* **60**, 121 (1988).
- [91] C. M. Gray, P. König, A. K. Engel, and W. Singer, Stimulus-Specific Neuronal Oscillations in Cat Visual Cortex Exhibit Inter-Columnar Synchronization Which Reflects Global Stimulus Properties, *Nature* **338**, 334 (1989).
- [92] W. Singer, Neuronal synchrony: a versatile code for the definition of relations?, *Neuron* **24**, 49 (1999), references for Reviews on the Binding Problem, pg. 111-125.
- [93] M. N. Shadlen and W. T. Newsome, The variable discharge of cortical neurons: implications for connectivity, computation and information coding, *J. Neurosci.* **18**, 3870 (1998).
- [94] S. A. Geršgorin, Über die Abgrenzung der Eigenwerte einer Matrix, *Izv. Akad. Nauk. SSSR, Ser. Fiz. Mat.* **6**, 749 (1931).

- [95] J. Stoer and R. Burlisch, *Introduction to Numerical Analysis* (Springer, New York, 1992).
- [96] O. Perron, Zur Theorie der Matrizen, *Math. Ann.* **64**, 248 (1907).
- [97] G. Frobenius, Über Matrizen aus positiven Elementen, *S.-B. K. Preuss. Akad. Wiss. Berlin* 471 (1908).
- [98] G. Frobenius, Über Matrizen aus positiven Elementen, *S.-B. K. Preuss. Akad. Wiss. Berlin* 514 (1909).
- [99] G. Frobenius, Über Matrizen aus nicht negativen Elementen, *S.-B. K. Preuss. Akad. Wiss. Berlin* 456 (1912).
- [100] H. Minc, *Nonnegative matrices* (Wiley, New York, 1988).
- [101] M. L. Mehta, *Matrix Theory* (Hindustan Publishing, Delhi, India, 1989).
- [102] E. P. Wigner, On the statistical distribution of the widths and spacings of nuclear resonance levels, *Proc. Camb. Phil. Soc.* **47**, 790 (1951).
- [103] *Statistical Theory of Spectra: Fluctuations*, edited by C. E. Porter (Academic Press, New York, 1965).
- [104] M. L. Mehta, *Random Matrices* (Academic Press, New York, 1991).
- [105] T. Guhr, A. Müller-Groeling, and H. A. Weidenmüller, Random-matrix theories in quantum physics: common concepts, *Phys. Rep.* **4–6**, 189 (1998).
- [106] O. Bohigas, M. J. Giannoni, and C. Schmit, Characterization of Chaotic Quantum Spectra and Universality of Level Fluctuations, *Phys. Rev. Lett.* **52**, 1 (1984).
- [107] F. Haake, *Quantum Signatures of Chaos* (Springer, New York, 2001).
- [108] A. D. Mirlin and Y. V. Fyodorov, Universality of level correlation function of sparse random matrices, *J. Phys. A* **24**, 2273 (1991).
- [109] Y. V. Fyodorov and A. D. Mirlin, Localization in Ensemble of Sparse Random Matrices, *Phys. Rev. Lett.* **67**, 2049 (1991).
- [110] A. J. Bray and G. J. Rodgers, Diffusion in a sparsely connected space: A model for glassy relaxation, *Phys. Rev. B* **38**, 11461 (1988).
- [111] G. J. Rodgers and A. J. Bray, Density of States of a sparse random matrix, *Phys. Rev. B* **37**, 3557 (1988).
- [112] V. L. Girko, Eigenvalues of Asymmetric Matrices, *Theory Probab. Appl.* **29**, 694 (1985).

- [113] H. Sommers, A. Crisanti, H. Sompolinsky, and Y. Stein, Spectrum of Large Random Asymmetric Matrices, *Phys. Rev. Lett.* **60**, 1895 (1988).
- [114] D. J. Watts, *Small Worlds* (Princeton University Press, Princeton, New Jersey, 1999).

Acknowledgments

This thesis has benefitted from the personal support of many people. I tried to prepare a succinct work in all other parts of this thesis. In this part – the acknowledgments – I see no reason and no chance for that.

I would like to thank Theo Geisel for giving me the possibility to work in his unique group, for many useful discussions, and for constant support. Thank you for your permanent efforts to create and retain the excellent environment in this group.

I would like to thank Fred Wolf, an ingenious researcher and competent teacher. He was not always present in Göttingen, but when he was, I learned a lot from him about how to attack problems, how to give talks, how to write papers, and how to convince editors and referees. Fred also strongly motivated me in times of trouble, no matter where it came from. He (and his absence) gave me the freedom to work on fields of my interest, whether they were related to the topic of this thesis or not. Thank you for guiding me through my thesis work.

Special thanks are due to Björn Naundorf with whom I shared an office for more than a year. Beginning in the time Björn was my office mate and continuing until to date, we share many ideas, scientific and private, whether they make sense or not. Thanks Björn.

I would like to thank him and Wolf-Dieter Brandt, Markus Diesmann, Ragnar Fleischmann, Denny Fliegner, Gerhard Nolte, and Yorck-Fabian Temme for constant support in all questions related to computers. Without your support, this thesis would not have come into existence.

Besides general support in many questions related to my thesis research, Markus also taught me a number of specialties about a certain computer algebra program. Thank you.

Michael Denker and Alexander Zumdieck, supported by Fred's and Markus' frequent absence, gave me the possibility to advise learning diploma students in doing research. I learned a lot as well and I hope, you enjoyed it like I did. I thank you for this opportunity.

Abigail Morrison, supported by Ellie Livesey, “brought me English by”, at least to some

extent. Unlike the definition of CM (center of mass), which is of minor importance in this thesis, BM (Bananenmilch) and AM both became dicta. Thanks to you, Abigail and Ellie, for your constant support, not only scientifically.

Dirk Brockmann supplied me with a huge number of “Germanism” via email and writing. He also taught me something about how stochastic processes do and do not work. He showed me – about one hundred times – that $\mu \approx 1$ is optimal not only for searching for food or interesting patches in pictures, but also for calculating functions. Thank you Dirk.

I would like to thank Udo Ernst for supporting me during my first year here in Göttingen. You not only introduced me to the model on which my thesis is based, but also answered any detailed questions I had during the beginning of my studies.

I gratefully acknowledge the help of Roland Ketzmerick and Tsampikos Kottos in all questions concerning the writing, submission, and permanent resubmission of papers, up to seventh order. Thank you.

Special thanks are due to Rita Bartels, Alexandra Behling, Corinna Trautsch, and Regina Wunderlich for supporting me in all questions concerning everyday survival, not only administratively.

The above-mentioned people as well as Steffen Arnrich, Oliver Bendix, Dmitri Bibitchkov, Kai Bröking, Michael Buschermöhle, Silke Dodel, Sven Goedeke, Michael Herrmann, Moritz Hiller, Lars Hufnagel, Matthias Kaschube, Karsten Kruse, Norbert Mayer, Alexandre Ossipov, Marc-Felix Otto, Felix Petri, Hans-Ekkehard Pleßer, Mathias Puhlmann, Holger Schanz, Michael Schnabel, Dennis Springguth, Frank Steinbach, Tom Tetzlaff, and Matthias Weiss were always open-minded, towards all kinds of questions. You all contributed your own, personal part to the distinct atmosphere.

I would also like to thank Ingeborg Krämer for providing me with even the most hidden journal articles. Under all circumstances, you found a way to get them very rapidly.

I greatly acknowledge useful discussions with visiting scientists as well as the help of people, who supported me scientifically under various circumstances, in particular Leonid Bunimovich (Institute of Mathematics, Georgia University of Technology), Michael Biehl (Institute for Theoretical Physics, University of Würzburg), Stefan Bornholdt (Center for Bioinformatics, University of Leipzig), Sonja Grün (Max Planck Institute for Brain Research, Frankfurt/Main), Andreas Herz (Faculty of Biology, Humboldt University of Berlin), Michael Holicki (Institute of Mathematics, University of Leipzig), Jürgen Kurths (Nonlinear Dynamics Group, University of Potsdam), and Carl van Vreeswijk (Laboratory for Neurophysics and Physiology of Motor Systems, Centre National de la Recherche Scientifique, University Rene Descartes, Paris).

Stefan Großkinsky. Where would I be without you? You constantly answered questions I had as a human being and as a non-mathematician. We wrote a very special paper

together, where I learned the difference between exact and rigorous, between single and unique. We also met very often for scientific and non-scientific issues, had quite a number of phone calls, and a lot of fun. Very special thanks for – you.

Last, but not least, I would like to thank my parents and grandparents for personal and financial support during my studies. Without them, my studies and hence this thesis would never have been possible. Thank you.

I acknowledge financial support by the European Physical Society, the WE-Heraeus Foundation, and the Max Planck Society.